Title: Drying summers threaten western North American river ecosystems and a keystone migratory fish

Authors: Sacha W. Ruzzante[1*], Tom Gleeson[1], Jonathan W. Moore[2], Marta E. Ulaski[2], Todd Hatfield[3], Markus Schnorbus[4], Stephanie J. Peacock[5]

Affiliations:

[1]Department of Civil Engineering, University of Victoria; Victoria, Canada.

[2]Earth to Ocean Research Group, Simon Fraser University; Burnaby, Canada.

[3]Trinity Consultants Canada; Victoria, Canada

[4]Pacific Climate Impacts Consortium, University of Victoria; Victoria, Canada.

[5]Pacific Salmon Foundation; Vancouver, Canada.

*Corresponding author. Email: sruzzante@uvic.ca

Abstract: Climate change threatens river ecosystems by altering the seasonal streamflow patterns to which aquatic species have adapted, including keystone species like Chinook salmon in western North America. Chinook salmon display diverse life-history adaptations to local hydrologic regimes, contributing to their past resilience but leaving locally adapted populations vulnerable to changing conditions. Here we show that moderate climate change will cause extreme hydrologic changes across western North America: August streamflow could halve in one quarter of the streams we studied by 2100, and one third will probably experience a 500-year return period drought by 2035. Concurrently, increasing agricultural water demand will conflict with ecological needs. Variation in Chinook migration timing across streams and populations poses diverse local challenges but also illustrates possible adaptations and species-level resilience.

Main Text:

River ecosystems are under threat globally as streamflow regimes change and species struggle to adapt to conditions very different from those under which they evolved (*1–5*). Globally, many streamflow regimes have already been pushed far outside pre-industrial conditions (*6–8*) and future changes are expected to be severe (*7*, *9*, *10*). Aquatic species are sensitive to alterations in the magnitude, timing, frequency, duration, and rate of change of flows, as well as changes in temperature, nutrients, and water chemistry (*11*). Of particular concern are high-elevation and polar regions, which are warming faster than the average (*12*, *13*) with severe consequences on the hydrologic cycle and the socioecological systems these regions support (*2*, *7*, *14*, *15*). Changes in average conditions have received much attention but extreme climate events can pose severe and immediate threats to river biodiversity (*16*).

While climate change is a global challenge, societal and ecological impacts are felt locally, vary significantly in space, and require local analyses and solutions (*17–19*). Regional analyses of climate impacts on hydrology usually lack the local specificity in physical and ecological data required for local-scale prediction and management. We solve this shortcoming by combining global climate change projections with locally tuned statistical hydrologic models and local ecological data across hundreds of sites. We apply this approach to the North American habitat range of Chinook salmon, a predominantly mountainous region that reveals the diverse hydrologic changes and tradeoffs between ecological and societal needs that are likely to afflict global regions dependent on the world's water towers (*20*).

Chinook salmon are a cultural, economic, and ecological keystone species that faces mounting pressures due to human impacts, including changing freshwater conditions during their spawning migration (*21–25*). Indeed, profound changes to streamflow have been widely predicted and increasingly observed across western North America (*26–30*). Chinook salmon have developed a rich diversity of life histories of life histories and life history timings in response to diverse hydrologic regimes throughout their range (*31*). This combined hydrologic and biological diversity controls the exposure of each population to climate and other anthropogenic pressures, and as a result some populations continue to thrive while most are in decline and some have been extirpated (*32–35*). However, the impact of climate change on spawning migrations throughout the range is largely unknown because previous studies have focused on small geographic domains (*36–38*) or ignored variation in migration timing between streams and regions (*24*, *30*, *39–41*).

We project future streamflow changes at 399 gauged near-natural streams in river basins that support Chinook salmon and explicitly link projections to Chinook salmon presence and run timings at each location. We develop highly skilled statistical hydrologic models for each gauge, including the effects of glacier loss, and project monthly streamflow for each gauge to the year 2100 using a weighted ensemble of 47 CMIP6 models. For a subset of gauges we also project water temperatures, accounting for the effects of streamflow. We present hydrologic projections for all 399 watersheds across the range, which we divide into 10 regions (see methods and Figure S7). We link these projections to local Chinook salmon migration timing for the 258 streams accessible to Chinook, and all of these results are available in the interactive supplement at https://sruzzante.shinyapps.io/streamflow_projections/, which also includes spawning timing, spawner abundance data, and conservation status where available. Here we illustrate stream-scale methods and results with four 'sentinel' streams chosen to represent the diverse hydrology, life histories, and climate-related threats to Chinook salmon populations. The Kenai River (Alaska) is a northern coastal stream with a snowmelt-glacier regime, and two Chinook salmon

runs (early and late) (*43*). The North Thompson River (British Columbia) is a mid-latitude, interior snowmelt-glacier dominated stream, with both spring and summer runs; these fish are stream-type, meaning juveniles spend more than a year in freshwater before migrating to the ocean (*44*). The North Fork Stillaguamish River (Washington) is a coastal mid-latitude rainfall-dominated stream that supports summer-run Chinook salmon with a primarily ocean-type life history, meaning juveniles migrate to the ocean a few months after hatching (*45*). Deer Creek is a southern rainfall-dominated stream that supports spring, fall, and late fall runs (*46*).

We quantify impacts on aquatic ecosystems using environmental flow methods, as well as on Chinook salmon specifically by examining how streamflow changes in the sentinel streams could threaten diverse aspects of Chinook salmon freshwater life stages. Reduced streamflow during upriver migration can make migration barriers impassable, such as riffles, waterfalls, and artificial structures (*46*, *47*). Low streamflow also reduces usable spawning and rearing habitat, limiting productivity (*23*). Chinook salmon are a cold-water species, and drier streams have the potential to get hotter; heat stress, migration blockage, and mass mortality events have been observed during riverine heat waves (*21*, *48*). Increases in streamflow can also prevent salmon migration, since high water velocities increase the energetic demands of swimming or introduce velocity barriers (*49*, *50*). Other impacts, including scouring of redds during high flow events, have also been observed (*51*).

Environmental flows can be in direct conflict with human water uses. Many populations of Chinook salmon have migration timing that runs through July and August, when river levels are generally low and irrigation water demand peaks. Agricultural operations divert a substantial fraction of summer streamflow from Chinook salmon streams in many parts of their range, and conflicts over this dwindling resource have already been seen (*52–54*). In California, water right curtailment regulations are explicitly tied to the presence of Chinook salmon and other aquatic species, and in British Columbia water rights have been curtailed 11 times since 2016 to protect fish populations (Table S4), leading to as-yet uncalculated economic losses and protests by affected farmers.

Widespread decreases to average late-summer streamflow

Late summer water availability will decrease in almost all streams south of Alaska. Below 60º latitude 94% of streams will see a decrease in median August streamflow, with an average reduction of 39% by the end of the century under a moderate emissions scenario (Fig. 1A and B). Projected flow decreases are greatest at mid-latitudes (*eg*. 47% and 63% in the North Thompson and Stillaguamish Rivers, Fig. 1C). Decreases are more moderate farther south (*eg.* 19% in Deer Creek), because changes in summer air temperature are predicted to be more modest (Fig. S9), July and August precipitation is expected to increase slightly (Fig. S8), and streamflow in this region does not respond as strongly to air temperature (Fig. S10). The lower sensitivity of streamflow to air temperature is likely because of the mediterranean climate in California, wherein most precipitation falls in the winter, and evaporative demand in the summer already far exceeds moisture availability; summer evapotranspiration in these catchments is thus more water-limited than energy-limited so increases in temperature do not lead to large increases in evapotranspiration (*55*, *56*). In the north, glacier retreat and increases in evapotranspiration may be offset by increases in precipitation. In the Kenai River, for example, glacier runoff historically provided about 27% of August streamflow, an amount which is projected to halve by the end of the century. However, increased precipitation could compensate for this loss, and August streamflow is projected to increase slightly by 3%.

There is good agreement among the climate models about the direction of change, but some uncertainty about the magnitude. In 90% of the 276 streams that are expected to see a decrease in August flow of greater than 20%, all of the 47 climate models predict a decrease (medium emissions scenario, end-of-century). Overall, there is at least 90% agreement on the direction of change in 83% of the catchments. However, there is uncertainty about the magnitude of change: regarding catchments where August flows are projected to decrease, on average 80% of models predict a change within ± 13% of the median decrease. For catchments with projected increases the uncertainty is higher: the 10th percentile of projected changes is, on average, 35% lower than the median, and the 90th percentile is 70% higher.

Competition between ecological flows and agricultural uses will probably intensify in the four southern regions, as increased agricultural water demand puts additional pressure on dwindling streamflow. Peak agricultural water demand usually occurs in July and August, when the largest decreases in streamflow are projected. In California and the Columbia Basin, challenges are likely to be basin-wide: 14% and 10% of land is agricultural, respectively, and we project increases to the climate moisture deficit (a proxy for irrigation water demand) of 7-8% in August (Fig. S15). In the Pacific Northwest Coast, Salish Sea, and Fraser Basins, agriculture is less extensive (2.7%, 2.7%, and 1.1% of land, respectively) but localized effects on individual watersheds will still be important. August climate moisture deficit will increase by 16% in the Salish Sea region, while the Pacific Northwest Coast and Fraser Basins will see increases of 6% and 7% under a medium emissions scenario. In each of the five northern regions agriculture occupies less than 0.3% of land, but water-intensive industrial activities such as mining are putting pressure on water resources and salmon habitats (*57–59*).

Disappearing glacier runoff

Glacier runoff will not buffer against streamflow declines for very much longer in the vast majority of rivers. As glacier melt rates accelerate, summer glacier runoff increases to a maximum – 'peak water' (*15*) – after which runoff declines because of reductions in glacier storage. Of the 183 catchments in our dataset with >0.01% glacier cover, 164 have already reached peak water and all but two will reach peak water by 2050 (Fig. S16). This includes the North Thompson River, where glaciers occupy just 1.8% of the catchment area but over the 20th century provided about 10% of August streamflow. However, glaciers in the North Thompson watershed have been retreating for decades and will probably be more than 95% gone by the end of the century.

Outside of southern Alaska and the Transboundary region, glacier runoff in most glaciated catchments will be reduced to less than one quarter of its historical mean (1901-2000) August levels before 2070. These declines will have serious consequences for streamflow and water temperature, as glacier runoff has historically contributed large volumes of cold water to summer streamflow.

Comparison to previous models

The regression models developed here perform better than all previously published models at predicting historical year-to-year changes in summer streamflow for the study area. Figures S3-S6 compare performance of our regression model to 17 models with publicly available simulation outputs, based on the Nash-Sutcliffe Efficiency (NSE) of log-transformed streamflow (Figs. S3 and S4) and Kling-Gupta Efficiency (KGE) of inverse-transformed streamflow (Figs S5 and S6). The comparison models include operational models such as the National Water Model (*60*) and the global Long Short-Term Memory model developed by Nearing *et al.* (*61*), as

well as state-of the-art research-grade process based, hybrid, and machine learning models (see Table S1). Three of the comparison models have also been used for climate change projection. The regression performance for year-round flows is exceeded only by the Long Short-Term Memory model developed by Kratzert *et al.* (*62*), while the regression models are better than all comparison models at predicting changes in August flows.

The decreases in August streamflow projected here are similar on average to previous regional studies in the Fraser (*29*), and Columbia (*28*, *63*) basins, but there are some differences in spatial patterns. Our projections for California show more extreme decreases in August flow than predicted previously (*64*). See supplementary text and Figs. S23-S26 for more details.

The modelling approach used here also accurately represents the direction of historical changes in streamflow. When forced with climate model data, the regression models accurately predict the direction of trends in August streamflow 90% of the time (Fig. S11). However, observed trends over 1951-2024 are about twice as large as these simulated trends, because the observed changes in temperature and precipitation have outpaced the changes predicted by the climate models. When forced with observed climate data, the observed and modelled trends match very closely (Fig. S12).

Extreme droughts are likely in the next 10 years

Extreme droughts are likely to occur soon in many streams, particularly in the middle latitudes of the Chinook salmon range (Figs. 2A and 2B). 67% of streams we studied in the Salish Sea region will probably experience (>50% probability) an August streamflow drought with a 500-year return period within 10 years (medium emissions scenario, SSP 2-4.5). For example, in the Stillaguamish River, we estimate the probability of a 500-year drought in the next decade to be 93%. The return levels are calculated using the Unprecedented Simulated Extreme Ensemble approach (*65*) with 61800 simulated years of data for the years 1901-2000. Over the next 10 years, 23% of ensemble simulations for the Stillaguamish predict streamflow below this threshold each year, for a cumulative probability of 93% (Figure 2C). From the Columbia Basin all the way to the BC North Coast region the median probability of a 500-year drought ranges from 34% to 67%. In the North Thompson River, the probability is 75%. Probabilities are lower in California and in the north (23% in Deer Creek and 0.8% in the Kenai River). Throughout the full range, 32% (126/399) of streams have a greater than 50% probability of experiencing a 500-year drought within 10 years and 253 will probably experience a 100-year drought (Figure S17). At this short time scale the probabilities are relatively insensitive to the emissions scenario. 500-year droughts will probably occur in 114/399 streams in a low-emissions scenario (SSP 1-2.6), and 147/399 streams in a high-emissions scenario SSP 5-8.5).

Range-wide threats to environmental flows

The projected changes will have profound impacts on river ecosystems throughout the range, as can be seen by applying environmental flow needs thresholds by three methods. First, streamflow will be outside of the sustainability boundaries prescribed by Richter's presumptive standard (a change of less than 20% relative to historical flows – see methods for more details) (*66*) for six or more months of the year in 373 of 399 streams under a medium emissions scenario by the end of the century (Fig. S18). Even under the lowest emissions scenario (SSP 1-1.9, consistent with 1.4 ºC of warming), 234 of 399 streams will exceed this sustainability boundary for at least half the year.

Future streamflow will be far outside the historical envelope of variability unless stringent emissions targets are met. We follow the Planetary Boundaries framework (*6*) and evaluate if the boundary will be permanently transgressed by 2090 (*i.e.,* the boundary is transgressed by 2090 and values do not return to normal by the end of the century – see methods). Using this definition, we estimate that boundaries will be permanently transgressed in at least one month of the year in 362 streams, and in at least six months of the year in 14 streams under the medium emissions scenario (Fig. S19). While the highest emissions scenario would see 199 streams with permanent transgressions for more than half the year, the lowest emissions scenario would see none. Thus, we predict that limiting global warming to 1.5 °C or 2 °C would avoid permanent transgressions of planetary boundaries for most streams and most months.

Lastly, there will be an increase in violations of the Tennant minimum flow threshold (10% of the mean annual discharge) (*67*). Some streams in the range experience flows below this threshold even under historical conditions (see Fig. 3C), but the number of streams where median monthly flows in the summer (June-September) drop below the Tennant threshold is expected to grow from 44 (20th century) to 81 (end of 21st century, medium emissions scenario) (Fig. S20). Thirteen of these new violations are in the Salish Sea basin and eleven are in the Columbia Basin. These high-level environmental flows methods portend dire impacts on aquatic ecosystems, including Chinook. However, the impacts will differ due to diverse life histories and geomorphic conditions within rivers, and local planning requires more locally relevant analyses.

Diverse impacts on Chinook salmon

Migrating and spawning Chinook salmon will see lower streamflow in almost all streams. Figure 3 shows changes in monthly flows during migration for the 258 gauge locations accessible to Chinook salmon. Panel A shows the interannual distribution of monthly streamflow for the historical and end-of-century periods for the four sentinel rivers. Panel B illustrates, for the North Fork Stillaguamish, how this information can be summarized into a 'hydrograph change plot', and panel C shows these plots for each of the 258 streams. In 66 of the 74 streams where Chinook salmon migrate during the lowest flows of the year, these flows are projected to decline.

In some streams lower streamflow can expose **physical migration barriers**, but some populations have adapted to avoid migration during critical low flow months. In Deer Creek summer flows in the lower watershed are too low for Chinook salmon passage, and consequently three distinct runs of Chinook salmon have developed. Spring-run Chinook salmon (a threatened population) quickly pass through the lower watershed from March to May (*68*) and then hold in colder pools in the upper watershed, while fall-run and late fall-run fish enter after mid-October, when autumn rains swell the river.

We predict that the summer low-flow period during which the lower reaches of Deer Creek are impassable will lengthen, and spring-run Chinook salmon will need to enter the upper watershed earlier and spend more time holding. While the shift in migration timing may be feasible, the prolonged holding period in the upper watershed, where water temperatures will increase, may harm reproductive success (*48*).

Moreover, extreme dry years are possible in the near future and may harm long-term adaptive capacity: There is a small but non-negligible (17%) probability of April flows in Deer Creek falling below the critical flow for Chinook salmon passage within the next decade (see supplementary text). If this occurs most of the spawning population could be prevented from reaching spawning grounds in the upper watershed, reducing the total abundance of the stream's spawning population and their life history and genetic diversity. For example, recent work from

other California rivers has documented how low flow events such as this can contract spatial and temporal diversity of migrating salmon (*69*).

In other streams the forecasted flow decreases will **limit usable spawning and rearing habitat**. In the North Fork Stillaguamish River, for example, median September flows will be reduced from a historic average of 16.3 m^3s^{-1} to only 8.0 m^3s^{-1}, which could reduce usable spawning habitat for summer-run Chinook salmon by 94% (*70*). Notably, spawning grounds in the Stillaguamish are already considered degraded due to human modifications to the landscape. This and other pressures have caused Stillaguamish Chinook salmon abundance to decline to only 7% of historical levels (*45*), with the spring-run population thought to be extinct (*71*). Nonetheless, extensive river restoration efforts, informed by climate change projections and supported by the Stillaguamish Tribe and the Stillaguamish Watershed Council, offer some hope for a more resilient future (*72*).

In some rivers, the combination of increased air temperature and reduced streamflow will lead to **stressful or lethal water temperatures**. Drier rivers have the potential to get hotter because the ratio of volume to contact area (with the substrate and the air) is smaller, so more heat is absorbed per unit volume. We quantified the sensitivity of water temperatures to air temperature and streamflow in 47 of our streams, including the North Thompson River (SI text and Figs. S21 and S22). We found that in the North Thompson River water temperature increases by 0.5 °C for each degree of air temperature, and by 2.3 °C for a halving of streamflow. Under a medium emissions scenario, we predict that 30-year mean August water temperatures could increase from 14.1 °C during the 20th century to 18.3 °C by late-21st century due to the dual impacts of increases in air temperatures and decreases in streamflow.

These hotter temperatures may endanger the migration, spawning, and juvenile rearing of spring and summer-run populations, both of which are listed as endangered by the Committee on the Status of Endangered Wildlife in Canada (*73*, *74*). Spring-run Chinook salmon begin arriving at the North Thompson River in late July, while summer-run fish migrate from mid-August to mid-September. Given significant year-to-year variability in temperature, it is likely that hot years could see August water temperatures exceeding 22 ºC, temperatures that have been documented as being lethal in some Chinook salmon populations (*27*). Spawning, which occurs from mid-August for spring-run fish and early September for the summer run, requires colder temperatures, optimally below about 12 °C to 15 °C (*27*, *75*). The exposure of these populations to temperatures significantly above this range prior to or during spawning will likely reduce productivity by damaging gametes and increasing egg mortality (*75*). Lastly, the North Thompson populations are stream-type Chinook salmon, meaning that they rear for more than a year in freshwater. Juveniles are thus exposed to the hottest period of the summer, and temperatures in almost all years will likely exceed the optimum for juvenile rearing, documented as being 14.8 °C at natural feeding regimes (*75*). Cold-water refuges, often resulting from groundwater influx, snowmelt, or glacier runoff, may mitigate the impacts of increases in average water temperature (*76*), but as winter snow accumulation declines, glaciers disappear, and groundwater warms, these refuges may shrink and provide less respite (*77*, *78*). The expected rise in water temperature varies significantly between streams (see supplementary text) leading to unique challenges for each population.

Large increases in streamflow, which are predicted in some northern streams, may impair adult migration if water velocities exceed Chinook salmon swimming abilities. However, mean water velocity scales sublinearly with discharge in natural streams (*79*), so increases in water velocity will be less dramatic than increases in streamflow. In the Kenai River, for example, the projected

13% increase in median July flows corresponds to an 8% increase in water velocity (based on field observations taken by the United States Geological Survey at the gauge site – see supplementary materials). Water velocity in the Kenai River is currently not thought to substantially impede Chinook salmon migration (*80*), and the projected increases are unlikely to cause major problems for Kenai Chinook salmon, which have a relatively short-distance freshwater migration. However, velocities may cause problems in other northern streams, especially in the upper Yukon basin where the migration distance is extremely long and energetically demanding (*81*, *82*). We project increases to streamflow in many upper Yukon basin streams during the Chinook salmon migration but data on water velocity in this region is lacking and a general survey of velocity barriers has not been conducted. We expect that high water velocities could block access to some spawning grounds, in some years, under moderate climate change. This problem could be compounded by declines in Chinook salmon body sizes, since smaller fish are weaker swimmers (*83*).

Conclusions

Climate change threatens aquatic ecosystems and biodiversity by altering freshwater flows and temperatures. For the first time, we have produced hydrologic projections for streams across the range of Chinook salmon in North America, including the effects of changing climate and declines in glacier runoff, and linked these projections with environmental flow metrics, Chinook salmon life-history timing, and agricultural water demand. The threats are profound, severe, and immediate. Unless emissions are rapidly reduced soon, by the end of the century August flows will decrease by more than 50% in one quarter of the studied streams and environmental flow transgressions will occur in all regions. 500-year return period droughts are more likely than not to occur in one third of streams over the next decade, and these extreme events could profoundly impact aquatic biodiversity (*16*). At the same time, agricultural and other water demands are likely to increase, setting the stage for ongoing and future water conflicts.

There are hundreds of locally adapted Chinook salmon populations across the diverse landscapes of western North America, and this diversity in life histories will control the exposure of each population to oncoming hydrologic changes and other anthropogenic pressures in each watershed. Prior to this study, this life-history and hydrologic diversity has posed a challenge for evaluating the climate vulnerability of the species across its range (*24*, *84–86*). Our results reveal that each population faces a unique constellation of challenges, as seen in the interactive supplement. The steepest declines in streamflow and most extreme droughts are likely to occur in the middle of the range and will overlap with increasing demand for water to grow food. These challenges will be most acute in the heavily agricultural Columbia Basin and around the densely populated Salish Sea, where agricultural water demand could increase by 8% and 16%, respectively. The results presented here, which represent a bottom-up approach built from local hydrologic models and local information about Chinook salmon migration timing, begin to illustrate how the constellation of challenges varies across rivers to inform climate mitigation and adaptation efforts.

At the local scale, authorities may consider several courses of action to mitigate climate impacts on aquatic species. First, existing anthropogenic stressors can be reduced to lessen cumulative impacts (*87*, *88*); for example, climate change assessments can be used to target locations for habitat restoration that will provide suitable habitat in a warmer climate (*27*, *37*). In the Stillaguamish River, the Stillaguamish Tribe and the Washington Department of Fisheries and Wildlife are restoring floodplain and estuarine habitats to provide rearing habitat for salmon and dissipate winter floods, which are projected to increase in magnitude with climate warming (*89*).

In other watersheds flow management can be employed to protect environmental flows. In Deer Creek, for example, water rights curtailments are explicitly linked to the presence of Chinook salmon and steelhead trout (*90*). Fisheries can be an additional responsive management lever and be reduced or closed to try to avoid overharvesting salmon in years with poor returns or forecasted poor survival during their migrations. For example, commercial fisheries for sockeye salmon in the Fraser River of BC are adaptively managed for climate change, with fisheries being reduced when the river is predicted to be so hot that the combination of heat stress and encounters with fishing gear could reduce sockeye spawner abundance below target escapement levels (*91*).

Range-wide, the hydrologic and water temperature changes projected here are setting in motion a major reorganization of salmon populations. The existing remarkable population diversity of Chinook salmon life-histories are an outcome of local adaptations to historic flow and temperatures regimes and other habitat factors (*31*, *92*). Salmon will be increasingly exposed to flow and temperature regimes to which they are not locally adapted. Some historic salmon rivers and habitats may cease to support Chinook salmon, yet climate change will also open up new habitats (*57*, *93*, *94*). A key question is: will salmon adapt to these oncoming changes? Under strong selective pressures such as shifts in flow and temperature regimes, salmon could rapidly evolve different life-history timings (*95*). In addition, dispersal and gene flow among watersheds could be a key process for adaptation, as evidenced by impressive rates of colonization of habitats following barrier removal (*96*). Human interventions can also support the natural adaptive capacity of species. For Chinook salmon such interventions can include hatchery programs, transplanting stocks from rivers with strong runs to rivers with depleted natural populations, assisted migration across natural or anthropogenic barriers, and genetic engineering (*97*). These strategies entail risks that are difficult to quantify and could cause more harm than good, but are increasingly advocated and employed (*98–100*). Regardless, the oncoming reorganization of freshwater flows will challenge the adaptive capacity of Chinook salmon and other species in these watersheds.

All efforts at conservation and mitigation will entail some cost and compromise between the natural world and human needs, including agricultural, fisheries, hydropower, mining, forestry, and other industrial sectors. The social-ecological challenges arising from these compromises over the next 75 years in western North America will demand locally relevant and community-led climate mitigation. The locally tuned projections and ecological information we have presented can help support such efforts.

References and Notes

1. H. Wang, J. Liu, M. Klaar, A. Chen, L. Gudmundsson, J. Holden, Anthropogenic climate change has influenced global river flow seasonality. *Science* **383**, 1009–1014 (2024).
2. M. A. Palmer, D. P. Lettenmaier, N. L. Poff, S. L. Postel, B. Richter, R. Warner, Climate Change and River Ecosystems: Protection and Adaptation Options. *Environmental Management* **44**, 1053–1068 (2009).
3. N. L. Poff, J. D. Allan, M. B. Bain, J. R. Karr, K. L. Prestegaard, B. D. Richter, R. E. Sparks, J. C. Stromberg, The Natural Flow Regime. *BioScience* **47**, 769–784 (1997).
4. C. J. Vörösmarty, P. B. McIntyre, M. O. Gessner, D. Dudgeon, A. Prusevich, P. Green, S. Glidden, S. E. Bunn, C. A. Sullivan, C. R. Liermann, P. M. Davies, Global threats to human water security and river biodiversity. *Nature* **467**, 555–561 (2010).
5. A. J. Reid, A. K. Carlson, I. F. Creed, E. J. Eliason, P. A. Gell, P. T. J. Johnson, K. A. Kidd, T. J. MacCormack, J. D. Olden, S. J. Ormerod, J. P. Smol, W. W. Taylor, K. Tockner, J. C. Vermaire, D. Dudgeon, S. J. Cooke, Emerging threats and persistent conservation challenges for freshwater biodiversity. *Biol Rev Camb Philos Soc* **94**, 849–873 (2019).
6. M. Porkka, V. Virkki, L. Wang-Erlandsson, D. Gerten, T. Gleeson, C. Mohan, I. Fetzer, F. Jaramillo, A. Staal, S. te Wierik, A. Tobian, R. van der Ent, P. Döll, M. Flörke, S. N. Gosling, N. Hanasaki, Y. Satoh, H. Müller Schmied, N. Wanders, J. S. Famiglietti, J. Rockström, M. Kummu, Notable shifts beyond pre-industrial streamflow and soil moisture conditions transgress the planetary boundary for freshwater change. *Nat Water* **2**, 262–273 (2024).
7. L. Gudmundsson, M. I. Brunner, P. Döll, E. Fluet-Chouinard, N. Frolova, S. N. Gosling, Y. Hirabayashi, M. B. Kireeva, X. Liu, H. Müller Schmied, D. Magritskiy, L. J. Slater, L. Stein, Y. Tramblay, K. Wang, C. Wasko, D. Yamazaki, X. Zhou, Past and future change in global river flows. *Nat Rev Earth Environ* **7**, 7–23 (2026).
8. L. Gudmundsson, J. Boulange, H. X. Do, S. N. Gosling, M. G. Grillakis, A. G. Koutroulis, M. Leonard, J. Liu, H. Müller Schmied, L. Papadimitriou, Y. Pokhrel, S. I. Seneviratne, Y. Satoh, W. Thiery, S. Westra, X. Zhang, F. Zhao, Globally observed trends in mean and extreme river flow attributed to climate change. *Science* **371**, 1159–1162 (2021).
9. Y. Zhang, H. Zheng, X. Zhang, L. R. Leung, C. Liu, C. Zheng, Y. Guo, F. H. S. Chiew, D. Post, D. Kong, H. E. Beck, C. Li, G. Blöschl, Future global streamflow declines are probably more severe than previously estimated. *Nat Water* **1**, 261–271 (2023).
10. G. Wu, J. Chen, X. Shi, J.-S. Kim, J. Xia, L. Zhang, Impacts of Global Climate Warming on Meteorological and Hydrological Droughts and Their Propagations. *Earth's Future* **10**, e2021EF002542 (2022).
11. B. D. Richter, J. V. Baumgartner, J. Powell, D. P. Braun, A Method for Assessing Hydrologic Alteration within Ecosystems. *Conservation Biology* **10**, 1163–1174 (1996).
12. N. C. Pepin, E. Arnone, A. Gobiet, K. Haslinger, S. Kotlarski, C. Notarnicola, E. Palazzi, P. Seibert, S. Serafin, W. Schöner, S. Terzago, J. M. Thornton, M. Vuille, C. Adler, Climate Changes and Their Elevational Patterns in the Mountains of the World. *Reviews of Geophysics* **60**, e2020RG000730 (2022).

13. N. Pepin, R. S. Bradley, H. F. Diaz, M. Baraer, E. B. Caceres, N. Forsythe, H. Fowler, G. Greenwood, M. Z. Hashmi, X. D. Liu, J. R. Miller, L. Ning, A. Ohmura, E. Palazzi, I. Rangwala, W. Schöner, I. Severskiy, M. Shahgedanova, M. B. Wang, S. N. Williamson, D. Q. Yang, Mountain Research Initiative EDW Working Group, Elevation-dependent warming in mountain regions of the world. *Nature Clim Change* **5**, 424–430 (2015).

14. T. P. Barnett, J. C. Adam, D. P. Lettenmaier, Potential impacts of a warming climate on water availability in snow-dominated regions. *Nature* **438**, 303–309 (2005).

15. M. Huss, R. Hock, Global-scale hydrological response to future glacier mass loss. *Nature Clim Change* **8**, 135–140 (2018).

16. J. D. Tonkin, T. Siqueira, J. Merder, T. Datry, N. L. Poff, J. Talbot-Jones, J. D. Olden, Extreme events and river biodiversity under climate change. *Nat. Rev. Biodivers.*, doi: 10.1038/s44358-026-00131-7 (2026).

17. A. W. R. Seddon, M. Macias-Fauria, P. R. Long, D. Benz, K. J. Willis, Sensitivity of global terrestrial ecosystems to climate variability. *Nature* **531**, 229–232 (2016).

18. V. Reyes-García, D. García-del-Amo, S. Álvarez-Fernández, P. Benyei, L. Calvet-Mir, A. B. Junqueira, V. Labeyrie, X. Li, S. Miñarro, V. Porcher, A. Porcuna-Ferrer, A. Schlingmann, C. Schunko, R. Soleymani, A. Tofighi-Niaki, M. Abazeri, E. M. N. A. N. Attoh, A. Ayanlade, J. V. D. C. Ávila, D. Babai, R. C. Bulamah, J. Campos-Silva, R. Carmona, J. Caviedes, R. Chakauya, M. Chambon, Z. Chen, F. Chengula, E. Conde, A. Cuní-Sanchez, C. Demichelis, E. Dudina, Á. Fernández-Llamazares, E. K. Galappaththi, C. Geffner-Fuenmayor, D. Gerkey, M. Glauser, E. Hirsch, T. Huanca, J. T. Ibarra, A. E. Izquierdo, L. Junsberg, M. Lanker, Y. López-Maldonado, J. Mariel, G. Mattalia, M. D. Miara, M. Torrents-Ticó, M. Salimi, A. Samakov, R. Seidler, V. Sharakhmatova, U. B. Shrestha, A. Sharma, P. Singh, T. Ulambayar, R. Wu, I. S. Zakari, Indigenous Peoples and local communities report ongoing and widespread climate change impacts on local social-ecological systems. *Commun Earth Environ* **5**, 29 (2024).

19. IPCC, *Climate Change 2022: Impacts, Adaptation, and Vulnerability.* (Cambridge University Press, 2022; https://www.ipcc.ch/report/ar6/wg2/chapter/summary-for-policymakers/).

20. W. W. Immerzeel, A. F. Lutz, M. Andrade, A. Bahl, H. Biemans, T. Bolch, S. Hyde, S. Brumby, B. J. Davies, A. C. Elmore, A. Emmer, M. Feng, A. Fernández, U. Haritashya, J. S. Kargel, M. Koppes, P. D. A. Kraaijenbrink, A. V. Kulkarni, P. A. Mayewski, S. Nepal, P. Pacheco, T. H. Painter, F. Pellicciotti, H. Rajaram, S. Rupper, A. Sinisalo, A. B. Shrestha, D. Viviroli, Y. Wada, C. Xiao, T. Yao, J. E. M. Baillie, Importance and vulnerability of the world's water towers. *Nature* **577**, 364–369 (2020).

21. V. R. von Biela, L. Bowen, S. D. McCormick, M. P. Carey, D. S. Donnelly, S. Waters, A. M. Regish, S. M. Laske, R. J. Brown, S. Larson, S. Zuray, C. E. Zimmerman, Evidence of prevalent heat stress in Yukon River Chinook salmon. *Can. J. Fish. Aquat. Sci.* **77**, 1878–1892 (2020).

22. D. Tonina, J. A. McKean, D. Isaak, R. M. Benjankar, C. Tang, Q. Chen, Climate Change Shrinks and Fragments Salmon Habitats in a Snow-Dependent Region. *Geophysical Research Letters* **49**, e2022GL098552 (2022).

23. L. Warkentin, C. K. Parken, R. Bailey, J. W. Moore, Low summer river flows associated with low productivity of Chinook salmon in a watershed with shifting hydrology. *Ecological Solutions and Evidence* **3**, e12124 (2022).

24. N. Mantua, I. Tohver, A. Hamlet, Climate change impacts on streamflow extremes and summertime stream temperature and their possible consequences for freshwater salmon habitat in Washington State. *Climatic Change* **102**, 187–223 (2010).

25. C. J. Sergeant, J. R. Bellmore, C. McConnell, J. W. Moore, High salmon density and low discharge create periodic hypoxia in coastal rivers. *Ecosphere* **8**, e01846 (2017).

26. S. W. Ruzzante, T. Gleeson, Rising Temperatures Drive Lower Summer Minimum Flows Across Hydrologically Diverse Catchments in British Columbia. *Water Resources Research* **61**, e2024WR038057 (2025).

27. T. Beechie, H. Imaki, J. Greene, A. Wade, H. Wu, G. Pess, P. Roni, J. Kimball, J. Stanford, P. Kiffney, N. Mantua, Restoring Salmon Habitat for a Changing Climate. *River Research and Applications* **29**, 939–960 (2013).

28. A. F. Hamlet, M. M. Elsner, G. S. Mauger, S.-Y. Lee, I. Tohver, R. A. Norheim, An Overview of the Columbia Basin Climate Change Scenarios Project: Approach, Methods, and Summary of Key Results. *Atmosphere-Ocean* **51**, 392–415 (2013).

29. M. Schnorbus, "VIC Glacier (VIC-GL) - Description of VIC model changes and upgrades, VIC Generation 2 Deployment Report volume 1" (Pacific Climate Impacts Consortium, University of Victoria, Victoria, BC, 2018); https://dspace.library.uvic.ca/server/api/core/bitstreams/850d5363-e326-4b13-bddc-f5cd6227c928/content.

30. S. ul Islam, S. J. Déry, A. T. Werner, Future Climate Change Impacts on Snow and Water Resources of the Fraser River Basin, British Columbia. *Journal of Hydrometeorology* **18**, 473–496 (2017).

31. A. Potapova, J. W. Moore, C. K. Parken, M. Sloat, W. Atlas, L. A. Jones, Range-wide life history diversity and climate exposure in adult Chinook salmon. *Ecosphere* **17**, e70572 (2026).

32. W. I. Atlas, M. R. Sloat, W. H. Satterthwaite, T. W. Buehrens, C. K. Parken, J. W. Moore, N. J. Mantua, J. Hart, A. Potapova, Trends in Chinook salmon spawner abundance and total run size highlight linkages between life history, geography and decline. *Fish and Fisheries* **24**, 595–617 (2023).

33. P. G. Carvalho, W. H. Satterthwaite, M. R. O'Farrell, C. Speir, E. P. Palkovacs, Role of maturation and mortality in portfolio effects and climate resilience. *Can. J. Fish. Aquat. Sci.* **80**, 924–941 (2023).

34. W. H. Satterthwaite, S. M. Carlson, Weakening portfolio effect strength in a hatchery-supplemented Chinook salmon population complex. *Can. J. Fish. Aquat. Sci.* **72**, 1860–1875 (2015).

35. B. M. Connors, M. R. Siegle, J. Harding, S. Rossi, B. A. Staton, M. L. Jones, M. J. Bradford, R. Brown, B. Bechtol, B. Doherty, S. Cox, B. J. G. Sutherland, Chinook salmon diversity contributes to fishery stability and trade-offs with mixed-stock harvest. *Ecological Applications* **32**, e2709 (2022).

36. L. G. Crozier, B. J. Burke, B. E. Chasco, D. L. Widener, R. W. Zabel, Climate change threatens Chinook salmon throughout their life cycle. *Commun Biol* **4**, 222 (2021).

37. J. Battin, M. W. Wiley, M. H. Ruckelshaus, R. N. Palmer, E. Korb, K. K. Bartz, H. Imaki, Projected impacts of climate change on salmon habitat restoration. *Proc Natl Acad Sci U S A* **104**, 6720–6725 (2007).

38. C. S. Shanley, D. M. Albert, Climate Change Sensitivity Index for Pacific Salmon Habitat in Southeast Alaska. *PLoS One* **9**, e104799 (2014).

39. J. C. Iacarella, J. D. Weller, Predicting favourable streams for anadromous salmon spawning and natal rearing under climate change. *Can. J. Fish. Aquat. Sci.* **81**, 1–13 (2024).

40. H. Wu, J. S. Kimball, M. M. Elsner, N. Mantua, R. F. Adler, J. Stanford, Projected climate change impacts on the hydrology and temperature of Pacific Northwest rivers. *Water Resources Research* **48** (2012).

41. D. Blaskey, Y. Cheng, A. J. Newman, J. C. Koch, M. N. Gooseff, K. N. Musselman, Alaskan Hydrology in Transition: Changing Precipitation and Evapotranspiration Patterns Are Projected to Reshape Seasonal Streamflow and Water Temperature by Midcentury (2035–64). doi: 10.1175/JHM-D-24-0121.1 (2025).

42. X. Augerot, Atlas of Pacific Salmon. *icbi* **45**, 952–952 (2005).

43. Alaska Dept of Fish and Game, Fish Count Data Search; https://www.adfg.alaska.gov/sf/FishCounts/.

44. Department of Fisheries and Oceans, NuSEDS-New Salmon Escapement Database System, version 20240110 (2024); https://open.canada.ca/data/en/dataset/c48669a3-045b-400d-b730-48aafe8c5ee6.

45. Stillaguamish Implementation Review Committee, "Stillaguamish Watershed Chinook Salmon Recovery Plan" (Snohomish County Department of Public Works, Everett, WA, 2005); https://www.snohomishcountywa.gov/ArchiveCenter/ViewFile/Item/2163.

46. D. Haas, M. Gard, W. Cowan, P. Uttley, "INSTREAM FLOW EVALUATION: Temperature and Passage Assessment for Salmonids in DEER CREEK, Tehama County" (17–2, California Department of Fish and Wildlife, 2017); https://nrm.dfg.ca.gov/FileHandler.ashx?DocumentID=150435&inline.

47. D. W. Reiser, C. Huang, S. Beck, M. Gagner, E. Jeanes, Defining Flow Windows for Upstream Passage of Adult Anadromous Salmonids at Cascades and Falls. *Transactions of the American Fisheries Society* **135**, 668–679 (2006).

48. A. Richter, S. A. Kolmes, Maximum Temperature Limits for Chinook, Coho, and Chum Salmon, and Steelhead Trout in the Pacific Northwest. *Reviews in Fisheries Science* **13**, 23–49 (2005).

49. Patrick D. Powers, John F. Orsborn, "An Investigation of the Physical and Biological Conditions Affecting Fish Passage Success at Culverts and Waterfalls" (Bonneville Power Administration, 1985).

50. M. J. Wright, M. Hurson, K. A. Robinson, D. A. Patterson, J. G. Venditti, A typology of potential hydraulic barriers to adult salmon migration in a bedrock river. *Can. J. Fish. Aquat. Sci.* **82**, 1–19 (2025).

51. J. R. Goode, J. M. Buffington, D. Tonina, D. J. Isaak, R. F. Thurow, S. Wenger, D. Nagel, C. Luce, D. Tetzlaff, C. Soulsby, Potential effects of climate change on streambed scour and risks to salmonid survival in snow-dominated mountain basins. *Hydrological Processes* **27**, 750–765 (2013).

52. T. G. Safford, K. C. Norman, Water water everywhere, but not enough for salmon? Organizing integrated water and fisheries management in Puget Sound. *Journal of Environmental Management* **92**, 838–847 (2011).

53. Andrew MacLeod, Scarce Water: On the Frontlines of BC's Drought, *The Tyee* (2023). https://thetyee.ca/News/2023/08/31/On-Frontlines-BC-Drought/.

54. M. R. Moore, A. Mulville, M. Weinberg, Water Allocation in the American West: Endangered Fish Versus Irrigated Agriculture. *Natural Resources Journal* **36**, 319–357 (1996).

55. T. Maurer, F. Avanzi, S. D. Glaser, R. C. Bales, Drivers of drought-induced shifts in the water balance through a Budyko approach. *Hydrology and Earth System Sciences* **26**, 589–607 (2022).

56. M. G. Cooper, J. R. Schaperow, S. W. Cooley, S. Alam, L. C. Smith, D. P. Lettenmaier, Climate Elasticity of Low Flows in the Maritime Western U.S. Mountains. *Water Resources Research* **54**, 5602–5619 (2018).

57. J. W. Moore, K. J. Pitman, D. Whited, N. T. Marsden, E. K. Sexton, C. J. Sergeant, M. Connor, Mining stakes claim on salmon futures as glaciers retreat. *Science* **382**, 887–889 (2023).

58. M. Braz Pires, N. Baltus, A. Marques, R. Kleijn, M. Buxton, V. Maus, V. Barbarossa, Freshwater Conservation Priority Areas Are Threatened by Global Mining Activities. *Global Change Biology* **32**, e70774 (2026).

59. S. Giljum, V. Maus, L. Sonter, S. Luckeneder, T. Werner, S. Lutter, J. Gershenzon, M. J. Cole, J. Siqueira-Gay, A. Bebbington, Metal mining is a global driver of environmental change. *Nat Rev Earth Environ* **6**, 441–455 (2025).

60. B. Cosgrove, D. Gochis, T. Flowers, A. Dugger, F. Ogden, T. Graziano, E. Clark, R. Cabell, N. Casiday, Z. Cui, K. Eicher, G. Fall, X. Feng, K. Fitzgerald, N. Frazier, C. George, R. Gibbs, L. Hernandez, D. Johnson, R. Jones, L. Karsten, H. Kefelegn, D. Kitzmiller, H. Lee, Y. Liu, H. Mashriqui, D. Mattern, A. McCluskey, J. L. McCreight, R. McDaniel, A. Midekisa, A. Newman, L. Pan, C. Pham, A. RafieeiNasab, R. Rasmussen, L. Read, M. Rezaeianzadeh, F. Salas, D. Sang, K. Sampson, T. Schneider, Q. Shi, G. Sood, A. Wood, W. Wu, D. Yates, W. Yu, Y. Zhang, NOAA's National Water Model: Advancing operational hydrology through continental-scale modeling. *JAWRA Journal of the American Water Resources Association* **60**, 247–272 (2024).

61. G. Nearing, D. Cohen, V. Dube, M. Gauch, O. Gilon, S. Harrigan, A. Hassidim, D. Klotz, F. Kratzert, A. Metzger, S. Nevo, F. Pappenberger, C. Prudhomme, G. Shalev, S. Shenzis, T. Y. Tekalign, D. Weitzner, Y. Matias, Global prediction of extreme floods in ungauged watersheds. *Nature* **627**, 559–563 (2024).

62. F. Kratzert, M. Gauch, D. Klotz, G. Nearing, HESS Opinions: Never train a Long Short-Term Memory (LSTM) network on a single basin. *Hydrology and Earth System Sciences* **28**, 4187–4201 (2024).

63. N. Mizukami, E. D. Gutmann, A. W. Wood, B. Nijssen, J. M. Harrell, C. D. Frans, M. D. Warner, C. Mueller, A century long ensemble streamflow dataset in the Pacific Northwest to support water security assessments. *Sci Data*, doi: 10.1038/s41597-026-06865-5 (2026).

64. California Water Commission, Climate Change Projections for Water Storage Investment Program (WSIP), (2019); https://data.ca.gov/dataset/climate-change-projections-for-water-storage-investment-program-wsip.

65. H. W. van den Brink, G. P. Können, J. D. Opsteegh, G. J. van Oldenborgh, G. Burgers, Estimating return periods of extreme events from ECMWF seasonal forecast ensembles. *International Journal of Climatology* **25**, 1345–1354 (2005).

66. B. D. Richter, M. M. Davis, C. Apse, C. Konrad, A Presumptive Standard for Environmental Flow Protection. *River Research and Applications* **28**, 1312–1321 (2012).

67. D. L. Tennant, Instream Flow Regimens for Fish, Wildlife, Recreation and Related Environmental Resources. *Fisheries* **1**, 6–10 (1976).

68. R. Revnak, Monitoring adult spring-run Chinook salmon throughout the adult lifespan on Deer and Mill Creek, Environmental Data Initiative (2024); https://doi.org/10.6073/PASTA/EE8EAD98742FB149E753ED533B4CE324.

69. S. M. Carlson, K. C. Pregler, M. Obedzinski, S. P. Gallagher, S. J. Rhoades, C. Woelfle-Hazard, N. Queener, S. E. Thompson, M. E. Power, Anatomy of a range contraction: Flow-phenology mismatches threaten salmonid fishes near their trailing edge. *Proc Natl Acad Sci U S A* **122**, e2415670122 (2025).

70. S. S. Embrey, "The relation of streamflow to habitat for anadromous fish in the Stillaguamish River basin, Washington" (U.S. Geological Survey, Tacoma, WA, 1987); https://doi.org/10.3133/wri864326.

71. W. Nehlsen, J. E. Williams, J. A. Lichatowich, Pacific Salmon at the Crossroads: Stocks at Risk from California, Oregon, Idaho, and Washington. *Fisheries* **16**, 4–21 (1991).

72. T. J. . Beechie, A. Goodman, M. Lowe, O. Stefankiv, B. TImpane-Padgham, J. Jorgensen, "Evaluating Effects of Climate Change, Restoration Scenarios, and Hatchery Effects on Chinook Salmon in the Stillaguamish River Basin with the HARP Model" (NOAA Contract Report NMFS-NWFSC-CR-2023-09., U.S. Department of Commerce, 2023); https://doi.org/10.25923/963j-pd86.

73. COSEWIC, "Chinook Salmon (Oncorhynchus tshawytscha): COSEWIC assessment and status report 2018 (Part one – Designatable units with no or low levels of artificial releases in the last 12 years)" (program results;research, Ottawa, 2019); https://www.canada.ca/en/environment-climate-change/services/species-risk-public-registry/cosewic-assessments-status-reports/chinook-salmon-2018.html.

74. COSEWIC, "COSEWIC assessment and status report on the Chinook Salmon Oncorhynchus tshawytscha, Designatable Units in Southern British Columbia (Part Two – Designatable Units with High Levels of Artificial Releases in the Last 12 Years)"

(COSEWIC, Committee on the Status of Endangered Wildlife in Canada = COSEPAC, Comité sur la situation des espèces en péril au Canada, Ottawa, ON, 2020).

75. A. Richter, S. A. Kolmes, Maximum Temperature Limits for Chinook, Coho, and Chum Salmon, and Steelhead Trout in the Pacific Northwest. *Reviews in Fisheries Science* **13**, 23–49 (2005).

76. M. N. Snyder, N. H. Schumaker, J. B. Dunham, J. L. Ebersole, M. L. Keefer, J. Halama, R. L. Comeleo, P. Leinenbach, A. Brookes, B. Cope, J. Wu, J. Palmer, Tough places and safe spaces: Can refuges save salmon from a warming climate? *Ecosphere* **13**, e4265 (2022).

77. S. A. Benz, D. J. Irvine, G. C. Rau, P. Bayer, K. Menberg, P. Blum, R. C. Jamieson, C. Griebler, B. L. Kurylyk, Global groundwater warming due to climate change. *Nat. Geosci.* **17**, 545–551 (2024).

78. J. A. Leach, R. D. Moore, Empirical Stream Thermal Sensitivities May Underestimate Stream Temperature Response to Climate Warming. *Water Resources Research* **55**, 5453–5467 (2019).

79. L. B. Leopold, T. M. Jr, "The hydraulic geometry of stream channels and some physiographic implications" (252, U.S. Government Printing Office, 1953); https://doi.org/10.3133/pp252.

80. D. W. Welch, A. D. Porter, P. Winchell, Migration behavior of maturing sockeye (Oncorhynchus nerka) and Chinook salmon (O. tshawytscha) in Cook Inlet, Alaska, and implications for management. *Anim Biotelemetry* **2**, 35 (2014).

81. K. R. Courtney, J. A. Falke, M. K. Cox, J. Nichols, Energetic Status of Alaskan Chinook Salmon: Interpopulation Comparisons and Predictive Modeling Using Bioelectrical Impedance Analysis. *North American Journal of Fisheries Management* **40**, 209–224 (2020).

82. A. Murdoch, B. M. Connors, N. W. R. Lapointe, J. Mills Flemming, S. J. Cooke, C. Mantyka-Pringle, Multiple environmental drivers across life stages influence Yukon River Chinook salmon productivity. *Can. J. Fish. Aquat. Sci.* **81**, 97–114 (2024).

83. K. B. Oke, C. J. Cunningham, P. a. H. Westley, M. L. Baskett, S. M. Carlson, J. Clark, A. P. Hendry, V. A. Karatayev, N. W. Kendall, J. Kibele, H. K. Kindsvater, K. M. Kobayashi, B. Lewis, S. Munch, J. D. Reynolds, G. K. Vick, E. P. Palkovacs, Recent declines in salmon body size impact ecosystems and fisheries. *Nat Commun* **11**, 4155 (2020).

84. L. G. Crozier, J. E. Siegel, A Comprehensive Review of the Impacts of Climate Change on Salmon: Strengths and Weaknesses of the Literature by Life Stage. *Fishes* **8**, 319 (2023).

85. J. D. Weller, R. D. (Dan) Moore, J. C. Iacarella, Stream thermalscape scenarios for British Columbia, Canada. *Canadian Water Resources Journal / Revue canadienne des ressources hydriques* **49**, 233–252 (2024).

86. A. M. FitzGerald, S. N. John, T. M. Apgar, N. J. Mantua, B. T. Martin, Quantifying thermal exposure for migratory riverine species: Phenology of Chinook salmon populations predicts thermal stress. *Global Change Biology* **27**, 536–549 (2021).

87. J. W. Moore, M. E. Ulaski, K. L. Wilson, T. G. Martin, S. D. Kuiper, S. J. Peacock, D. C. Braun, S. M. Naman, K. J. Pitman, A. J. Reid, J. S. Rosenfeld, N. C. Sainsbury, S. M.

Wilson, B. J. Zdasiuk, A Safe Operating Space for Salmon Watersheds Under Rapid Climate Change. *Fish and Fisheries* **26**, 1213–1228 (2025).

88. M. E. Ulaski, J. W. Moore, D. Carlson, K. F. Taddei, K. Kriese, J. Griggs, C. C. Murray, M. Adams, K. L. Wilson, A. Reid, N. Sainsbury, S. Cannon, E. Griggs, T. G. Martin, Barriers and opportunities for the effective management of cumulative effects in salmon ecosystems in British Columbia, Canada. *FACETS* **10**, 1–25 (2025).

89. Ingrid Tohver, Lara Whitely Binder, Guillaume Mauger, Meade Krosby, "Summary of projected changes in physical conditions in the Stillaguamish watershed and ceded area" (2015).

90. California State Water Resources Control Board, Curtailment of Diversions on Mill and Deer Creeks Due to Insufficient Flow for Specific Fisheries (2022). https://www.waterboards.ca.gov/drought/mill_deer_creeks/docs/2022-readoption-reg-text.pdf.

91. D. A. Patterson, S. J. Cooke, S. G. Hinch, K. A. Robinson, N. Young, A. P. Farrell, K. M. Miller, A perspective on physiological studies supporting the provision of scientific advice for the management of Fraser River sockeye salmon (Oncorhynchus nerka). *Conserv Physiol* **4**, cow026 (2016).

92. T. Beechie, E. Buhle, M. Ruckelshaus, A. Fullerton, L. Holsinger, Hydrologic regime and the conservation of salmon life history diversity. *Biological Conservation* **130**, 560–572 (2006).

93. K. J. Pitman, J. W. Moore, M. Huss, M. R. Sloat, D. C. Whited, T. J. Beechie, R. Brenner, E. W. Hood, A. M. Milner, G. R. Pess, G. H. Reeves, D. E. Schindler, Glacier retreat creating new Pacific salmon habitat in western North America. *Nat Commun* **12**, 6816 (2021).

94. C. Carothers, T. L. Sformo, S. Cotton, J. C. George, P. A. H. Westley, Pacific Salmon in the Rapidly Changing Arctic: Exploring Local Knowledge and Emerging Fisheries in Utqiaġvik and Nuiqsut, Alaska. *ARCTIC* **72**, 273–288 (2019).

95. T. E. Reed, D. E. Schindler, M. J. Hague, D. A. Patterson, E. Meir, R. S. Waples, S. G. Hinch, Time to Evolve? Potential Evolutionary Responses of Fraser River Sockeye Salmon to Climate Change and Effects on Persistence. *PLOS ONE* **6**, e20380 (2011).

96. G. R. Pess, M. L. McHenry, K. Denton, J. H. Anderson, M. C. Liermann, R. J. Peters, J. R. McMillan, S. J. Brenkman, T. R. Bennett, J. J. Duda, K. M. Hanson, Initial responses of Chinook salmon (Oncorhynchus tshawytscha) and steelhead (Oncorhynchus mykiss) to removal of two dams on the Elwha River, Washington State, U.S.A. *Front. Ecol. Evol.* **12** (2024).

97. L. G. Crozier, J. E. Siegel, From threats to solutions: A literature review of climate adaptation in anadromous salmon and trout. *Ecosphere* **16**, e70054 (2025).

98. M. Kardos, E. E. Armstrong, S. W. Fitzpatrick, S. Hauser, P. W. Hedrick, J. M. Miller, D. A. Tallmon, W. C. Funk, The crucial role of genome-wide genetic variation in conservation. *Proceedings of the National Academy of Sciences* **118**, e2104642118 (2021).

99. P. W. Hedrick, F. W. Allendorf, R. S. Waples, Genetic engineering in conservation. *Nature* **502**, 303–303 (2013).

100. G. Torda, K. M. Quigley, Drivers of adaptive capacity in wild populations: Implications for genetic interventions. *Front. Mar. Sci.* **9** (2022).

101. H. V. Gupta, H. Kling, K. K. Yilmaz, G. F. Martinez, Decomposition of the mean squared error and NSE performance criteria: Implications for improving hydrological modelling. *Journal of Hydrology* **377**, 80–91 (2009).

102. RGI Consortium, Randolph Glacier Inventory - A Dataset of Global Glacier Outlines, Version 6, National Snow and Ice Data Center (2017); https://doi.org/10.7265/4M1F-GD79.

103. L. M. Wake, S. J. Marshall, Assessment of current methods of positive degree-day calculation using in situ observations from glaciated regions. *Journal of Glaciology* **61**, 329–344 (2015).

104. E. Luedeling, L. Caspersen, E. Fernandez, chillR: Statistical Methods for Phenology Analysis in Temperate Fruit Trees, version 0.76 (2024); https://cran.r-project.org/web/packages/chillR/index.html.

105. F. Maussion, A. Butenko, N. Champollion, M. Dusch, J. Eis, K. Fourteau, P. Gregor, A. H. Jarosch, J. Landmann, F. Oesterle, B. Recinos, T. Rothenpieler, A. Vlug, C. T. Wild, B. Marzeion, The Open Global Glacier Model (OGGM) v1.1. *Geoscientific Model Development* **12**, 909–931 (2019).

106. R. Hugonnet, R. McNabb, E. Berthier, B. Menounos, C. Nuth, L. Girod, D. Farinotti, M. Huss, I. Dussaillant, F. Brun, A. Kääb, Accelerated global glacier mass loss in the early twenty-first century. *Nature* **592**, 726–731 (2021).

107. A. J. Cannon, Multivariate quantile mapping bias correction: an N-dimensional probability density function transform for climate model simulations of multiple variables. *Clim Dyn* **50**, 31–49 (2018).

108. A. J. Cannon, S. R. Sobie, T. Q. Murdock, Bias Correction of GCM Precipitation by Quantile Mapping: How Well Do Methods Preserve Changes in Quantiles and Extremes? *Journal of Climate* **28**, 6938–6959 (2015).

109. A. J. Cannon, H. Alford, R. R. Shrestha, M. C. Kirchmeier-Young, M. R. Najafi, Canadian Large Ensembles Adjusted Dataset version 1 (CanLEADv1): Multivariate bias-corrected climate model outputs for terrestrial modelling and attribution studies in North America. *Geoscience Data Journal* **9**, 288–303 (2022).

110. M. C. Kirchmeier-Young, F. W. Zwiers, N. P. Gillett, A. J. Cannon, Attributing extreme fire risk in Western Canada to human emissions. *Climatic Change* **144**, 365–379 (2017).

111. Z. Hausfather, K. Marvel, G. A. Schmidt, J. W. Nielsen-Gammon, M. Zelinka, Climate simulations: recognize the 'hot model' problem. *Nature* **605**, 26–29 (2022).

112. S. C. Sherwood, M. J. Webb, J. D. Annan, K. C. Armour, P. M. Forster, J. C. Hargreaves, G. Hegerl, S. A. Klein, K. D. Marvel, E. J. Rohling, M. Watanabe, T. Andrews, P. Braconnot, C. S. Bretherton, G. L. Foster, Z. Hausfather, A. S. von der Heydt, R. Knutti, T. Mauritsen, J. R. Norris, C. Proistosescu, M. Rugenstein, G. A. Schmidt, K. B. Tokarska, M. D. Zelinka, An Assessment of Earth's Climate Sensitivity Using Multiple Lines of Evidence. *Reviews of Geophysics* **58**, e2019RG000678 (2020).

113. A. J. Cannon, The Impact of "Hot Models" on a CMIP6 Ensemble Used by Climate Service Providers in Canada: Do Global Constraints Lead to Appreciable Differences in Regional Projections? *Journal of Climate* **37**, 2141–2154 (2024).

114. F. Garcia, N. Folton, L. Oudin, Which objective function to calibrate rainfall–runoff models for low-flow index simulations? *Hydrological Sciences Journal* **62**, 1149–1166 (2017).

115. G. Thirel, L. Santos, O. Delaigue, C. Perrin, On the use of streamflow transformations for hydrological model calibration. *Hydrology and Earth System Sciences* **28**, 4837–4860 (2024).

116. S. W. Ruzzante, W. J. M. Knoben, T. Wagener, T. Gleeson, M. Schnorbus, Technical Note: High Nash Sutcliffe Efficiencies conceal poor simulations of interannual variance in tropical, alpine, and polar catchments. *EGUsphere*, 1–27 (2025).

117. Cyril Thébault, FUSE simulations. https://www.hydroshare.org/resource/d450bfdfdb944548ac0577f04dd60529/.

118. Cyril Thébault, FUSE-Dynamic-Combination-Sim-Paper, *CUAHSI HydroShare* (2026). https://www.hydroshare.org/resource/cd5cd3116bc544488c223122b4af5516/.

119. A. J. Cannon, MBC: Multivariate Bias Correction of Climate Model Outputs, version 0.10-7 (2024); https://doi.org/10.32614/CRAN.package.MBC.

120. AdaptWest Project, Gridded current and projected climate data for North America at 1km resolution, generated using the ClimateNA v7.30 software (T. Wang et al., 2022), (2022); adaptwest.databasin.org.

121. T. Wang, A. Hamann, D. Spittlehouse, C. Carroll, Locally Downscaled and Spatially Customizable Climate Data for Historical and Future Periods for North America. *PLOS ONE* **11**, e0156720 (2016).

122. Commission for Environmental Cooperation, North American Land Cover, 2020 (Landsat, 30m), version 2020 (2024); https://www.cec.org/north-american-environmental-atlas/land-cover-30m-2020/.

123. V. Thompson, N. J. Dunstone, A. A. Scaife, D. M. Smith, J. M. Slingo, S. Brown, S. E. Belcher, High risk of unprecedented UK rainfall in the current climate. *Nat Commun* **8**, 107 (2017).

124. M. Porkka, V. Virkki, L. Wang-Erlandsson, D. Gerten, T. Gleeson, C. Mohan, I. Fetzer, F. Jaramillo, A. Staal, S. te Wierik, A. Tobian, R. van der Ent, P. Döll, M. Flörke, S. Gosling, N. Hanasaki, Y. Satoh, H. M. Schmied, N. Wanders, J. Rockstrom, M. Kummu, Global water cycle shifts far beyond pre-industrial conditions – planetary boundary for freshwater change transgressed. (2022).

125. A. Y. Hoekstra, M. M. Mekonnen, A. K. Chapagain, R. E. Mathews, B. D. Richter, Global Monthly Water Scarcity: Blue Water Footprints versus Blue Water Availability. *PLOS ONE* **7**, e32688 (2012).

126. M. E. Ulaski, L. Warkentin, S. M. Naman, J. W. Moore, Spatially variable effects of streamflow on water temperature and thermal sensitivity within a salmon-bearing watershed in interior British Columbia, Canada. *River Research and Applications* **39**, 2036–2047 (2023).

127. D. J. Isaak, S. J. Wenger, E. E. Peterson, J. M. Ver Hoef, D. E. Nagel, C. H. Luce, S. W. Hostetler, J. B. Dunham, B. B. Roper, S. P. Wollrab, G. L. Chandler, D. L. Horan, S. Parkes-Payne, The NorWeST Summer Stream Temperature Model and Scenarios for the Western U.S.: A Crowd-Sourced Database and New Geospatial Tools Foster a User Community and Predict Broad Climate Warming of Rivers and Streams. *Water Resources Research* **53**, 9181–9205 (2017).

128. E. D. Lindley, K. M. Dunmall, P. A. H. Westley, Assessing the Role of Incubation Temperature as a Barrier to Successful Establishment of Coho Salmon (Oncorhynchus kisutch) in a Rapidly Warming Arctic. *Ecology and Evolution* **15**, e70797 (2025).

129. J. Pellerin, F. Nzokou Tanekou, "Reference Hydrometric Basin Network Update" (Environment and Climate Change Canada, Gatineau, QC, 2020).

130. J. A. Falcone, "GAGES-II: Geospatial Attributes of Gages for Evaluating Streamflow" (U.S. Geological Survey, 2011); https://doi.org/10.3133/70046617.

131. N. Dawson, J. Fischer, M. Kuhn, A. Pasotti, mhugent, D. Rouzaud, T. Sutton, A. Bruy, M. Dobias, M. Pellerin, V. Olaya, W. Macho, P. Blottiere, R. Blazek, G. Sherman, E. Rouault, N. Woodrow, H. Sant-anna, rldhont, L. Bartoletti, signedav, L. Shaffer, N. Belgacem, J. Cabieces, S. Larosa, V. Cloarec, S. Mani, S. Santilli, P. Cavallini, S. Natsis, qgis/QGIS: 3.28.8, Zenodo (2023); https://doi.org/10.5281/zenodo.8074945.

132. V. Maus, S. Giljum, D. M. da Silva, J. Gutschlhofer, R. P. da Rosa, S. Luckeneder, S. L. B. Gass, M. Lieber, I. McCallum, An update on global mining land use. *Sci Data* **9**, 433 (2022).

133. M. Mulligan, A. van Soesbergen, L. Sáenz, GOODD, a global dataset of more than 38,000 georeferenced dams. *Sci Data* **7**, 31 (2020).

134. H. MacDonald, D. W. McKenney, P. Papadopol, K. Lawrence, J. Pedlar, M. F. Hutchinson, North American historical monthly spatial climate dataset, 1901–2016. *Sci Data* **7**, 411 (2020).

135. J. Eis, L. van der Laan, F. Maussion, B. Marzeion, Reconstruction of Past Glacier Changes with an Ice-Flow Glacier Model: Proof of Concept and Validation. *Front. Earth Sci.* **9** (2021).

136. J.-H. Malles, B. Marzeion, Twentieth century global glacier mass change: an ensemble-based model reconstruction. *The Cryosphere* **15**, 3135–3157 (2021).

137. I. Harris, T. J. Osborn, P. Jones, D. Lister, Version 4 of the CRU TS monthly high-resolution gridded multivariate climate dataset. *Sci Data* **7**, 109 (2020).

138. A. R. Bevington, B. Menounos, Accelerated change in the glaciated environments of western Canada revealed through trend analysis of optical satellite imagery. *Remote Sensing of Environment* **270**, 112862 (2022).

139. I. Dussaillant, R. Hugonnet, M. Huss, E. Berthier, J. Bannwart, F. Paul, M. Zemp, Annual mass change of the world's glaciers from 1976 to 2024 by temporal downscaling of satellite data with in situ observations. *Earth System Science Data* **17**, 1977–2006 (2025).

140. D. Farinotti, M. Huss, J. J. Fürst, J. Landmann, H. Machguth, F. Maussion, A. Pandit, A consensus estimate for the ice thickness distribution of all glaciers on Earth. *Nat. Geosci.* **12**, 168–173 (2019).

141. D. R. Rounce, R. Hock, F. Maussion, R. Hugonnet, W. Kochtitzky, M. Huss, E. Berthier, D. Brinkerhoff, L. Compagno, L. Copland, D. Farinotti, B. Menounos, R. W. McNabb, Global glacier change in the 21st century: Every increase in temperature matters. *Science* **379**, 78–83 (2023).

142. S. M. Wilson, S. J. Peacock, Freshwater life-cycle timing of Pacific salmon and steelhead (Oncorhynchus spp.) in Canada. *Can. J. Fish. Aquat. Sci.* **82**, 1–17 (2025).

143. R. Brenner, Daily salmon escapement counts from the OceanAK database, Alaska, 1921-2017, Knowledge Network for Biocomplexity (2017); https://doi.org/10.5063/P26WJJ.

144. R. W. Williams, L. A. Phinney, "A Catalog of Washington streams and salmon utilization." (Washington Dept. of Fisheries., 1975); https://docs.streamnetlibrary.org/WashingtonStreamCatalog/WRIAs.pdf.

145. J. M. Myers, R. G. Kope, G. J. Bryant, D. Teel, L. J. Lierheimer, T. C. Wainwright, W. S. Grant, F. W. Waknitz, K. Neely, S. T. Lindley, R. S. Waples, "Status review of chinook salmon from Washington, Idaho, Oregon, and California" (NMFS-NWFSC-35, National Oceanic and Atmospheric Administration, 1998); https://repository.library.noaa.gov.

146. J. Bowers, Fish Life Stage Timing Tables, version June 2023 (2023); https://nrimp.dfw.state.or.us/DataClearinghouse/default.aspx?p=202&XMLname=42654.xml.

147. S. Baste, D. Klotz, E. Acuña Espinoza, A. Bardossy, R. Loritz, Unveiling the limits of deep learning models in hydrological extrapolation tasks. *Hydrology and Earth System Sciences* **29**, 5871–5891 (2025).

148. J. P. Bohl, R. R. Wood, C. Frank, P. C. Astagneau, J. Peters, M. I. Brunner, Hybrid models generalize better to warmer climate conditions than process-based and purely data-driven models. *EGUsphere*, 1–45 (2025).

149. Y. Song, K. Sawadekar, J. M. Frame, M. Pan, M. P. Clark, W. J. M. Knoben, A. W. Wood, K. E. Lawson, T. Patel, C. Shen, Physics-Informed, Differentiable Hydrologic Models for Capturing Unseen Extreme Events. *Water Resources Research* **62**, e2025WR040414 (2026).

150. L. Flores, J. Mojica, A. Fletcher, P. Casey, Z. Christin, C. Armistead, D. Batker, "The Value of Natural Capital in the Columbia River Basin: A Comprehensive Analysis" (1.5, Tacoma, WA, 2017); https://ucut.org/wp-content/uploads/2025/09/ValueNaturalCapitalColumbiaRiverBasinDec2017-1.pdf.

151. S. A. Hall, A. Whittemore, J. Padowski, M. Yourek, G. G. Yorgey, K. Rajagopalan, S. McLarty, F. V. Scarpare, M. Liu, C. Asante-Sasu, A. Kondal, M. Brady, R. Gustine, M. Downes, M. Callahan, J. C. Adam, Concurrently assessing water supply and demand is critical for evaluating vulnerabilities to climate change. *JAWRA Journal of the American Water Resources Association* **60**, 543–571 (2024).

152. E. Ehsanzadeh, T. B. M. J. Ouarda, H. M. Saley, A simultaneous analysis of gradual and abrupt changes in Canadian low streamflows. *Hydrological Processes* **25**, 727–739 (2011).

153. D. H. Burn, M. A. Hag Elnur, Detection of hydrologic trends and variability. *Journal of Hydrology* **255**, 107–122 (2002).

154. P. R. Kormos, C. H. Luce, S. J. Wenger, W. R. Berghuijs, Trends and sensitivities of low streamflow extremes to discharge timing and magnitude in Pacific Northwest mountain streams. *Water Resources Research* **52**, 4990–5007 (2016).

155. N. Mizukami, O. Rakovec, A. J. Newman, M. P. Clark, A. W. Wood, H. V. Gupta, R. Kumar, On the choice of calibration metrics for "high-flow" estimation using hydrologic models. *Hydrology and Earth System Sciences* **23**, 2601–2614 (2019).

156. M. Schnorbus, "VIC-Glacier (VIC-GL): Model set-up and deployment for the Peace, Fraser, and Columbia: VIC generation 2 deployment report, volume 6" (Pacific Climate Impacts Consortium (PCIC), 2020); https://hdl.handle.net/1828/21635.

157. B. Lehner, G. Grill, Global river hydrography and network routing: baseline data and new approaches to study the world's large river systems. *Hydrological Processes* **27**, 2171–2186 (2013).

158. F. Kratzert, CAMELS benchmark models, HydroShare (2019); https://doi.org/10.4211/hs.474ecc37e7db45baa425cdb4fc1b61e1.

159. A. J. Newman, N. Mizukami, M. P. Clark, A. W. Wood, B. Nijssen, G. Nearing, Benchmarking of a Physically Based Hydrologic Model. *Journal of Hydrometeorology* **18** (2017).

160. J. Seibert, M. J. P. Vis, E. Lewis, H. j. van Meerveld, Upper and lower benchmarks in hydrological modelling. *Hydrological Processes* **32**, 1120–1125 (2018).

161. Y. Song, T. Bindas, C. Shen, H. Ji, W. J. M. Knoben, L. Lonzarich, M. P. Clark, J. Liu, K. van Werkhoven, S. Lamont, M. Denno, M. Pan, Y. Yang, J. Rapp, M. Kumar, F. Rahmani, C. Thébault, R. Adkins, J. Halgren, T. Patel, A. Patel, K. A. Sawadekar, K. Lawson, High-Resolution National-Scale Water Modeling Is Enhanced by Multiscale Differentiable Physics-Informed Machine Learning. *Water Resources Research* **61**, e2024WR038928 (2025).

162. R. S. Regan, K. E. Juracek, L. E. Hay, S. L. Markstrom, R. J. Viger, J. M. Driscoll, J. H. LaFontaine, P. A. Norton, The U. S. Geological Survey National Hydrologic Model infrastructure: Rationale, description, and application of a watershed-scale model for the conterminous United States. *Environmental Modelling & Software* **111**, 192–203 (2019).

163. Y. Yang, D. Feng, H. E. Beck, W. Hu, A. Abbas, A. Sengupta, L. Delle Monache, R. Hartman, P. Lin, C. Shen, M. Pan, Global Daily Discharge Estimation Based on Grid Long Short-Term Memory (LSTM) Model and River Routing. *Water Resources Research* **61**, e2024WR039764 (2025).

164. D. Bi, M. Dix, S. Marsland, S. O'Farrell, A. Sullivan, R. Bodman, R. Law, I. Harman, J. Srbinovsky, H. A. Rashid, P. Dobrohotoff, C. Mackallah, H. Yan, A. Hirst, A. Savita, F. B. Dias, M. Woodhouse, R. Fiedler, A. Heerdegen, Configuration and spin-up of ACCESS-CM2, the new generation Australian Community Climate and Earth System Simulator Coupled Model. *JSHESS* **70**, 225–251 (2020).

165. T. Ziehn, M. A. Chamberlain, R. M. Law, A. Lenton, R. W. Bodman, M. Dix, L. Stevens, Y.-P. Wang, J. Srbinovsky, The Australian Earth System Model: ACCESS-ESM1.5. *JSHESS* **70**, 193–214 (2020).

166. T. Semmler, S. Danilov, T. Rackow, D. Sidorenko, D. Barbi, J. Hegewald, D. Sein, Q. Wang, T. Jung, AWI AWI-CM1.1MR model output prepared for CMIP6 CMIP, Earth System Grid Federation (2018); https://doi.org/10.22033/ESGF/CMIP6.359.

167. C. Danek, Ö. Gürses, P. Gierz, M. Andrés-Martínez, J. Hauck, AWI AWI-ESM1REcoM model output prepared for CMIP6 ScenarioMIP, Earth System Grid Federation (2023); https://doi.org/10.22033/ESGF/CMIP6.17723.

168. C. Danek, P. Gierz, C. Stepanek, G. Lohmann, "Equilibrium Climate Sensitivity in AWI-ESM: Mechanisms and Effects" (Copernicus Meetings, Vienna, 2020; https://meetingorganizer.copernicus.org/EGU2020/EGU2020-17981.html).

169. T. Wu, Y. Lu, Y. Fang, X. Xin, L. Li, W. Li, W. Jie, J. Zhang, Y. Liu, L. Zhang, F. Zhang, Y. Zhang, F. Wu, J. Li, M. Chu, Z. Wang, X. Shi, X. Liu, M. Wei, A. Huang, Y. Zhang, X. Liu, The Beijing Climate Center Climate System Model (BCC-CSM): the main progress from CMIP5 to CMIP6. *Geoscientific Model Development* **12**, 1573–1600 (2019).

170. X. Rong, J. Li, H. Chen, Y. Xin, J. Su, L. Hua, T. Zhou, Y. Qi, Z. Zhang, G. Zhang, J. Li, The CAMS Climate System Model and a Basic Evaluation of Its Climatology and Climate Variability Simulation. *J Meteorol Res* **32**, 839–861 (2018).

171. H. Zhang, M. Zhang, J. Jin, K. Fei, D. Ji, C. Wu, J. Zhu, J. He, Z. Chai, J. Xie, X. Dong, D. Zhang, X. Bi, H. Cao, H. Chen, K. Chen, X. Chen, X. Gao, H. Hao, J. Jiang, X. Kong, S. Li, Y. Li, P. Lin, Z. Lin, H. Liu, X. Liu, Y. Shi, M. Song, H. Wang, T. Wang, X. Wang, Z. Wang, Y. Wei, B. Wu, Z. Xie, Y. Xu, Y. Yu, L. Yuan, Q. Zeng, X. Zeng, S. Zhao, G. Zhou, J. Zhu, Description and Climate Simulation Performance of CAS-ESM Version 2. *Journal of Advances in Modeling Earth Systems* **12**, e2020MS002210 (2020).

172. G. Danabasoglu, J.-F. Lamarque, J. Bacmeister, D. A. Bailey, A. K. DuVivier, J. Edwards, L. K. Emmons, J. Fasullo, R. Garcia, A. Gettelman, C. Hannay, M. M. Holland, W. G. Large, P. H. Lauritzen, D. M. Lawrence, J. T. M. Lenaerts, K. Lindsay, W. H. Lipscomb, M. J. Mills, R. Neale, K. W. Oleson, B. Otto-Bliesner, A. S. Phillips, W. Sacks, S. Tilmes, L. van Kampenhout, M. Vertenstein, A. Bertini, J. Dennis, C. Deser, C. Fischer, B. Fox-Kemper, J. E. Kay, D. Kinnison, P. J. Kushner, V. E. Larson, M. C. Long, S. Mickelson, J. K. Moore, E. Nienhouse, L. Polvani, P. J. Rasch, W. G. Strand, The Community Earth System Model Version 2 (CESM2). *Journal of Advances in Modeling Earth Systems* **12**, e2019MS001916 (2020).

173. Y. Lin, X. Huang, Y. Liang, Y. Qin, S. Xu, W. Huang, F. Xu, L. Liu, Y. Wang, Y. Peng, L. Wang, W. Xue, H. Fu, G. J. Zhang, B. Wang, R. Li, C. Zhang, H. Lu, K. Yang, Y. Luo, Y. Bai, Z. Song, M. Wang, W. Zhao, F. Zhang, J. Xu, X. Zhao, C. Lu, Y. Chen, Y. Luo, Y. Hu, Q. Tang, D. Chen, G. Yang, P. Gong, Community Integrated Earth System Model (CIESM): Description and Evaluation. *Journal of Advances in Modeling Earth Systems* **12**, e2019MS002036 (2020).

174. A. Cherchi, P. G. Fogli, T. Lovato, D. Peano, D. Iovino, S. Gualdi, S. Masina, E. Scoccimarro, S. Materia, A. Bellucci, A. Navarra, Global Mean Climate and Main Patterns of Variability in the CMCC-CM2 Coupled Model. *Journal of Advances in Modeling Earth Systems* **11**, 185–209 (2019).

175. T. Lovato, D. Peano, M. Butenschön, S. Materia, D. Iovino, E. Scoccimarro, P. G. Fogli, A. Cherchi, A. Bellucci, S. Gualdi, S. Masina, A. Navarra, CMIP6 Simulations With the

CMCC Earth System Model (CMCC-ESM2). *Journal of Advances in Modeling Earth Systems* **14**, e2021MS002814 (2022).

176. A. Voldoire, D. Saint-Martin, S. Sénési, B. Decharme, A. Alias, M. Chevallier, J. Colin, J.-F. Guérémy, M. Michou, M.-P. Moine, P. Nabat, R. Roehrig, D. Salas y Mélia, R. Séférian, S. Valcke, I. Beau, S. Belamari, S. Berthet, C. Cassou, J. Cattiaux, J. Deshayes, H. Douville, C. Ethé, L. Franchistéguy, O. Geoffroy, C. Lévy, G. Madec, Y. Meurdesoif, R. Msadek, A. Ribes, E. Sanchez-Gomez, L. Terray, R. Waldman, Evaluation of CMIP6 DECK Experiments With CNRM-CM6-1. *Journal of Advances in Modeling Earth Systems* **11**, 2177–2213 (2019).

177. R. Séférian, P. Nabat, M. Michou, D. Saint-Martin, A. Voldoire, J. Colin, B. Decharme, C. Delire, S. Berthet, M. Chevallier, S. Sénési, L. Franchisteguy, J. Vial, M. Mallet, E. Joetzjer, O. Geoffroy, J.-F. Guérémy, M.-P. Moine, R. Msadek, A. Ribes, M. Rocher, R. Roehrig, D. Salas-y-Mélia, E. Sanchez, L. Terray, S. Valcke, R. Waldman, O. Aumont, L. Bopp, J. Deshayes, C. Éthé, G. Madec, Evaluation of CNRM Earth System Model, CNRM-ESM2-1: Role of Earth System Processes in Present-Day and Future Climate. *Journal of Advances in Modeling Earth Systems* **11**, 4182–4227 (2019).

178. N. C. Swart, J. N. S. Cole, V. V. Kharin, M. Lazare, J. F. Scinocca, N. P. Gillett, J. Anstey, V. Arora, J. R. Christian, S. Hanna, Y. Jiao, W. G. Lee, F. Majaess, O. A. Saenko, C. Seiler, C. Seinen, A. Shao, M. Sigmond, L. Solheim, K. von Salzen, D. Yang, B. Winter, The Canadian Earth System Model version 5 (CanESM5.0.3). *Geoscientific Model Development* **12**, 4823–4873 (2019).

179. M. Sigmond, J. Anstey, V. Arora, R. Digby, N. Gillett, V. Kharin, W. Merryfield, C. Reader, J. Scinocca, N. Swart, J. Virgin, C. Abraham, J. Cole, N. Lambert, W.-S. Lee, Y. Liang, E. Malinina, L. Rieger, K. von Salzen, C. Seiler, C. Seinen, A. Shao, R. Sospedra-Alfonso, L. Wang, D. Yang, Improvements in the Canadian Earth System Model (CanESM) through systematic model analysis: CanESM5.0 and CanESM5.1. *Geoscientific Model Development* **16**, 6553–6591 (2023).

180. J. R. Christian, K. L. Denman, H. Hayashida, A. M. Holdsworth, W. G. Lee, O. G. J. Riche, A. E. Shao, N. Steiner, N. C. Swart, Ocean biogeochemistry in the Canadian Earth System Model version 5.0.3: CanESM5 and CanESM5-CanOE. *Geoscientific Model Development* **15**, 4393–4424 (2022).

181. R. Döscher, M. Acosta, A. Alessandri, P. Anthoni, T. Arsouze, T. Bergman, R. Bernardello, S. Boussetta, L.-P. Caron, G. Carver, M. Castrillo, F. Catalano, I. Cvijanovic, P. Davini, E. Dekker, F. J. Doblas-Reyes, D. Docquier, P. Echevarria, U. Fladrich, R. Fuentes-Franco, M. Gröger, J. v. Hardenberg, J. Hieronymus, M. P. Karami, J.-P. Keskinen, T. Koenigk, R. Makkonen, F. Massonnet, M. Ménégoz, P. A. Miller, E. Moreno-Chamarro, L. Nieradzik, T. van Noije, P. Nolan, D. O'Donnell, P. Ollinaho, G. van den Oord, P. Ortega, O. T. Prims, A. Ramos, T. Reerink, C. Rousset, Y. Ruprich-Robert, P. Le Sager, T. Schmith, R. Schrödner, F. Serva, V. Sicardi, M. Sloth Madsen, B. Smith, T. Tian, E. Tourigny, P. Uotila, M. Vancoppenolle, S. Wang, D. Wårlind, U. Willén, K. Wyser, S. Yang, X. Yepes-Arbós, Q. Zhang, The EC-Earth3 Earth system model for the Coupled Model Intercomparison Project 6. *Geoscientific Model Development* **15**, 2973–3020 (2022).

182. B. He, Q. Bao, X. Wang, L. Zhou, X. Wu, Y. Liu, G. Wu, K. Chen, S. He, W. Hu, J. Li, J. Li, G. Nian, L. Wang, J. Yang, M. Zhang, X. Zhang, CAS FGOALS-f3-L Model Datasets

for CMIP6 Historical Atmospheric Model Intercomparison Project Simulation. *Adv. Atmos. Sci.* **36**, 771–778 (2019).

183. Y. Pu, H. Liu, R. Yan, H. Yang, K. Xia, Y. Li, L. Dong, L. Li, H. Wang, Y. Nie, M. Song, J. Xie, S. Zhao, K. Chen, B. Wang, J. Li, L. Zuo, CAS FGOALS-g3 Model Datasets for the CMIP6 Scenario Model Intercomparison Project (ScenarioMIP). *Adv. Atmos. Sci.* **37**, 1081–1092 (2020).

184. Y. Bao, Z. Song, F. Qiao, FIO-ESM Version 2.0: Model Description and Evaluation. *Journal of Geophysical Research: Oceans* **125**, e2019JC016036 (2020).

185. N. Scafetta, Impacts and risks of "realistic" global warming projections for the 21st century. *Geoscience Frontiers* **15**, 101774 (2024).

186. J. P. Dunne, L. W. Horowitz, A. J. Adcroft, P. Ginoux, I. M. Held, J. G. John, J. P. Krasting, S. Malyshev, V. Naik, F. Paulot, E. Shevliakova, C. A. Stock, N. Zadeh, V. Balaji, C. Blanton, K. A. Dunne, C. Dupuis, J. Durachta, R. Dussin, P. P. G. Gauthier, S. M. Griffies, H. Guo, R. W. Hallberg, M. Harrison, J. He, W. Hurlin, C. McHugh, R. Menzel, P. C. D. Milly, S. Nikonov, D. J. Paynter, J. Ploshay, A. Radhakrishnan, K. Rand, B. G. Reichl, T. Robinson, D. M. Schwarzkopf, L. T. Sentman, S. Underwood, H. Vahlenkamp, M. Winton, A. T. Wittenberg, B. Wyman, Y. Zeng, M. Zhao, The GFDL Earth System Model Version 4.1 (GFDL-ESM 4.1): Overall Coupled Model Description and Simulation Characteristics. *Journal of Advances in Modeling Earth Systems* **12**, e2019MS002015 (2020).

187. M. Kelley, G. A. Schmidt, L. S. Nazarenko, S. E. Bauer, R. Ruedy, G. L. Russell, A. S. Ackerman, I. Aleinov, M. Bauer, R. Bleck, V. Canuto, G. Cesana, Y. Cheng, T. L. Clune, B. I. Cook, C. A. Cruz, A. D. Del Genio, G. S. Elsaesser, G. Faluvegi, N. Y. Kiang, D. Kim, A. A. Lacis, A. Leboissetier, A. N. LeGrande, K. K. Lo, J. Marshall, E. E. Matthews, S. McDermid, K. Mezuman, R. L. Miller, L. T. Murray, V. Oinas, C. Orbe, C. P. García-Pando, J. P. Perlwitz, M. J. Puma, D. Rind, A. Romanou, D. T. Shindell, S. Sun, N. Tausnev, K. Tsigaridis, G. Tselioudis, E. Weng, J. Wu, M. Yao, GISS-E2.1: Configurations and Climatology. *J Adv Model Earth Syst* **12**, e2019MS002025 (2020).

188. C. Orbe, D. Rind, J. Jonas, L. Nazarenko, G. Faluvegi, L. T. Murray, D. T. Shindell, K. Tsigaridis, T. Zhou, M. Kelley, G. A. Schmidt, GISS Model E2.2: A Climate Model Optimized for the Middle Atmosphere—2. Validation of Large-Scale Transport and Evaluation of Climate Response. *Journal of Geophysical Research: Atmospheres* **125**, e2020JD033151 (2020).

189. M. B. Andrews, J. K. Ridley, R. A. Wood, T. Andrews, E. W. Blockley, B. Booth, E. Burke, A. J. Dittus, P. Florek, L. J. Gray, S. Haddad, S. C. Hardiman, L. Hermanson, D. Hodson, E. Hogan, G. S. Jones, J. R. Knight, T. Kuhlbrodt, S. Misios, M. S. Mizielinski, M. A. Ringer, J. Robson, R. T. Sutton, Historical Simulations With HadGEM3-GC3.1 for CMIP6. *Journal of Advances in Modeling Earth Systems* **12**, e2019MS001995 (2020).

190. P. Swapna, M. K. Roxy, K. Aparna, K. Kulkarni, A. G. Prajeesh, K. Ashok, R. Krishnan, S. Moorthi, A. Kumar, B. N. Goswami, The IITM Earth System Model: Transformation of a Seasonal Prediction Model to a Long-Term Climate Model. doi: 10.1175/BAMS-D-13-00276.1 (2015).

191. E. M. Volodin, E. V. Mortikov, S. V. Kostrykin, V. Y. Galin, V. N. Lykossov, A. S. Gritsun, N. A. Diansky, A. V. Gusev, N. G. Iakovlev, A. A. Shestakova, S. V. Emelina, Simulation

of the modern climate using the INM-CM48 climate model. *Russian Journal of Numerical Analysis and Mathematical Modelling* **33**, 367–374 (2018).

192. E. M. Volodin, E. V. Mortikov, S. V. Kostrykin, V. Ya. Galin, V. N. Lykossov, A. S. Gritsun, N. A. Diansky, A. V. Gusev, N. G. Iakovlev, Simulation of the present-day climate with the climate model INMCM5. *Clim Dyn* **49**, 3715–3734 (2017).

193. O. Boucher, J. Servonnat, A. L. Albright, O. Aumont, Y. Balkanski, V. Bastrikov, S. Bekki, R. Bonnet, S. Bony, L. Bopp, P. Braconnot, P. Brockmann, P. Cadule, A. Caubel, F. Cheruy, F. Codron, A. Cozic, D. Cugnet, F. D'Andrea, P. Davini, C. de Lavergne, S. Denvil, J. Deshayes, M. Devilliers, A. Ducharne, J.-L. Dufresne, E. Dupont, C. Éthé, L. Fairhead, L. Falletti, S. Flavoni, M.-A. Foujols, S. Gardoll, G. Gastineau, J. Ghattas, J.-Y. Grandpeix, B. Guenet, E. Guez Lionel, E. Guilyardi, M. Guimberteau, D. Hauglustaine, F. Hourdin, A. Idelkadi, S. Joussaume, M. Kageyama, M. Khodri, G. Krinner, N. Lebas, G. Levavasseur, C. Lévy, L. Li, F. Lott, T. Lurton, S. Luyssaert, G. Madec, J.-B. Madeleine, F. Maignan, M. Marchand, O. Marti, L. Mellul, Y. Meurdesoif, J. Mignot, I. Musat, C. Ottlé, P. Peylin, Y. Planton, J. Polcher, C. Rio, N. Rochetin, C. Rousset, P. Sepulchre, A. Sima, D. Swingedouw, R. Thiéblemont, A. K. Traore, M. Vancoppenolle, J. Vial, J. Vialard, N. Viovy, N. Vuichard, Presentation and Evaluation of the IPSL-CM6A-LR Climate Model. *Journal of Advances in Modeling Earth Systems* **12**, e2019MS002010 (2020).

194. J. Lee, J. Kim, M.-A. Sun, B.-H. Kim, H. Moon, H. M. Sung, J. Kim, Y.-H. Byun, Evaluation of the Korea Meteorological Administration Advanced Community Earth-System model (K-ACE). *Asia-Pacific J Atmos Sci* **56**, 381–395 (2020).

195. G. Pak, Y. Noh, M.-I. Lee, S.-W. Yeh, D. Kim, S.-Y. Kim, J.-L. Lee, H. J. Lee, S.-H. Hyun, K.-Y. Lee, J.-H. Lee, Y.-G. Park, H. Jin, H. Park, Y. H. Kim, Korea Institute of Ocean Science and Technology Earth System Model and Its Simulation Characteristics. *Ocean Sci. J.* **56**, 18–45 (2021).

196. R. Stouffer, U of Arizona MCM-UA-1-0 model output prepared for CMIP6 CMIP, Earth System Grid Federation (2019); https://doi.org/10.22033/ESGF/CMIP6.2421.

197. M. Kawamiya, T. Hajima, K. Tachiiri, S. Watanabe, T. Yokohata, Two decades of Earth system modeling with an emphasis on Model for Interdisciplinary Research on Climate (MIROC). *Prog Earth Planet Sci* **7**, 64 (2020).

198. H. Tatebe, T. Ogura, T. Nitta, Y. Komuro, K. Ogochi, T. Takemura, K. Sudo, M. Sekiguchi, M. Abe, F. Saito, M. Chikira, S. Watanabe, M. Mori, N. Hirota, Y. Kawatani, T. Mochizuki, K. Yoshimura, K. Takata, R. O'ishi, D. Yamazaki, T. Suzuki, M. Kurogi, T. Kataoka, M. Watanabe, M. Kimoto, Description and basic evaluation of simulated mean state, internal variability, and climate sensitivity in MIROC6. *Geoscientific Model Development* **12**, 2727–2765 (2019).

199. T. Mauritsen, J. Bader, T. Becker, J. Behrens, M. Bittner, R. Brokopf, V. Brovkin, M. Claussen, T. Crueger, M. Esch, I. Fast, S. Fiedler, D. Fläschner, V. Gayler, M. Giorgetta, D. S. Goll, H. Haak, S. Hagemann, C. Hedemann, C. Hohenegger, T. Ilyina, T. Jahns, D. Jimenéz-de-la-Cuesta, J. Jungclaus, T. Kleinen, S. Kloster, D. Kracher, S. Kinne, D. Kleberg, G. Lasslop, L. Kornblueh, J. Marotzke, D. Matei, K. Meraner, U. Mikolajewicz, K. Modali, B. Möbis, W. A. Müller, J. E. M. S. Nabel, C. C. W. Nam, D. Notz, S.-S. Nyawira, H. Paulsen, K. Peters, R. Pincus, H. Pohlmann, J. Pongratz, M. Popp, T. J.

Raddatz, S. Rast, R. Redler, C. H. Reick, T. Rohrschneider, V. Schemann, H. Schmidt, R. Schnur, U. Schulzweida, K. D. Six, L. Stein, I. Stemmler, B. Stevens, J.-S. von Storch, F. Tian, A. Voigt, P. Vrese, K.-H. Wieners, S. Wilkenskjeld, A. Winkler, E. Roeckner, Developments in the MPI-M Earth System Model version 1.2 (MPI-ESM1.2) and Its Response to Increasing CO2. *Journal of Advances in Modeling Earth Systems* **11**, 998–1038 (2019).

200. S. Yukimoto, H. Kawai, T. Koshiro, N. Oshima, K. Yoshida, S. Urakawa, H. Tsujino, M. Deushi, T. Tanaka, M. Hosaka, S. Yabu, H. Yoshimura, E. Shindo, R. Mizuta, A. Obata, Y. Adachi, M. Ishii, The Meteorological Research Institute Earth System Model Version 2.0, MRI-ESM2.0: Description and Basic Evaluation of the Physical Component. *Journal of the Meteorological Society of Japan. Ser. II* **97**, 931–965 (2019).

201. J. Cao, L. Ma, F. Liu, J. Chai, H. Zhao, Q. He, B. Wang, Y. Bao, J. Li, Y. Yang, H. Deng, B. Wang, NUIST ESM v3 Data Submission to CMIP6. *Adv. Atmos. Sci.* **38**, 268–284 (2021).

202. Ø. Seland, M. Bentsen, D. Olivié, T. Toniazzo, A. Gjermundsen, L. S. Graff, J. B. Debernard, A. K. Gupta, Y.-C. He, A. Kirkevåg, J. Schwinger, J. Tjiputra, K. S. Aas, I. Bethke, Y. Fan, J. Griesfeller, A. Grini, C. Guo, M. Ilicak, I. H. H. Karset, O. Landgren, J. Liakka, K. O. Moseid, A. Nummelin, C. Spensberger, H. Tang, Z. Zhang, C. Heinze, T. Iversen, M. Schulz, Overview of the Norwegian Earth System Model (NorESM2) and key climate response of CMIP6 DECK, historical, and scenario simulations. *Geoscientific Model Development* **13**, 6165–6200 (2020).

203. W.-L. Lee, Y.-C. Wang, C.-J. Shiu, I. -chun Tsai, C.-Y. Tu, Y.-Y. Lan, J.-P. Chen, H.-L. Pan, H.-H. Hsu, Taiwan Earth System Model Version 1: description and evaluation of mean state. *Geoscientific Model Development* **13**, 3887–3904 (2020).

204. A. A. Sellar, C. G. Jones, J. P. Mulcahy, Y. Tang, A. Yool, A. Wiltshire, F. M. O'Connor, M. Stringer, R. Hill, J. Palmieri, S. Woodward, L. de Mora, T. Kuhlbrodt, S. T. Rumbold, D. I. Kelley, R. Ellis, C. E. Johnson, J. Walton, N. L. Abraham, M. B. Andrews, T. Andrews, A. T. Archibald, S. Berthou, E. Burke, E. Blockley, K. Carslaw, M. Dalvi, J. Edwards, G. A. Folberth, N. Gedney, P. T. Griffiths, A. B. Harper, M. A. Hendry, A. J. Hewitt, B. Johnson, A. Jones, C. D. Jones, J. Keeble, S. Liddicoat, O. Morgenstern, R. J. Parker, V. Predoi, E. Robertson, A. Siahaan, R. S. Smith, R. Swaminathan, M. T. Woodhouse, G. Zeng, M. Zerroukat, UKESM1: Description and Evaluation of the U.K. Earth System Model. *Journal of Advances in Modeling Earth Systems* **11**, 4513–4558 (2019).

Acknowledgments:

Generative AI tools (ChatGPT and Claude) were used for some coding tasks related to this study, and to search for peer-reviewed and grey literature. No AI tools were used to write or edit the manuscript.

Funding:

Natural Sciences and Engineering Research Council, Alexander Graham Bell Doctoral Scholarship (SWR)

Natural Sciences and Engineering Research Council, Discovery Grant (TG)

Author contributions:

Conceptualization: SWR, TG, MEU, JWM, TH

Methodology: SWR, TG

Investigation: SWR, TG

Visualization: SWR

Funding acquisition: SWR, TG

Project administration: SWR, TG

Supervision: TG

Writing – original draft: SWR

Writing – review & editing: SWR, TG, JWM, MEU, MS, SJP, TH

Competing interests: The authors declare that they have no competing interests.

Data, code, and materials availability: The historical and projected streamflow data, fitted regression models, salmon run timing data, gauge and catchment metadata, and summary PDF files for each catchment are available at https:/doi.org/10.20383/103.01675. The code required to reproduce the analyses in this paper is available at https://doi.org/10.5281/zenodo.20135654. All original data are available from their respective providers.

Supplementary Materials

Materials and Methods

Supplementary Text

Figs. S1 to S28

Tables S1 to S4

References (*101-204*)

Interactive map S1

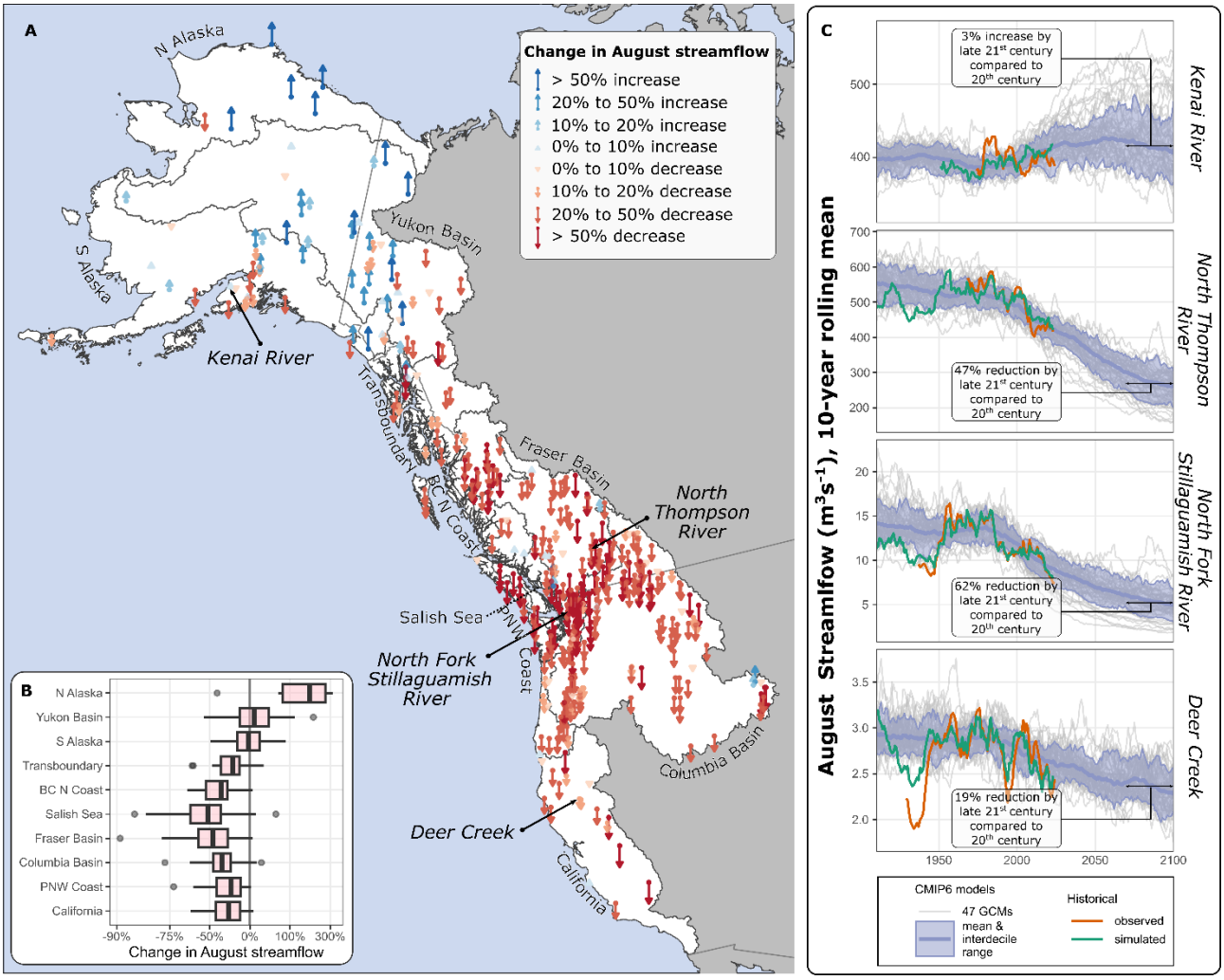

Fig. 1. Projected changes to August streamflow. (A) Changes in August streamflow by the end of the century (median of 2070-2099 compared to the median for 1901-2000) under moderate emissions (SSP 2-4.5). **(B)** Boxplots of data in A summarized across streams within each of the 10 regions. **(C)** Observed, simulated, and projected streamflow for the sentinel rivers. The CMIP6 projections are for the moderate emissions scenario (SSP 2-4.5, corresponding to an average global temperature rise of 3ºC).

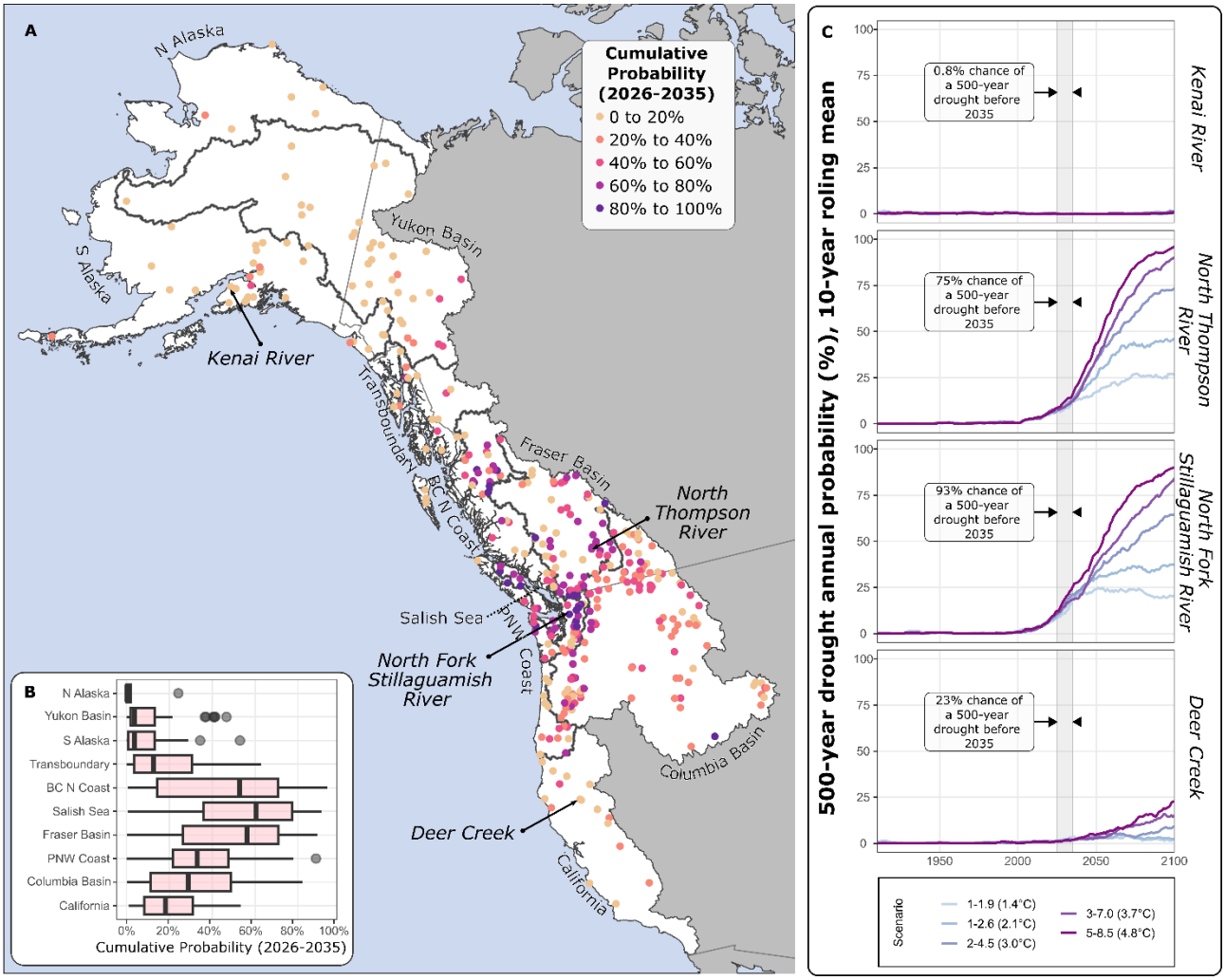

Fig. 2. Probability of 500-year August droughts. **(A)** Cumulative probability of 500-year droughts occurring between 2026-2035. Note that the baseline probability under a stationary climate would be ~2%. **(B)** Boxplots of data in A summarized across streams in each region. **(C)** Annual probability of a 500-year August drought for the sentinel rivers. The inset text refers to the medium emissions scenario but results are similar across scenarios.

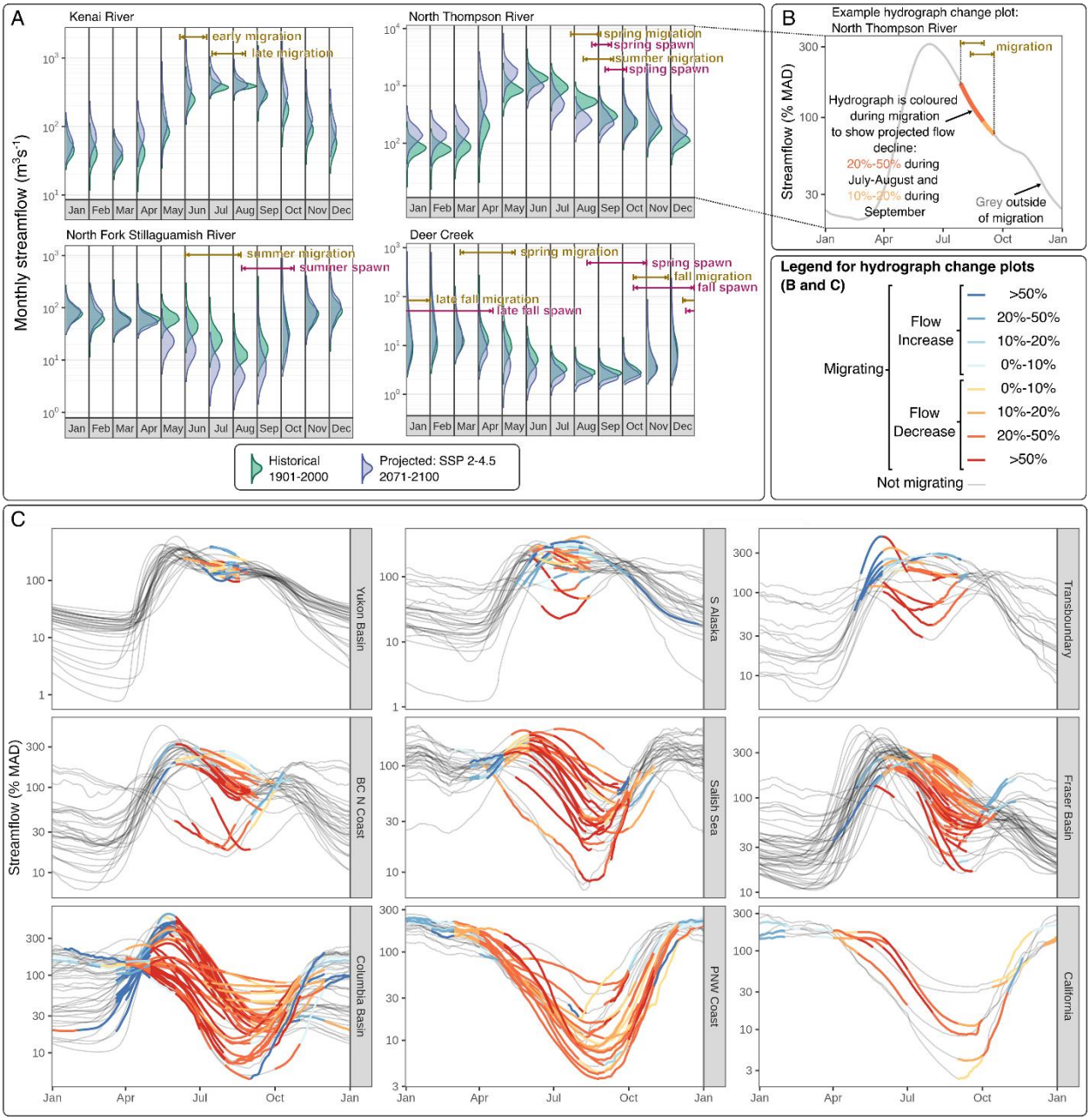

Fig. 3. Predicted changes to monthly flows during Chinook salmon migration. (A) Historical and future interannual distribution of monthly flows, in addition to Chinook salmon migration and spawning timing for the four sentinel rivers. **(B)** 'Hydrograph change plot' for the North Fork Stillaguamish River with the historical smoothed average annual hydrograph, coloured to show projected changes during Chinook salmon migration. **(C)** Hydrograph change plots for the 258 gauge locations accessible to Chinook salmon, grouped by region.

Science
AAAS

Supplementary Materials for

Drying summers threaten western North American river ecosystems and a keystone migratory fish

Sacha W. Ruzzante, Tom Gleeson, Jonathan W. Moore, Marta E. Ulaski, Todd Hatfield, Markus Schnorbus, Stephanie Peacock
Corresponding author: sruzzante@uvic.ca

The PDF file includes:

Other Supplementary Materials for this manuscript include the following:

Interactive map S1

Materials and Methods

Statistical Hydrologic Models

We develop regression-based models of monthly flows for each catchment, similar to those developed in earlier work to simulate historical changes in summer minimum flows (*26*) but including process-based glacier runoff predictions. Diagrams showing the data flow for glacier runoff model and the regression model fitting and use for projection are provides in Figures S1 and S2.

We use as the predictand the logarithm of non-glacial streamflow:

$$\log\left(Q - Q_{glacier\,melt} + \xi\right) = a * T_1 + b * T_2 + \cdots + \alpha * P_1 + \beta * P_2 + \cdots \varepsilon$$

Q is the observed monthly streamflow, $Q_{glacier\,melt}$ is the estimated glacier runoff (section M2). For some catchments, the difference $Q - Q_{glacier\,melt}$ is negative for some years and months. In these catchments we add ξ, a small value to ensure that the argument of the logarithm is positive. ξ is chosen to make the minimum value of the argument of the logarithm 0.05 mm/d.

The predictors T_1, T_2 ... and P_1, P_2 ... are the catchment-average air temperature and precipitation over various rolling windows. We use as candidates 1, 2, 3, 4, 6, 8, and 12 month rolling windows, up to and including the month that is being predicted. We select the most appropriate predictors for each catchment and each month using all-subsets regression, limited to a maximum of 6 predictor variables for computational efficiency, and including at least one precipitation variable. This results in 6349 candidate regression models.

For each fold, we hold out one fifth of the training data as a validation data set, train all candidate regression models on the remaining data, and evaluate the Kling-Gupta Efficiency (*101*) of the square-root transformed flow on the held-out validation data. We repeat the 5-fold cross-validation ten times and select the candidate regression model with the best average performance across all 50 folds.

Process-based glacier runoff model

188 of the catchments analyzed here have some glacier cover, from a combined 18,428 glaciers from the Randoph Glacier Inventory (*102*). To calculate $Q_{glacier\,melt}$ we use a temperature-index model combined with modeled glacier areas:

$$Q_{glacier\,melt} = A \times PDD \times m_f$$

A is the glacier area, PDD is the positive degree days, and m_f is the melt factor. This model is show schematically in Fig. S1.

The glacier melt is calculated for each glacier, and then the total glacier runoff contribution to streamflow is calculated by summing the glacier melt from all glaciers within each watershed. For glaciers that lie partially outside of a watershed, the contribution is scaled by the fraction of the glacier area that is within the watershed.

Calculation of PDD

PDD is calculated from gridded air temperature data. It is defined as the cumulative temperature above the melting point of 0°C over a given period (*103*). To calculate the PDD from monthly temperature, distributional assumptions must be made about the sub-monthly temperature variation. While a Gaussian distribution with a fixed standard deviation is often assumed, near a temperature of 0°C the diurnal range (and hence the standard deviation) is usually suppressed, particularly on glaciers and ice sheets, because of the latent heat of melting

and freezing (*103*). However, no globally-applicable formula for standard deviation as a function of monthly temperature has been developed.

We approximate this relationship using gridded daily temperature. For 500 randomly selected latitude/longitude points within the glaciers studied here, we extract daily maximum and minimum temperature from 1991 to 2020. We then reconstruct hourly temperatures using the chillR package (*104*) and calculate the mean monthly temperature and monthly standard deviation. We fit a locally estimated scatterplot smoothing (LOESS) function and call this function $sd(\mu)$.

We then extract the mean monthly temperature for each glacier and adjust the temperature using a temperature lapse rate of 6.5°C/km and the glacier hypsometry in 50-m elevation bands. For each elevation band we calculate the PDD assuming a Gaussian distribution with a standard deviation defined by the function $sd(\mu)$. Glacier hypsometry is not dynamically updated as glaciers recede.

Calculation of m_f

For each of the 18,428 glaciers we calibrate a melt factor m_f using the Open Global Glacier Model (*105*), 2-km gridded temperature and precipitation data, and geodetic mass balance observations from January 2000 – January 2020 (*106*). We set the precipitation factor to 1, the temperature bias to 0, and the melting temperature to 0ºC. We limit the melt factor to the range 0.5-17 kg m^{-2} day^{-1} K^{-1}. Dynamic changes in the melt factor are not considered.

Quantile Mapping

We quantile map climate model projections of monthly 2-m air temperature and precipitation using as a reference observation-based gridded monthly climate data from 1950-2014. For catchment-average temperature and precipitation, we use the Multivariate Bias Correction algorithm (MBCn) (*107*). For air temperature on glaciers, we use the computationally more efficient Quantile Delta Mapping (QDM) (*108*). In all cases, we apply the bias correction using 30-year and 3-month sliding windows, replacing the central 10 years and the central month (*109*). For example, the projected data for July from 2050-2059 are bias corrected using (i) historical observed data from June-August, 1950-2014, (ii) historical simulated data from 1950-2014, June-August, and (iii) future projected data from 2040-2069, June-August.

To avoid artificially suppressing the internal climatic variability, we bias-correct each ensemble member with a different variant from the same climate model where possible (*110*). This was not possible for seven of the 47 CMIP6 models, which had only one ensemble variant available for download.

Ensemble Averaging and Weighting

There is a recognized bias towards 'hot' models in the CMIP6 ensemble: the distribution of Equilibrium Climate Sensitivity (ECS) of the models does not match the assessed distribution of ECS from multiple lines of evidence (*111*, *112*). This means a simple average of all CMIP6 models will overestimate the warming associated with a particular Shared Socioeconomic Pathway (SSP). Following Cannon (*113*), to calculate ensemble mean (median) projections we first average all variants within each model and then take the weighted mean (median) of all models, with weights chosen such that the weighted distribution of model ECS matches the assessed ECS distribution (*112*).

Model performance comparison

We evaluate the performance of these models using two performance metrics commonly used to assess low-flow performance: the Nash-Sutcliffe Efficiency of log-transformed flows: NSE(log(Q)), and the Kling-Gupta Efficiency of inverse-transformed flows: KGE(1/Q) (*114*, *115*). We calculate these performance metrics for the full time series of monthly flows and also individually for August, in order to evaluate the ability of the models to simulate interannual variability distinctly from the seasonality of each catchment (*116*).

We compare the performance of our models to 17 published models that contain simulations for some of the same catchments. These models are listed in Table S1. The daily streamflow simulations from each model were summarized to mean monthly values before calculating performance metrics.

Unless otherwise specified, we evaluate all models on a common evaluation period of October 1989-September 1999 because this evaluation period was used for many of the comparison models. For the purpose of performance evaluation and comparison, we retrained all of our models excluding these years. Eight of the comparison models also held out these years of data for evaluation or did not use them for calibration. Two models were trained to predict streamflow in ungauged basins, and we used the 'test' data for these models. The other models were tested on data seen in calibration or a mix of data seen and not seen during calibration.

For the North America-wide FUSE simulations performed by Thébault (*117*), 78 model configurations are provided. For each catchment and evaluation metric, we choose the model that maximizes performance in the calibration period.

For the CONUS-wide FUSE simulations performed by Thébault (*118*) we choose the low-flow optimized simulations (optimized with KGE(1/Q)). Again, 78 model configurations are provided, and again for each catchment and evaluation metric we choose the model that maximizes performance in the calibration period. These FUSE simulations were calibrated to the period 1989-1998, and evaluated on the period 1999-2009, so we retrained our regression models excluding the years 1999-2009 to enable a like-for-like comparison.

The two FUSE simulations performed by Thébault (*117*, *118*) are at a slight comparative advantage over the regression models, because the model structure is chosen to maximize each evaluation metric, whereas the regression model structure is chosen to maximize the $\mathrm{KGE}\left(\sqrt{\mathrm{Q}}\right)$ for each month.

Hamlet et al. (*28*) recommend bias-correcting their streamflow predictions to match observations. For this model, we bias correct the simulations for the test period (October 1989-September 1999) using Quantile Delta Mapping (*108*, *119*), using all other years of data as the calibration period.

Peak Water

We evaluate when each watershed has reached or will reach 'peak water' (*15*) using the time series of August glacier runoff. We use the multi-model weighted mean runoff for each, and smooth it with a 5-year moving average. We then find the year of maximum runoff for the time series from 2000-2100, for SSP 2-4.5. We evaluate whether peak water has already occurred ($\leq$2025) or will occur sometime in the future.

Agricultural water demand

We calculate Hargreave's climatic moisture deficit (CMD) on a monthly basis using downscaled and bias-corrected climate normal data for North America at 1 km resolution (*120*).

CMD is a proxy for agricultural water demand and is the difference between potential evapotranspiration and precipitation. We use the same formulas that were used to calculate CMD on an annual basis (*121*). We calculated this variable on the same 1 km grid for the normal period of 1991-2020 and for the end of century (2071-2100) under SSP 2-4.5. For each of the 10 regions, we then summed the total CMD over all cropped land, as defined in the North American Land Cover dataset (*122*). We then calculate the change in CMD between the end-of-century and the normal period.

500-year Drought Analysis

We estimate return levels for August streamflow for return periods of 100 and 500 years using the UNSEEN methodology (*123*). The 100 and 500-year levels are estimated as the August flows that are exceeded in 99% and 99.8% of years across all of the historical simulations from 1901 to 2000 combined (a total of 61,600 simulated years). The exceedance of these levels is then evaluated for the projection period (2015 onwards). For each year *i*, we calculate the probability p_i as number of ensemble members with flows below the return level. To calculate the cumulative probability p_{cum} over a period of 10 years (2026-2035) we calculate:

$$p_{cum} = 1 - \prod_{i=2026}^{2035} (1 - p_i)$$

An important assumption in this analysis is that the elements of the variable (August streamflow) are independent and identically distributed (i.i.d.). This assumption may not be met for these data for at least two reasons. First, the simulations originating from different climate models may not be identically distributed (although the bias correction ensures the distributions are similar). Second, the simulations for consecutive years from the same simulation may not be independent. We therefore consider two other approaches for estimating the return levels and the probabilities.

First, to evaluate whether different distributions originating from different climate models affect the estimated probabilities, we calculate the return levels separately for each climate model. For this analysis we select only the 18 models that have at least 10 variants available for the historical period (*i.e.* 1000 years of data). We then compare the projection from each model to its respective return level before averaging across models.

Second, we used a block minima approach to evaluate whether dependence between consecutive years affects the estimated probabilities. We calculated the minimum August streamflow for each decade and ensemble member in the historical simulations calculated the 500-year return period as the flow that is exceed in 98% of decadal minima. Then we calculated the 10-year cumulative probability as the number of ensemble members with a minimum August flow below this level over the period 2026-2035.

We also compare the return levels estimated using the UNSEEN methodology to those estimated by fitting a generalized extreme value (GEV) function to (a) the historical observed streamflow data and (b) the historical simulations based on observed climate data. Due to large uncertainties in the observed climate data prior to 1950 we use the period 1951-2000 for this analysis.

Environmental flows thresholds

We evaluate transgressions of environmental flows using three methods: Richter's presumptive standard (*66*), the planetary boundaries framework (*124*), and the Tennant method (*67*).

Presumptive Standard

The presumptive standard was intended to provide conservative limits on human alterations to streamflow conditions, and is based on deviations from historical mean flows for each day of the year. The standard states that alterations beyond 20% are likely to result in "moderate or major changes to major changes in natural structure and ecosystem functions" (*66*). The standard has also been applied to monthly flows (*125*), as we do here. For each catchment, ensemble member, and scenario, we evaluate the number of months during which the projected change in streamflow between the end-of-century (2070-2099) and the 20th century (1901-2000) is greater than 20%. For each catchment, we first average across all variants within each climate model and then take the weighted average across all models.

Planetary Boundaries Framework

The planetary boundary for freshwater is defined using the 5th and 95th percentiles of historical streamflow (*124*)**.** We emulate this approach here. For each catchment, month, climate model, ensemble member, and scenario, we calculate the 5th and 95th streamflow percentiles of the historical period (1901-2000). We define a 'deviation' when the 10-year rolling mean flow for a month is lower than the 5th or higher than the 95th percentile of historical flows for that month. We consider the boundary to have been permanently transgressed if a deviation occurs by 2090 and the rolling mean does not return to within the 5th-95th percentile range by the end of the century. We evaluate the number of months with permanent transgressions and then take the mean across all realizations for each climate model and then the weighted mean across all climate models.

Tennant method

The Tennant method is widely applied across North America. It stipulates that a minimum flow of 10% of the long-term mean annual discharge (LTMAD) must be maintained to "sustain short-term survival habitat for most aquatic life forms" (*67*). We first calculate the LTMAD based on the simulations for 1901-2000, using observed climate data. For each catchment, ensemble member, scenario, and year, we identify transgressions when the minimum summer (June – September) flow is less than 10% LTMAD. We then calculate the fraction of years with transgressions for the historical (1901-2000) and future (2070-2099) periods. We average the number of transgressions first across all variants within each climate model and then take the weighted average across all models.

Water Temperature Projections

As an illustration of the value of stream-specific hydrologic projections, we also use the streamflow projections to predict changes in stream temperature. We use a simple model based on empirical streamflow sensitivities to air temperature and streamflow, similar to previous studies (*126*, *127*):

$$W = \alpha\, T + \beta \log(Q) + \epsilon$$

Where W is the water temperature, T is the air temperature, Q is streamflow, ϵ is an error term, and α and β are coefficients fit by multiple linear regression. We fit this regression model

to historical water temperature data from the two hottest months of the year (usually July and August). We then project water temperature using the projected air temperature and streamflow.

We compare our projected water temperature increases to projections of water temperature in British Columbia (*85*) and western United States (*127*). We calculated the historical and projected averages to match the time periods used in those studies: for British Columbia the historical period is 1981-2000 and the future period is 2081-2100, and for western United State the historical period is 1993-2011 and the future period is 2080-2089. For British Columbia we compare our projections for SSP 2-4.5 to projections for RCP 4.5. For western United States, results are reported for CMIP3 scenario A1B, which represents approximately 6 W/m^2 of additional radiative forcing by 2100. We therefore compare these projections to the average of our projections for SSP 2-4.5 and SSP 3-7.0, which represent additional forcings of 4.5 W/m^2 and 7.0 W/m^2, respectively.

Streamflow data

We use data from the United States Geological Survey (USGS) and the Water Survey of Canada (WSC) downloaded between December 2024 and July 2025. We filtered stations based on the following criteria:

- Within the habitat range of Pacific Salmon, *ie.,* Pacific drainages from California to Alaska. We also include northern Alaska as salmon may be driven northward as temperatures warm and all five species of Pacific salmon have recently been observed to spawn in Arctic rivers (*94*, *128*).
- At least 20 years of data from May to September, with no missing days.
- At least one full year of year-round streamflow observations, with no missing days
- A time series not ending prior to 2000.

We include only near-natural streams. In Canada, we included only basins in the 2020 version of the Reference Hydrometric Basin Network, or those that appeared in the 1999 version but were dropped because monitoring was discontinued (*129*). In the United States, we included basins from the GAGES-II dataset (*130*).

In Alaska there are relatively few basins considered to be of 'reference quality' by GAGES-II. However, GAGES-II was published in 2011, so we examined 33 gauged basins that were not evaluated in GAGES-II (neither determined to be reference quality nor non-reference quality). These basins were mostly established recently and did not have a long enough time series in 2011 to warrant evaluation. We evaluated whether these basins are near-natural using similar methods to GAGES-II: (i) we examined annual Water Data Reports (available at https://rconnect.usgs.gov/water-year-summary/) for evidence of regulation or anthropogenic land/water use) and (ii) we visualized basin polygons in QGIS (*131*) along with global mining area polygons (*132*), dam locations (*133*), OpenStreetMap, and ESRI topo. We determined 21 of these basins to be of reference quality, or 'near-natural'. These screening results are shown in Table S2.

Lastly, we removed some stations that have high levels of water use. In British Columbia we relied on water use estimates prepared by (*26*). In the contiguous United States we relied on water use estimates from (*130*). In Yukon and Alaska we assumed water use to be negligible relative to streamflow. We removed basins where the mean annual water use (m^3s^{-1}) was greater than 10% of the minimum observed flow from June to September in any individual year.

Historical climate data

We use historical gridded monthly temperature and precipitation data from 1900 to 2023 (*134*). These data are provided at 2 km spatial resolution and are interpolated from weather station data using the ANUSPLIN algorithm. We calculated the monthly mean temperature as the average of monthly mean daily maximum and minimum temperatures.

In previous work we found that this dataset outperformed other available datasets in terms of temporal consistency (*26*). However, data quality is poorer prior to 1950, when significantly fewer weather stations were operational. Data quality is also poorer in the far north and in remote coastal watersheds, where the weather station network is sparser.

Water Temperature Data

We compiled stream water temperature data from the Water Survey of Canada and the United State Geological Survey. Where data was hourly we first summarized it to the daily scale, discarding any days with more than 4 hours of data missing. We then summarized it to the monthly scale, discarding months with more than 6 days missing. Lastly, we discarded gauges with fewer than 20 valid monthly water temperature measurements from July and August.

Climate projection data

We use all models from the Sixth-generation Coupled Model Intercomparison Project (CMIP6) that were available for download as of May 2025. We required that each model report monthly precipitation and mean temperature, and report results for the historical experiment and the three primary scenarios (SSP 1-2.6, 'Sustainability', SSP 2-4.5, 'Middle of the Road', and SSP 5-8.5 'Fossil-fueled Development'). We also included scenarios SSP 1-1.9 (consistent with the Paris Climate Agreement warming goal of 1.5ºC above pre-industrial conditions) and SSP 3-7.0 ('Regional Rivalry').

In total 379 model runs across 47 models satisfied our criteria. An additional 289 model runs, across 29 of the models, were available for the historical experiment only. These were added for the purpose of calculating historical return levels in the UNSEEN methodology (500-year drought analysis). These models are listed in Table S2 along with their equilibrium climate sensitivity.

Historical glacier extent data

There are 18,428 glaciers within the basins studied here, based on the global compilation of glacier polygons from the Randolph Glacier Inventory (RGI) V6 (*102*). The RGI provides the glacier area for a reference year, which is usually close to the year 2000. However, for our analysis we need time series of annual glacier area for the historical and future periods. There is considerable uncertainty about historical glacier states, especially for regions like western North America where historical glaciological observations are sparse, and model-based reconstructions of glacier states are subject to large uncertainties (*135*).

Malles and Marzeion (*136*) developed gridded model-based reconstructions of glacier mass and area from 1901 to 2018, based on ten climate datasets. We used the reconstruction based on CRU TS 4.03 (*137*) which was found to perform best over the full time period (*136*). We extracted a time series of relative area for each glacier within our study basins from the Randolph Glacier Inventory (RGI) V6 (*102*). This time series was then scaled to match the glacier area for the reference year in the RGI. We extended the time series from for the years 2019 to 2023 using a linear extrapolation of the recession rate for 2015 to 2018. The data have large uncertainties,

especially for the first half of the 20th century, for which glaciological observations are largely unavailable to constrain the estimates.

We evaluated the suitability of two other historical glacier extent databases for this study. Bevington and Menounos (*138*) developed time series of glacier extents from 1984 to 2020 from satellite imagery. However, this dataset covers western Canada and a limited temporal range, and we found the time series contained unrealistic annual advances and retreats, possibly due to misidentification of snow cover on land or debris cover on glaciers, or due to cloud cover in the satellite imagery for some year. These annual fluctuations would lead to unrealistic predictions of glacier runoff, which would introduce errors into the regression models.

Dussaillant et al. (*139*) used geostatistical modelling to estimate annual mass changes for every glacier on earth from satellite and airborne altimetry data as well as in-situ glaciological observations. In western North America this time series begins in 1946 and extends to 2024. We tried adding these annual mass changes to the estimated glacier mass at the reference year for each glacier (*140*) to develop a time series of glacier mass. However, for parts of the range where glaciers advanced from the 1950s to the 1980s, this strategy led to negative mass at the beginning of the time series for many (mostly small) glaciers. In other places this method led to negative mass in recent years, even for glaciers that are still visible on satellite imagery. This indicates that either the reference year mass (*1*) is underestimated or the rate of change (*139*) is overestimated. We concluded that these data were not suitable for our analysis.

Projected glacier extent data

For the future period we rely on the projections developed by Rounce *et al.* (*141*), which provide glacier area from 2000 to 2100 using 10 CMIP6 models under four emissions scenarios. The projections are provided for each glacier. To improve consistency between the historical and future glacier extent data, we also scale the projections such that the glacier area at the reference year matches the reference area in the RGI.

Chinook life history timing data

We collected Chinook upstream migration and spawning timing data for each gauge location. These data were sourced from academic publications, grey literature, publicly available datasets, and in a few cases sport fishing reports.

In British Columbia and Yukon, we relied mostly on the NuSEDS database (*44*), which provides start and end dates of stream arrival and spawning for each year in which counts or surveys were taken. We defined the migration period as beginning on the the mean start date of stream arrival (STREAM_ARRIVAL_DT_FROM) and ending on the mean peak spawn date (PEAK_SPAWN_DT_FROM). We defined the spawning period as beginning on the mean start date of spawning (START_SPAWN_DT_FROM) and ending on the mean end date of spawning (END_SPAWN_DT_FROM). We also relied on (*142*) where stream-specific migration or timing data were unavailable from NuSEDS.

In Alaska and parts of Yukon, daily fish count data are available from (*43*, *143*). For each year of data, we found the date on which 2.5% and 97.5% of fish had passed, and then calculated the median of all years. Spawning timing data were generally not available for Alaskan streams.

In CONUS, we mostly relied on Chinook life stage timing tables compiled by various publications (*144–146*). However, in Deer Creek and Mill Creek (California), fish count data were available (*68*), and we used the same strategy as for Alaskan streams.

All life stage timing data and references are available in supplementary data 1, as well as in the catchment summary sheets linked in the interactive supplementary material: https://sruzzante.shinyapps.io/streamflow_projections/.

Delineation of ten salmon-producing regions

We defined ten salmon-producing regions based on natural hydrologic divides, management regions used by various jurisdictions within the range, similarity in hydrology and life history traits, and a previous effort to define 'Salmon Ecoregions' (*42*). We desired about ten regions, each with at least 5 stream gauging stations. The regions are shown in Fig. 9, and are defined as follows:

California: Pacific-draining basins in California, south of and including the Smith River.

PNW Coast: Outer coastal drainages in Washington, Oregon and Vancouver Island: on the mainland north of the Smith River, and south of and including the Quillayute River, and on Vancouver Island from the Gordon River clockwise to the Nimpkish River (not including those rivers).

Columbia Basin: All streams that drain through the Columbia mainstem at Skamokawa.

Fraser Basin: All streams that drain through the Fraser River bifurcation into the South and North arms at New Westminster.

Salish Sea: Pacific drainages on the mainland from north of the Quillayute River on the Olympic peninsula (Washington) to the Southgate River (British Columbia), excluding the Fraser River, and streams on Vancouver Island from the Nimpkish River clockwise to the Gordon River (inclusive).

BC North Coast: mainland pacific drainages north of the Southgate River (non-inclusive) to the Nass River (inclusive), as well as Haida Gwaii.

Transboundary region: Pacific drainages from the Nass River (non-inclusive) to Sea Otter Creek (inclusive).

S Alaska: Coastal drainages from north of Sea Otter Creek to the Yukon River.

Yukon River: All streams that drain through the Yukon River mainstem at Pilot Station.

N Alaska: All Pacific and Arctic drainages north of the Yukon River, up to but excluding the Mackenzie River.

Supplementary Text

Models outperform all previous models

Figures S3-S6 show empirical cumulative distributions of performance metrics for the regression models developed in this study and for fifteen other published hydrologic models. Distributions further to the right indicate better performance. Based NSE(log(Q)) (Fig S3) the regression models outperform all models except the long short-term memory model (LSTM) developed by Kratzert et al., (*62*). Based on the KGE(1/Q) (Fig S5), the regression model outperforms all comparison models.

The regression models are also better than all other models at predicting interannual variability in August flows, which is a main objective of this paper. The performance improvement is substantial, whether evaluated using the NSE(log(Q)) (Figure S4) or the KGE(1/Q) (Figure S6). These performance improvements in both simulating year-round flows and in simulating interannual variability in late-summer flows specifically indicate that the models presented here may result in more robust estimates of responses to climate change.

The only model that rivals the regression models in performance is the LSTM developed by Kratzert et al. (*62*). However, LSTMs have known issues in extrapolating to unseen climate conditions that are not easily overcome (*147–149*). In contrast, the regression models used here have simple but physically realistic and stable extrapolation behavior (*26*) and incorporate a process-based glacier model.

Robustness of 500-year drought probabilities

We compare the 500-year drought probabilities calculated using two alternative methods designed to test the i.i.d. assumption. Figure S27 shows the comparison to probabilities calculated using return levels calculated for each model independently, while Fig. S28 shows the comparison when a decadal block minima approach is used.

Calculating return levels for each model independently results in overall slightly higher probabilities, while the block minima approach reduces the highest probabilities somewhat. Under our standard approach, for SSP 2-4.5, 126 streams have a >50% probability of experiencing a 500-year drought within 10 years, while calculating return levels for each model independently for each model gives an estimate of 155 streams and using a block minima approach gives an estimate of 102 streams.

The 500-year return levels calculated using the UNSEEN methodology also agree reasonably well with return levels estimated by fitting generalized extreme value (GEV) functions. We consider the estimates to agree if the UNSEEN-estimated return level lies within the 95% confidence interval of a GEV function fit to historical data. For the GEV fit to historical simulated streamflow data there is 86% agreement across all 399 catchments. For the GEV fit to historical observed data there is 78% agreement across 127 catchments with at least 40 years of observed streamflow data between 1951-2000. In cases of disagreement, the UNSEEN-estimated return level is more extreme (smaller) than the return level estimated using historical simulated data (always) and historical observed data (75% of the time). Evaluating future projections against UNSEEN-estimated return levels is thus both robust and conservative.

Agricultural water demand

We predict mostly modest increases in agricultural water demand over the five southern regions (Fig. S15). Projected percentage increases are greatest for the Salish Sea. However, in

terms of total volume, the increase will probably be most noticeable in the California and the Columbia Basin.

In the Columbia Basin, where 10% of land is cropped, August agricultural water demand is estimated at 4000 m^3s^{-1} for the historical period (1991-2020), projected to increase by 8% under SSP 2-4.5 by the end of the century. Over this same period, August streamflow at the mouth of the Columbia averaged 4500 m^3s^{-1}, and across all study sites in the Columbia basin we project a median decrease in August streamflow of 29%.

It is important to note that not all of the agricultural water demand is satisfied, and probably will not be in the future. Approximately 64% of agricultural land in the Columbia Basin is not irrigated. On non-irrigated land an increase in agricultural water demand would more likely result in reduced productivity than increased water use. Previous authors have estimated August irrigation water demand in the Columbia Basin to be about 1000 m^3s^{-1} (*150*).

Our estimates also do not account for accelerated crop development in a warmer climate, leading to a reduction in time to maturity, increased water use efficiency under higher carbon dioxide concentrations, or earlier planting dates. Accounting for these factors, late-season irrigation water demand could actually decrease on average throughout the Columbia Basin, although many watersheds will still see increases (*151*).

Historical simulations match streamflow declines

Many of the streams in this regions have seen significant trends in streamflow since 1950 (*26*, *152–154*). We thus evaluate the ability of the regression models to simulate observed trends in streamflow when forced with temperature and precipitation from the historical runs of the climate models. Figure S11 shows this analysis. We compare the observed trend (Thiel-Sen slope) in August streamflow to the modelled trend for all gauges with at least 50 years of observed streamflow data between 1951 and 2024 (229 gauges).

There is adequate agreement between the observed streamflow trends and the trends simulated using the regression models forced with climate model data. The direction of the trend (positive or negative) is accurately predicted 90% of the time. However, the magnitude of the simulated trends is generally smaller than observed trends. The linear best fit line on Figure S11 has a slope of 0.55, indicating that observed changes are about twice as large as simulated changes.

The error (underestimation) derives mostly from the climate models. When forced with observed climate data the regression models correctly predict the trend direction 97% of the time and the simulated trend magnitudes lie very close to the observed trend magnitudes (Fig. S12). In addition, Fig. S13 shows that the magnitude of both wetting and drying trends in precipitation throughout the range has been underpredicted by the CMIP6 multi-model ensemble. In particular, strong drying trends in the summer near the middle of the range have been underpredicted. Figure S14 shows that most of the range has warmed faster than predicted by the CMIP6 ensemble: in particular, warming trends are underpredicted in the middle of the range for the summer and in the north for the winter.

If the strong trends in the observed climate data are a result of climate change then the climate models would be expected to have captured these changes. The underestimation of the trends would thus suggest that projected changes are also underestimated. However, this is highly uncertain as the trends in the observed climate data could also be affected by cyclical phenomena such as the Pacific Decadal Oscillation and the El Niño Southern Oscillation, or by

errors in the observed data deriving from changes in measurement techniques or weather station density.

Comparison to previous projections

We compare our projections to four other studies which projected streamflow changes for California (*64*), the Pacific Northwest (*28*, *155*), and the Fraser Basin (*29*, *156*).

In California, we compare our projections to projections prepared by the California Water Commission using a Variable Infiltration Capacity (VIC) model (*64*). The VIC projections are provided at the HUC-8 watershed level, for a combination of RCP 4.5 and RCP 8.5 scenarios, comparing historical (1991-2010) to future (2056-2085) condition. We compare our projections of the relative change in August streamflow to the same metric for HUC-8 watershed that covers each of the Californian gauges in our study. We calculate the change over the same historical and future periods, for a combination of SSP 2-4.5 and SSP 5-8.5.

We project much larger changes than the California Water Commission (*64*), as seen in Fig. S26. Our projections show decreases in August streamflow of up to 62%, while the VIC model projects changes no larger than 18%. Our projections show larger decreases in 14 of 17 locations.

Hamlet *et al.* (*28*) used a distributed Variable Infiltration Capacity (VIC) model over the Columbia Basin and the Washington and Oregon coasts, and provide simulations at 557 discrete locations, 37 of which are gauges used in our study. They simulated historical streamflow over the period 1915-2006, and use a 'hybrid delta' downscaling technique to adjust CMIP3 projections for the period 2070-2099. They produced projections for scenarios B1 and A1B. We compare the B1 scenario from Hamlet *et al.* to our projections for SSP 2-4.5 because the B1 scenario corresponds to 4.2 W/m^2 of additional radiative forcing by the end of the century, which is a close match to SSP 2-4.5 (4.5 W/m^2).

We project similar overall reductions in August streamflow than Hamlet *et al.*, as shown in Figure S24. Our projections are more extreme in 24 of 37 sites, and the median change is slightly larger (-42% vs -36%).

Also in the Pacific Northwest, Mizukami *et al.* (*63*) produced projections using the Structure for Unifying Multiple Modeling Alternatives (SUMMA), for SSP 2-4.5, SSP 3-7.0, and SSP 5-8.5. Mizukami *et al.* provide projections for 414 discrete locations, 57 of which are gauges used in our study. For this comparison, we recalculated the change factors using a historical period of 1955-2014 for both our models and for the SUMMA simulations. We also only include the 5 climate models included by Mizukami *et al.* Both models show decreases in August flow at almost all locations (56/57 locations in the regression models, 54/57 locations in the SUMMA model; Fig. S25). Overall, our projections show larger decreases at 34/57 locations under SSP 2-4.5 and 38/57 locations under SSP 5-8.5. Under SSP 2-4.5 the median change in SUMMA is -27% and -41% in our projections.

Schnorbus (*29*, *156*) used a VIC model with a glacier module (VIC-GL) to project streamflow for the Fraser Basin, for RCPs 4.5 and 8.5. We compare these simulations to our projections for SSPs 2-4.5 and 5-8.5. The VIC-GL model includes projections from six CMIP5 climate models, so for the sake of like-for-like comparison, for the regression model we include only the CMIP6 models that are successors to those six models: ACCESS-1.0 → ACCESS CM2, CCSM4 → CESM2, CNRM-CM5 → CNRM-CM6-1, CanESM2 → CanESM5, MPI-ESM-LR → MPI-ESM1-2-LR, and HadGEM2-ES → HadGEM3-GC31-LL. The regression models agree with the VIC-GL model that almost all locations will see decreases in August flow (43/44

locations in the regression models, 44/44 locations in the VIC-GL model ; Fig S23). The VIC-GL model predicts larger decreases in 31/44 locations, and predicts a median decrease of -53% compared to 40% in the regression models.

Temperature Projections

To illustrate the value of site-specific hydrologic projections for projecting other environmental variables, we present projections of water temperature change at 47 gauge locations in Figure S21. Under the medium emissions scenario water temperatures are predicted to change by between 0.5ºC and 5ºC by the end of the century. Water temperatures in the PNW Coast, Fraser Basin, and Salish Sea are projected to increase most significantly, along with three streams in the Columbia Basin.

These projections are based on simple empirical sensitivities to air temperature and streamflow and as such are subject to substantial uncertainty. Process-based stream temperature models would likely produce larger estimates of warming rates, particularly if they explicitly model the effects of snow cover, glacier loss, and groundwater warming (*78*).

In Figure S22 these projections are compared to 28 locations in the western United States also projected by (*127*) and 10 locations in British Columbia also projected by (*85*). The median projected warming is similar in both cases: in the western United States we project a median warming of 2.1ºC vs 2.4ºC by (*127*), and in British Columbia we project a median increase of 2.8ºC vs 3.2ºC by (*85*). However, we predict a much wider range of temperature changes than these regional models, suggesting that individual stream sites may warm significantly faster or slower than the regional average.

The variation in response among individual stream sites emphasizes the value of site-based hydrologic projections. Existing stream temperature projections for British Columbia (*85*) do not account for relationships with streamflow, while in the United States regional average observed streamflow was used to fit the models, and regional average streamflow projections from (*28*) were used in the projection step (*127*). Isaak *et al.* (*127*) recognize that creating a regional model in this way 'obscure[s] site-level variation in warming rates'. While it is not possible to conduct detailed site-specific investigations of every stream reach in western North America, the variation shown here can help set expectations about the uncertainty of regional warming rates.

Deer Creek migration barriers

In Deer Creek, an instream flow evaluation found that on April 29, 2014, water depths at a critical riffle in the lower watershed were below the minimum passage depth requirement for Chinook (0.9 ft) (*46*). On this date, flow at the upstream near-natural gauge (USGS 11383500) was 4 m^3s^{-1}. We use this value as the critical flow. However, there are multiple diversions downstream of the gauge that can reduce flow in the stream.

We evaluated the probability of flows falling below this threshold in the same way as for the 500-year drought estimation. In April (the peak of the spring migration) we predict a 17% probability of flows falling below 4 m^3s^{-1} within the next 10 years. In May, the tail end of the spring migration, we estimate this probability to be 94%.

North Fork Stillaguamish Spawning Habitat

Embrey developed spawning habitat-flow relationships using the instream flow incremental methodology for various spawning sites in the Stillaguamish basin (*70*). The site closest to gauge 12167000 (NF Stillaguamish River near Arlington, WA) is labelled 'North Fork Stillaguamish

River at Wiersma Bar' by Embrey. At this site, Chinook salmon spawning area was estimated to be maximized by a flow of 33 m^3s^{-1} (Table 7 in (*70*)). We used linear interpolations of the data in (*70*) to determine the usable spawning habitat for historical flows and for projected future conditions.

At historical median August flows of 13.0 m^3s^1, 19% of maximum usable spawning habitat would be available, but at future (end-of-century, SSP 2-4.5) conditions, only 2% would remain available. For September, the peak spawning month for summer Chinook salmon, historical conditions would make 48% of usable spawning habitat available, while future conditions would leave only 2.8% available, a reduction of 94%.

Kenai River water velocity

Mean channel velocity measurements were taken from USGS data for gauge 15266300 (Kenai R at Soldotna AK). These are plotted against discharge in Fig S31. Data appear to follow a power law scaling of velocity with the square root of discharge. We fit a regression line (R^2=0.95) to the data points with discharge greater than 200 m^3s^{-1}, to capture the relationship for higher flows.

Based on this regression, we calculate median July water velocities of 1.6 m/s for the historical period and 1.72 m/s for the future period, an increase of 8%. The median July discharge is projected to increase from 379 m^3s^{-1} to 429 m^3s^{-1}. During July-August 2013, when Chinook salmon were observed migrating in the Kenai River (*80*), the average water velocity is estimated at 1.75 m/s. We therefore do not expect future increases in water velocity to be particularly challenging for Chinook salmon in this river.

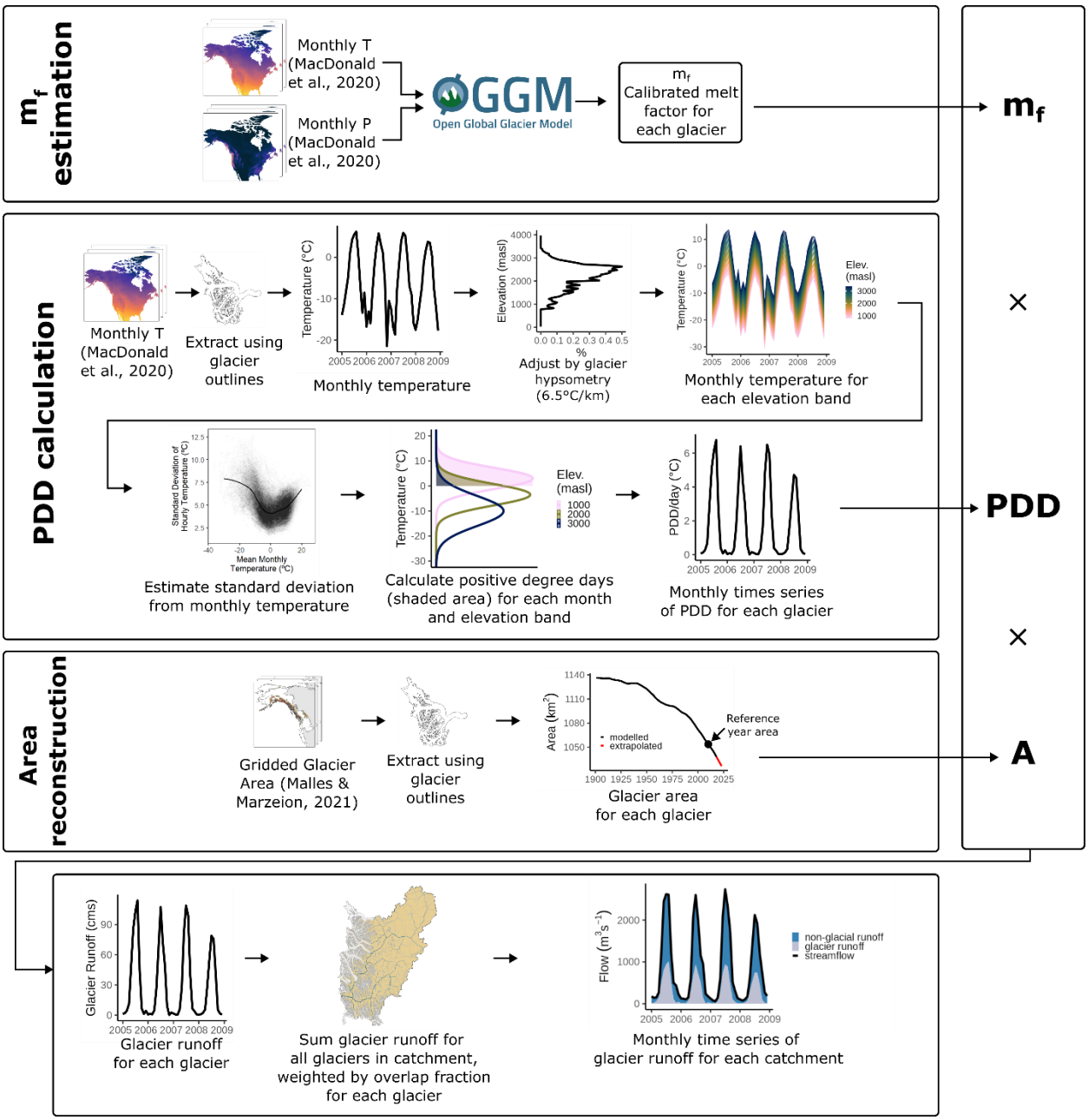

Fig. S1.

Glacier runoff model diagram for historical simulation. The runoff is the product of melt factor (m_f), positive degree days (PDD) and glacier area (A). For the CMIP6 projections, the monthly temperature time series (third figure within PDD calculation) is replaced by the bias-corrected temperature from each CMIP6 model, and the area is taken from the projections by Rounce et al. (*141*).

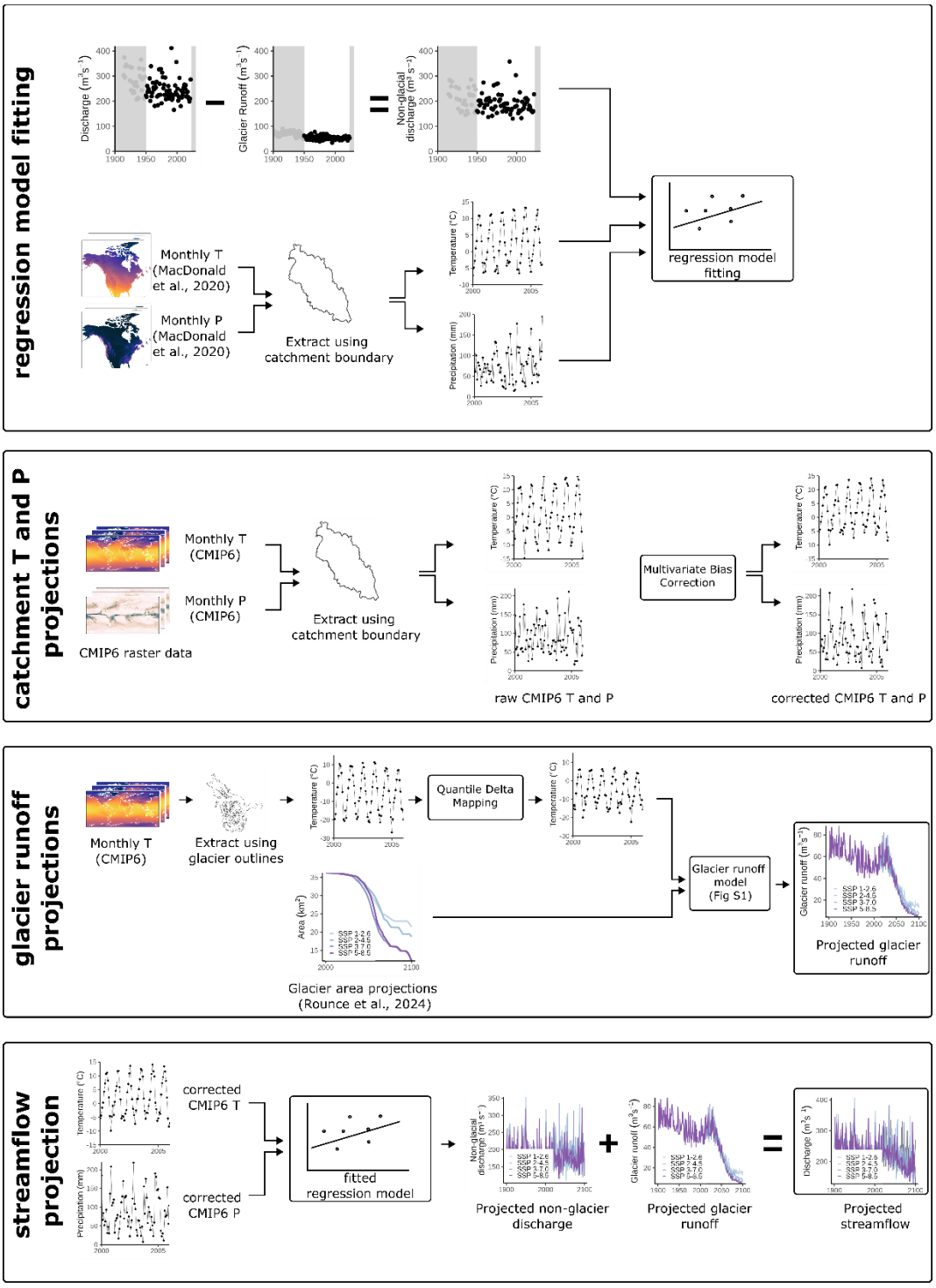

Fig. S2.

Data flow diagram for the streamflow projection models presented in this study. First, the regression models are fit to non-glacial streamflow. Next, CMIP6 T and P are bias-corrected. Third, glacier runoff is projected using bias-corrected CMIP6 T and glacier area projections from (*141*). Lastly, the bias-corrected T and P are fed to the fitted regression model to calculate non-glacial discharge, and then glacier runoff is added to calculate projected streamflow.

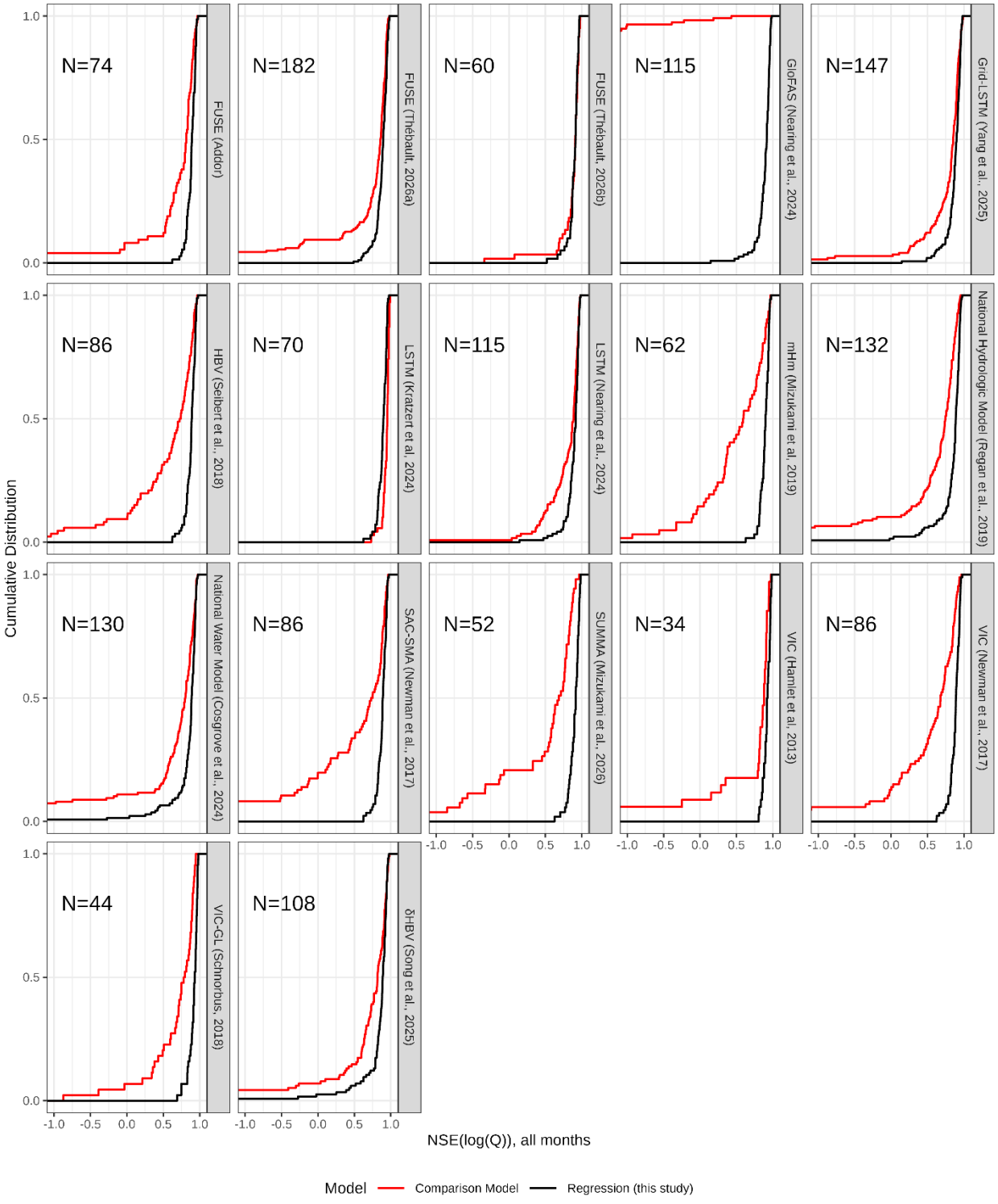

Fig. S3.

Performance comparison against 17 other models (model names are in strip text), based on the NSE of the log-transformed monthly flows for all months of the year. Higher values (further to the right) indicate better performance.

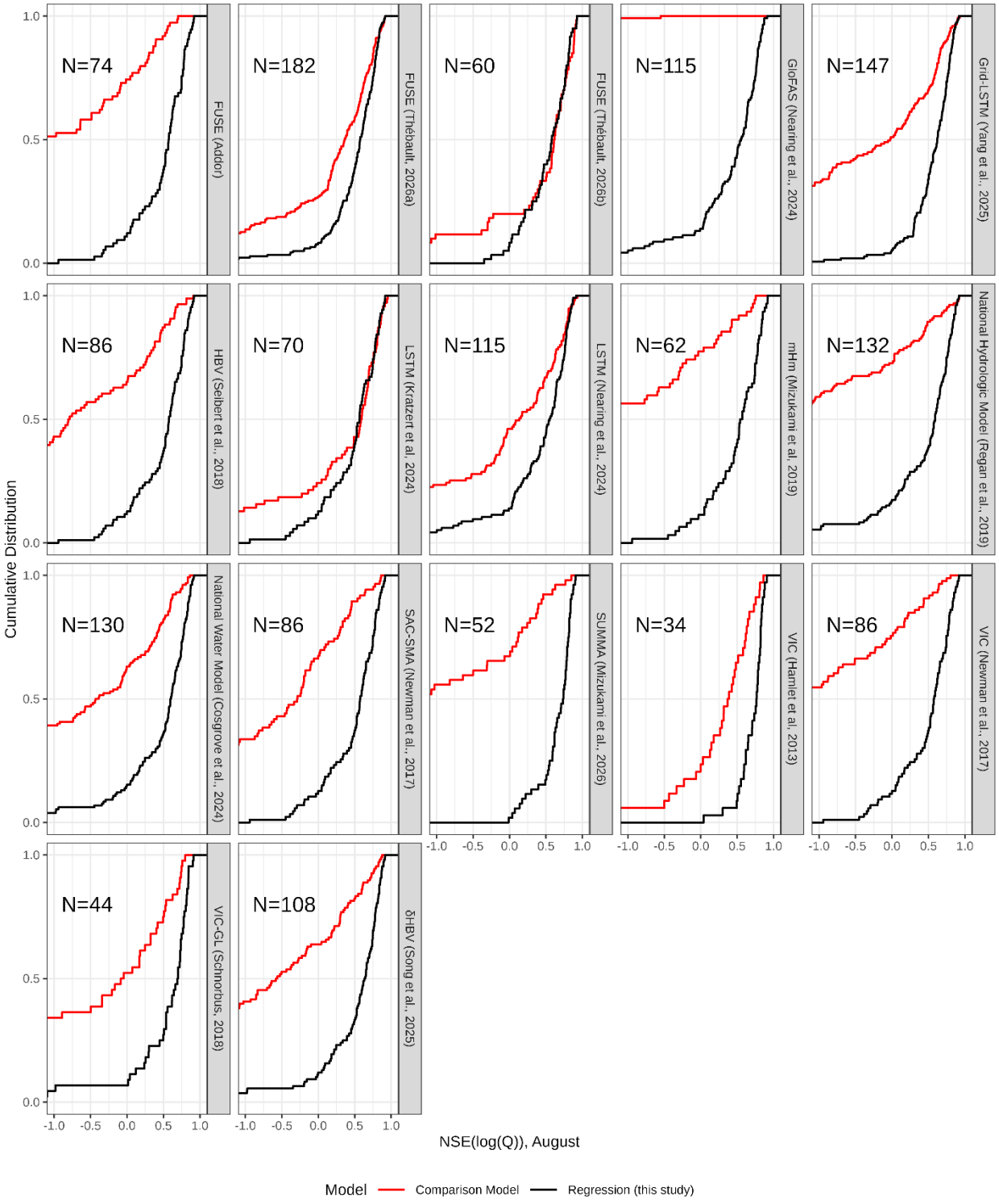

Fig. S4.

Performance comparison against 17 other models (model names are in strip text), based on the NSE of the log-transformed monthly flows for August. Higher values (further to the right) indicate better performance.

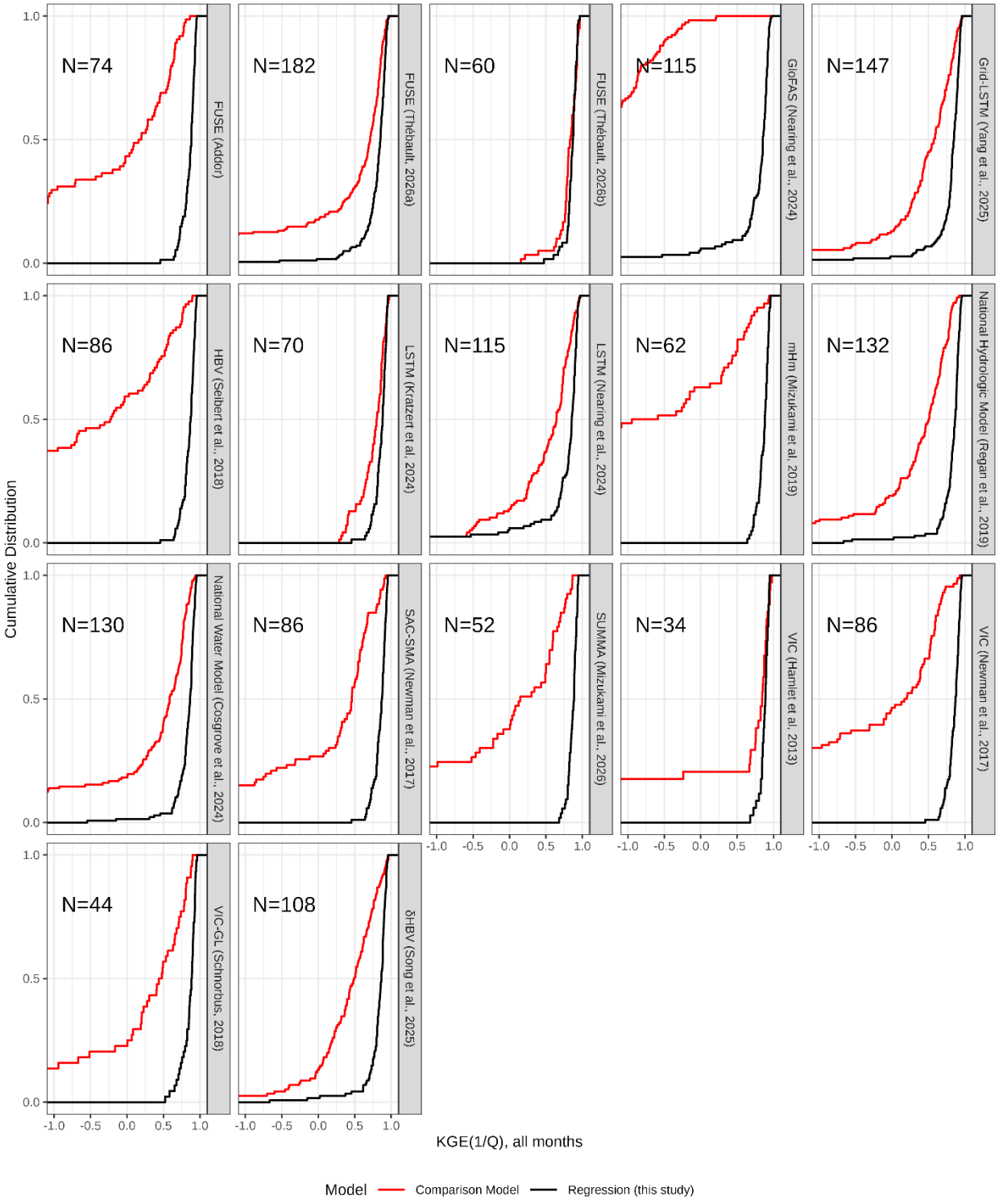

Fig. S5.

Performance comparison against 17 other models (model names are in strip text), based on the KGE of inverse-transformed monthly flows for all months of the year. Higher values (further to the right) indicate better performance.

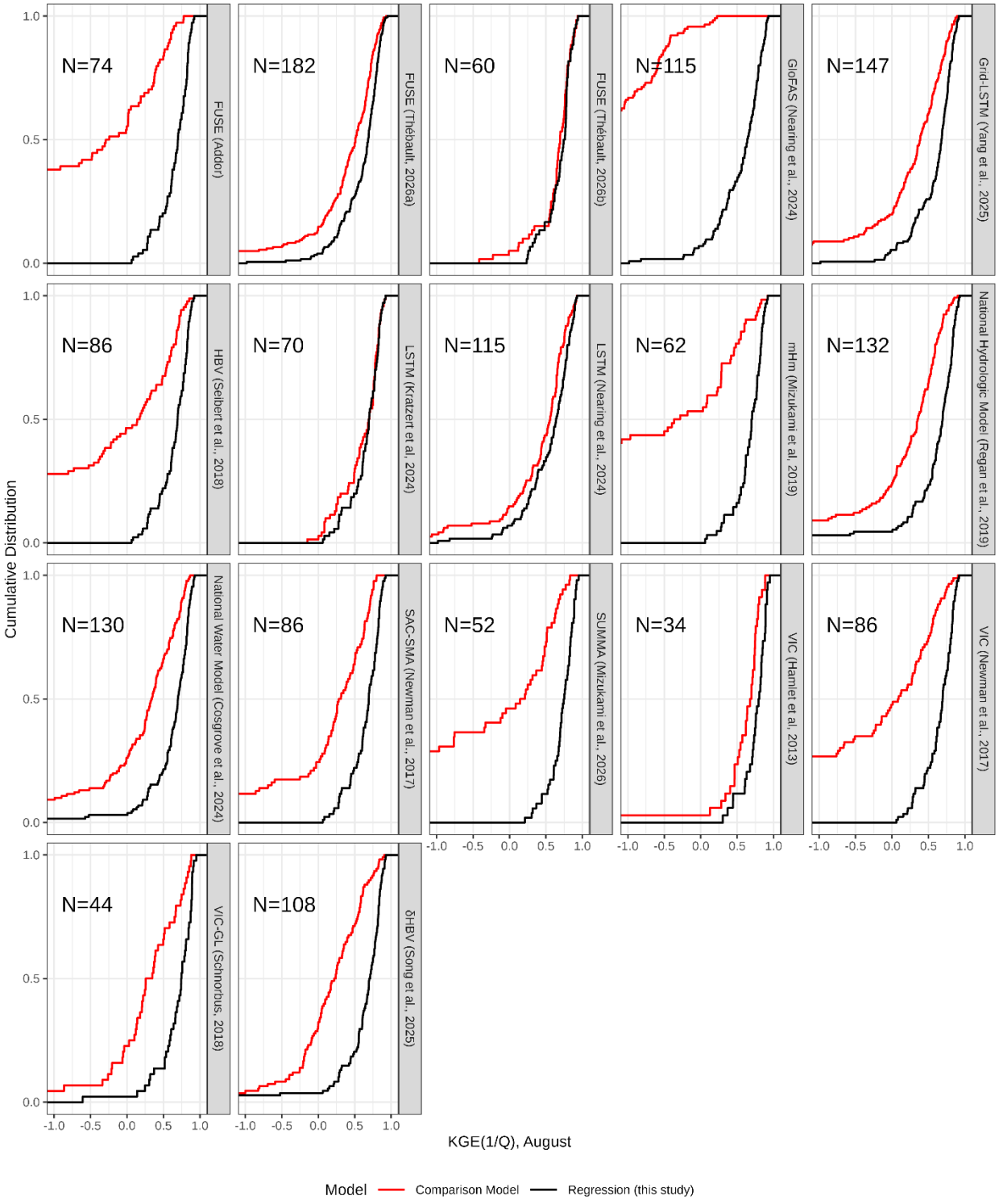

Fig. S6.

Performance comparison against 17 other models (model names are in strip text), based on the KGE of inverse-transformed monthly flows for August. Higher values (further to the right) indicate better performance.

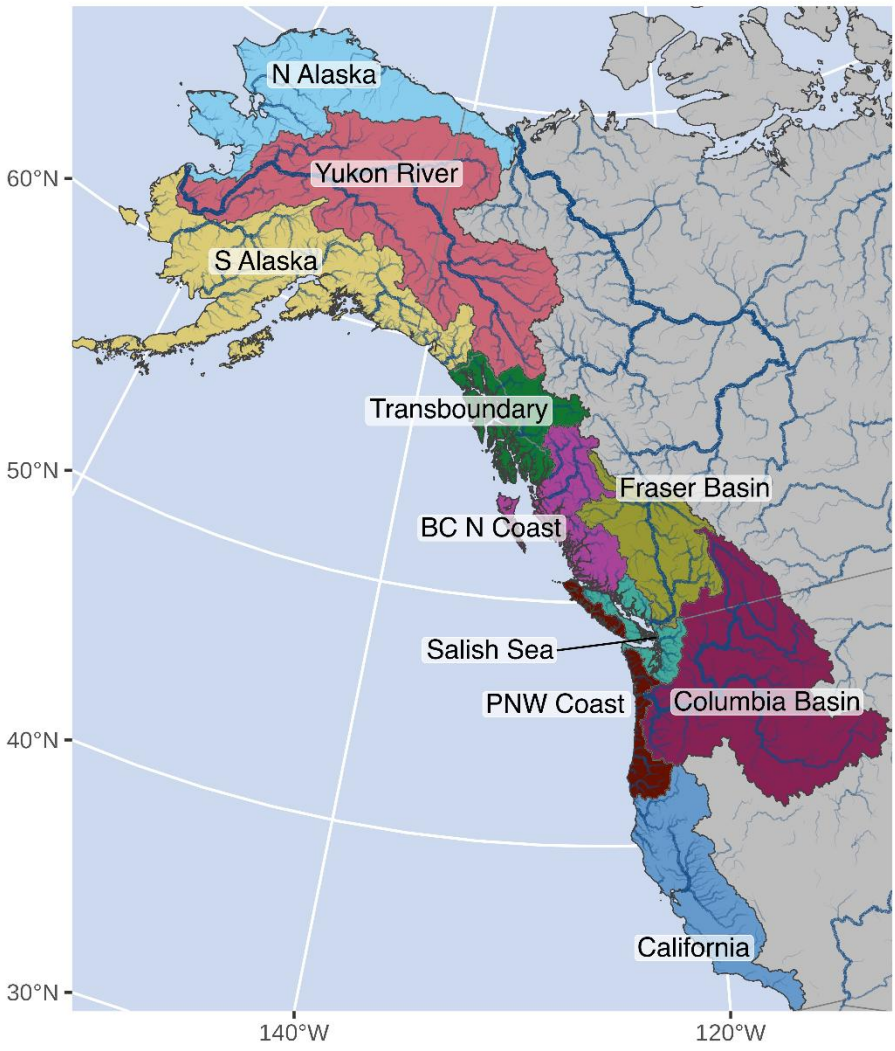

Fig. S7.

The 10 salmon-producing regions used in this study. The river network is based on data from (*157*).

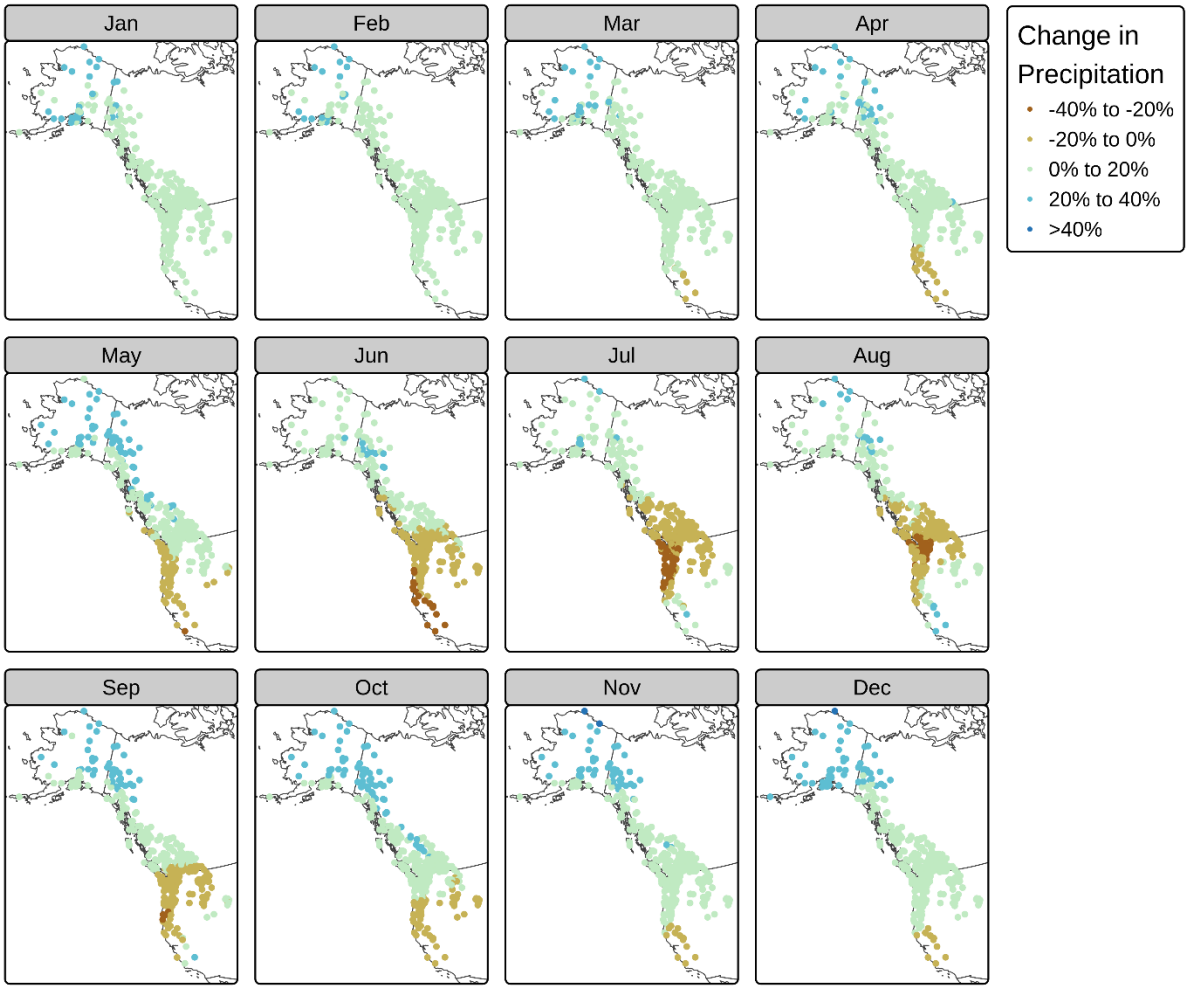

Fig. S8.

Projected change in precipitation by month for each of the 399 catchments, under SSP 2-4.5 at the end of the century (2070-2099). The values are the weighted median of all climate models.

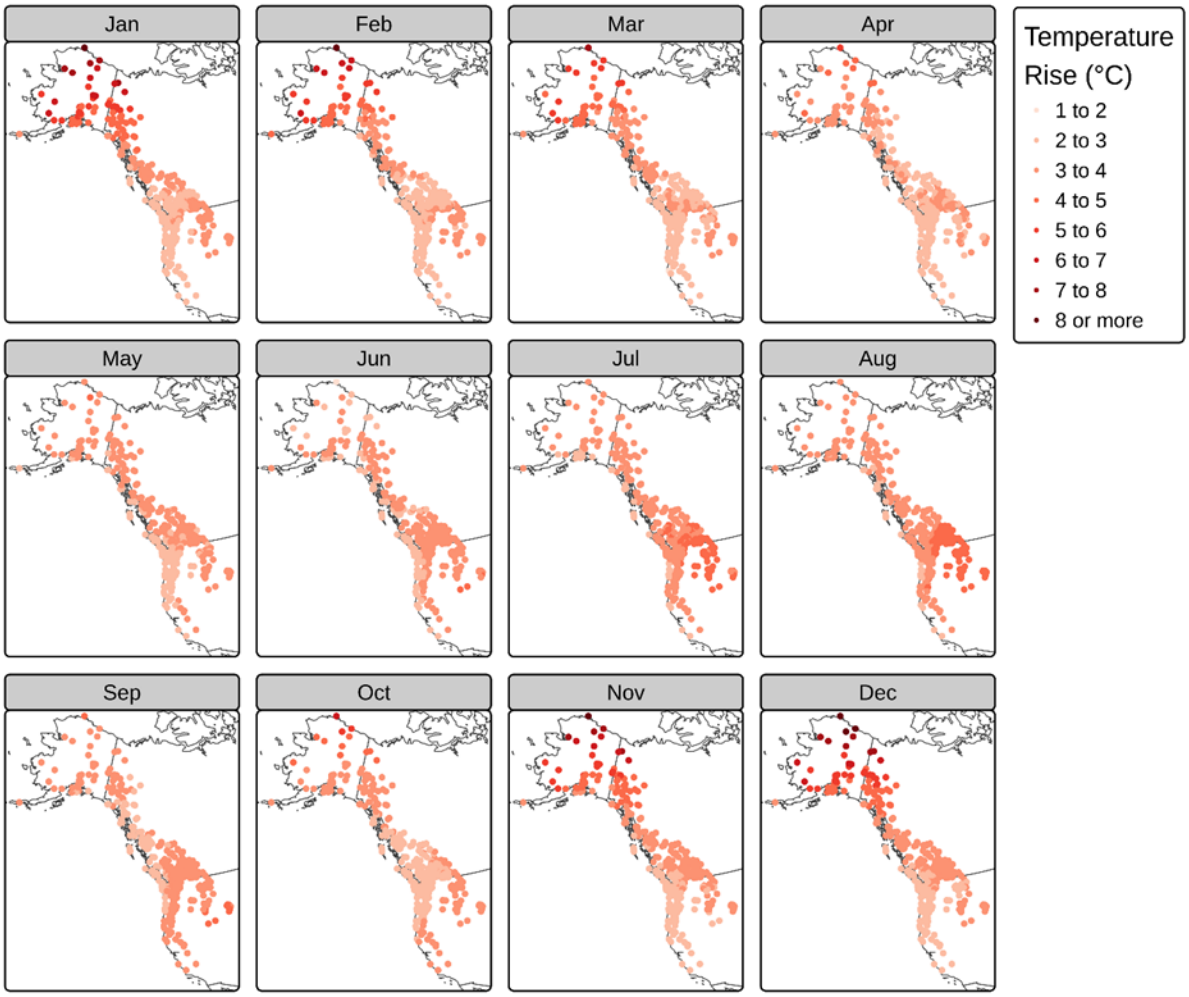

Fig. S9.

Projected increase in air temperature by month for each of the 399 catchments, under SSP 2-4.5 at the end of the century (2070-2099). The values are the weighted median of all climate models.

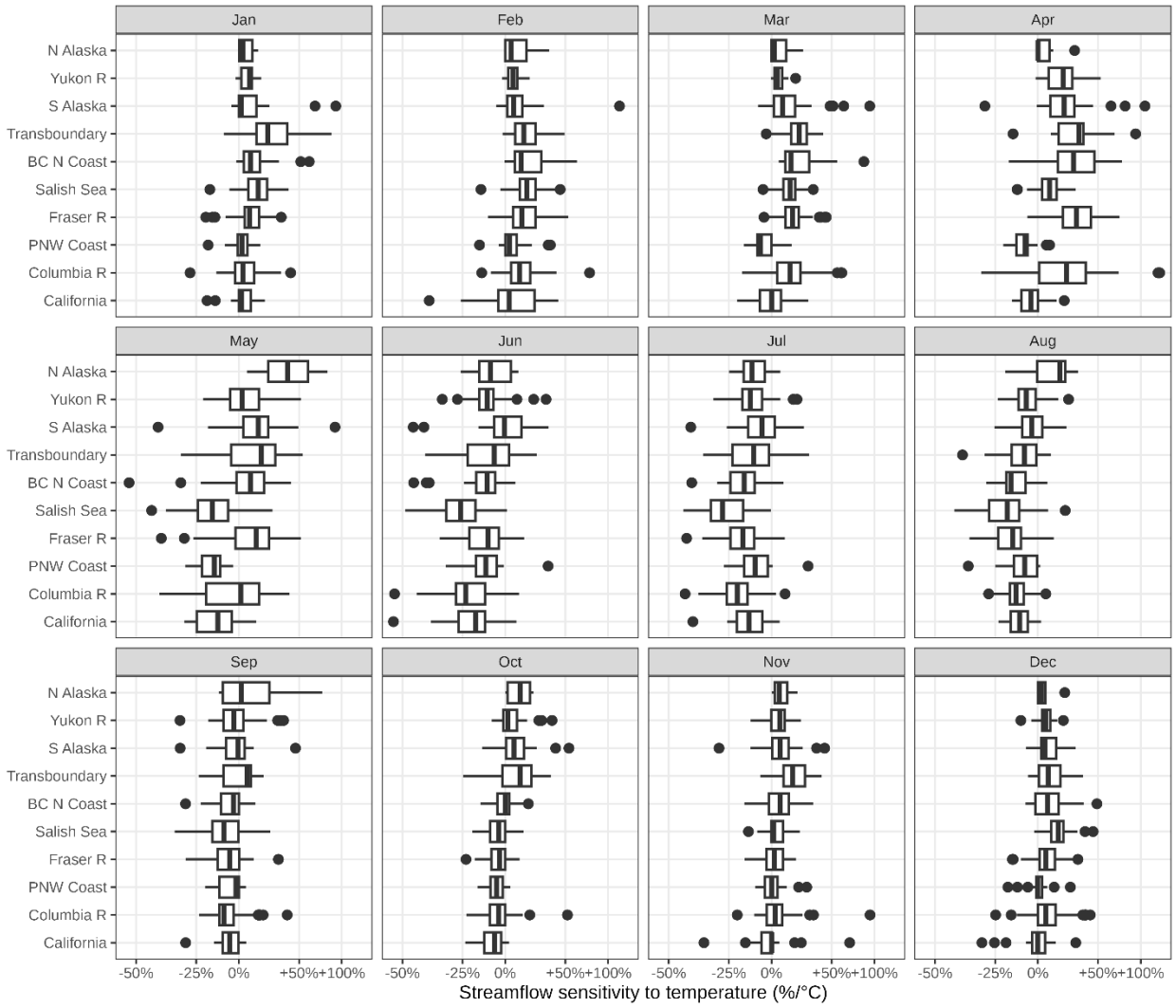

Fig. S10.

Streamflow sensitivity to air temperature. The x axis represents the change in streamflow associated with 1°C increase in average temperature. July and August streamflow in the Salish Sea, Fraser Basin, BC North Coast, and Columbia Basin regions is particularly sensitive to increasing temperatures.

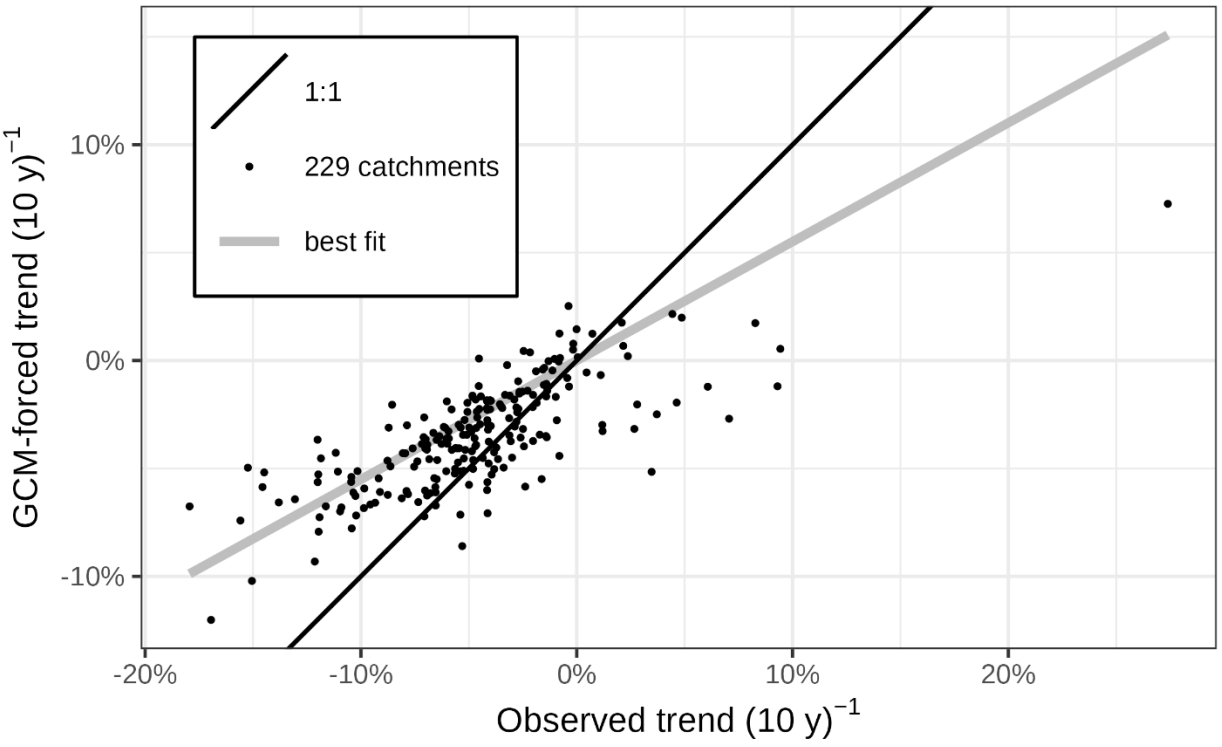

Fig. S11.

Comparison of GCM-forced and observed historical trends in August streamflow. The trends are the Thiel-Sen slope of observed streamflow (x-axis) and simulated streamflow by forcing the regression models with climate model (GCM) outputs. The data represent 229 catchments with at least 50 years of data from 1951-2024. The simulations correctly predict the direction of change 90% of the time but underestimate the magnitude. The linear best fit line (grey) is constrained to pass through (0,0) and has a slope of 0.55.

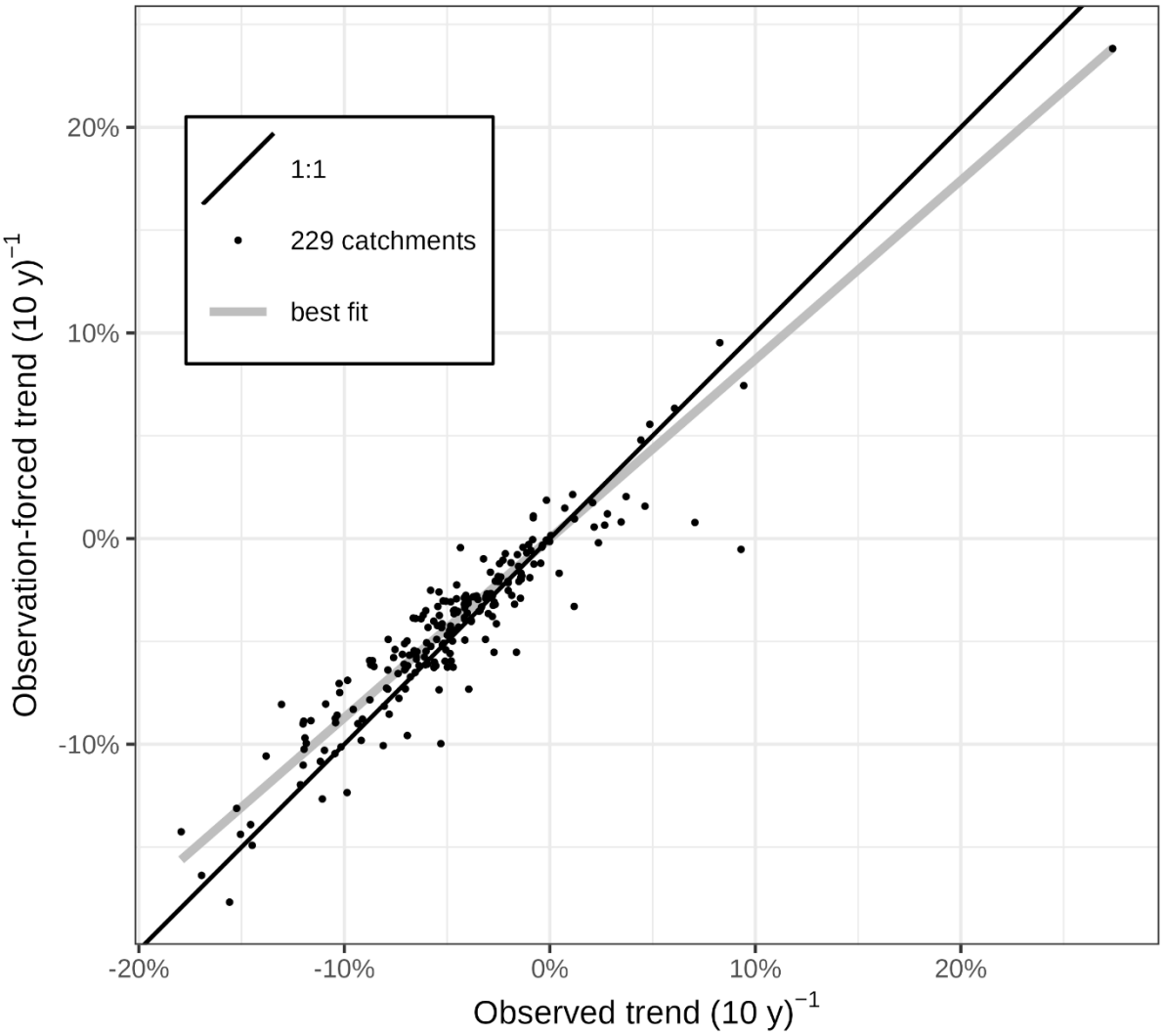

Fig. S12.

Comparison of observation-forced simulated and observed historical trends in August streamflow. The trends are the Thiel-Sen slope of observed streamflow (x-axis) and simulated streamflow by forcing the regression models with observed climate data. The data represent 229 catchments with at least 50 years of data from 1951-2024. The simulations correctly predict the direction of change 99% of the time but underestimate the magnitude. The linear best fit line (grey) is constrained to pass through (0,0) and has a slope of 0.87.

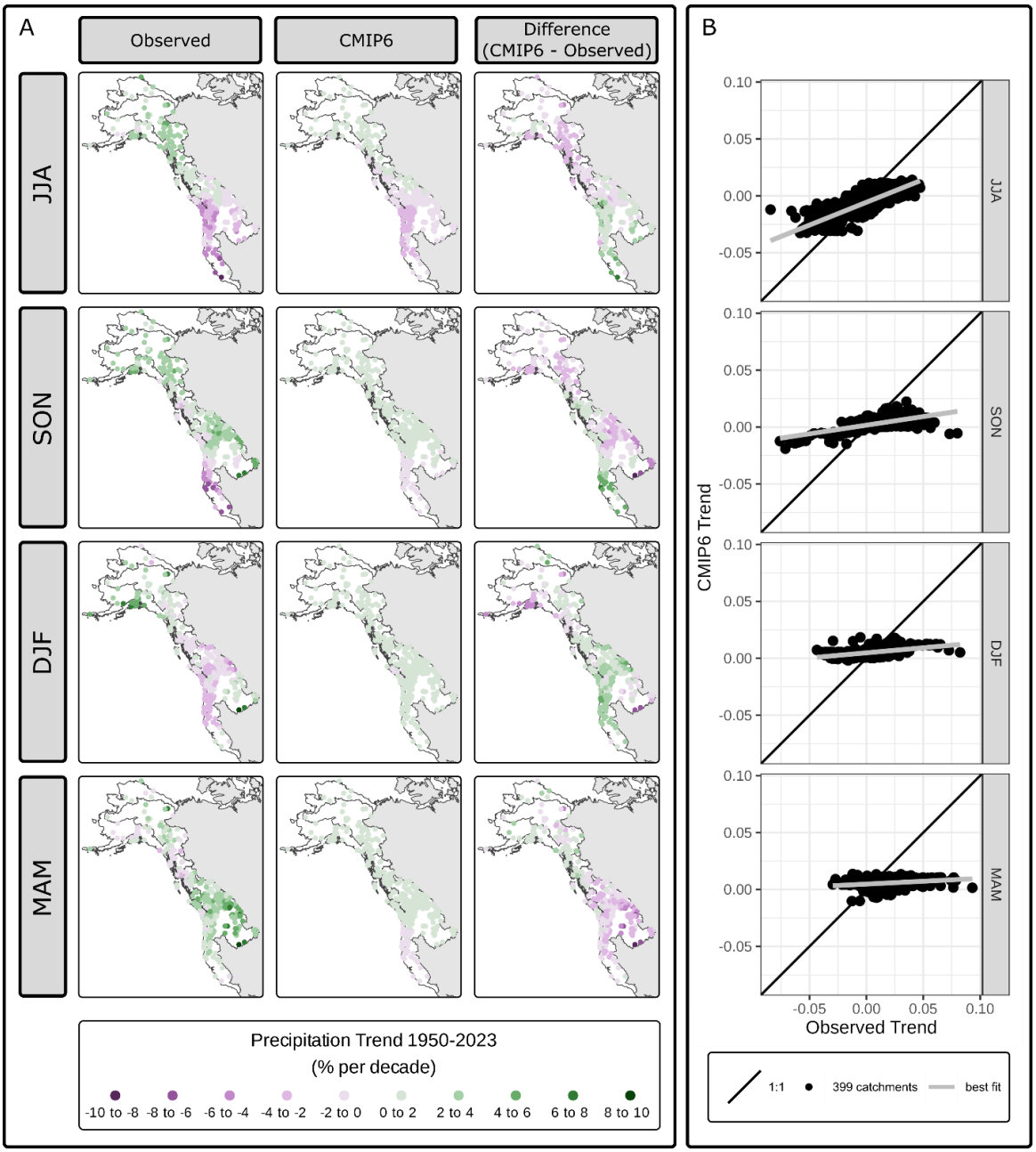

Fig. S13.

Comparison of observed and CMIP6 trends in precipitation over the historical period (1950-2023), for each of four seasons: summer (JJA), autumn (SON), winter (DJF), and spring (MAM). **(A)** Observed and CMIP6 trends, as well as the difference, in % per decade. **(B)** scatterplots of CMIP6 trends vs observed trends for each season. Both positive and negative trends are underpredicted by the CMIP6 models, with positive (wetting) trends in the north being underpredicted and negative (drying) trends in the south being underpredicted in the summer, autumn, and winter. Strong positive trends in the upper Columbia and Fraser basins are underpredicted in the autumn, winter, and spring.

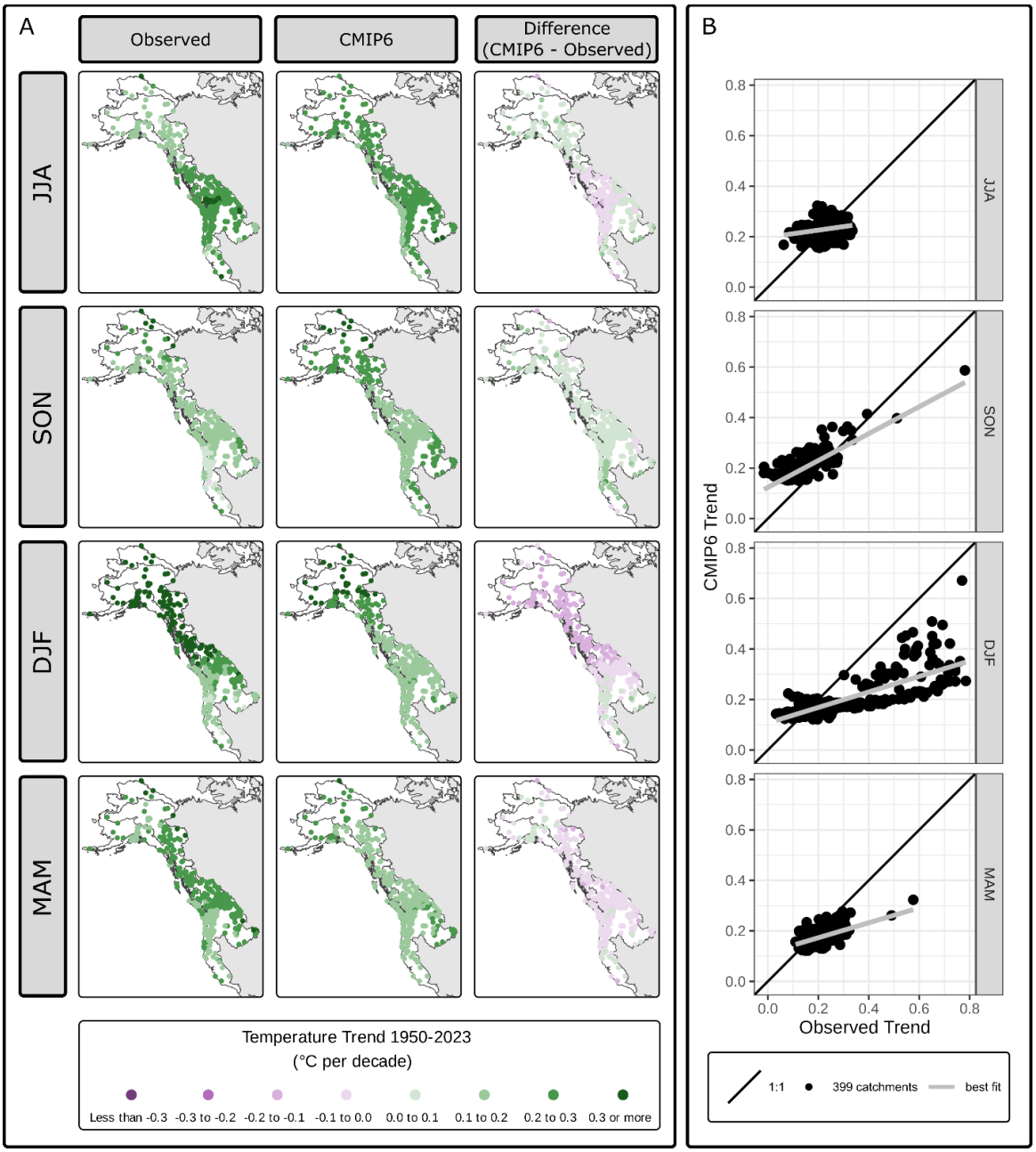

Fig. S14.

Comparison of observed and CMIP6 trends in temperature over the historical period (1950-2023), for each of four seasons: summer (JJA), autumn (SON), winter (DJF), and spring (MAM). **(A)** Observed and CMIP6 trends, as well as the difference, in ºC per decade. **(B)** scatterplots of CMIP6 trends vs observed trends for each season. Most of the strong positive (warming) trends are underpredicted: in the summer throughout the middle of the range, in the winter in the northern half of the range, and in the spring throughout most of the range. Warming trends in the autumn are overpredicted in most of the range.

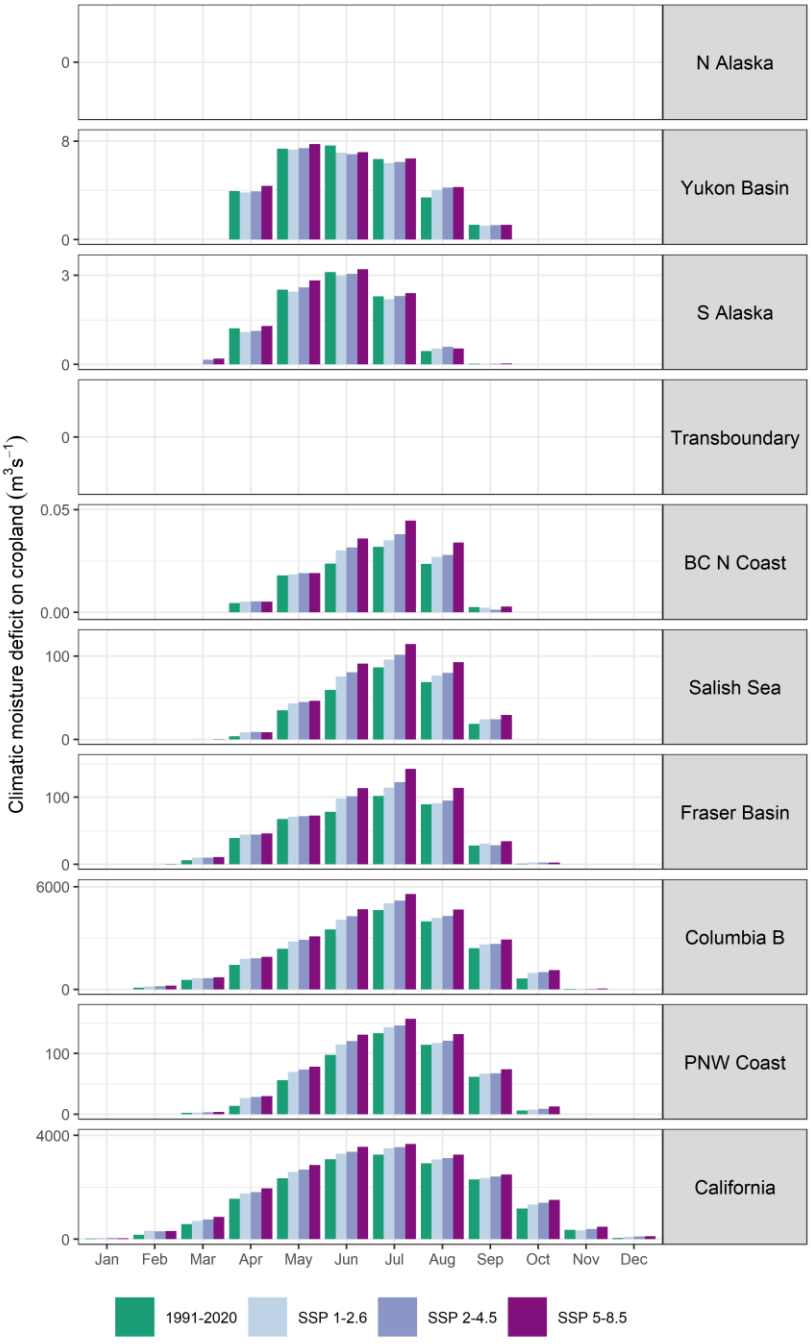

Fig. S15.

Total climatic moisture deficit over cropland for each region, for the historical normal period (1991-2020) and for the end-of-century under three CMIP6 scenarios. Note differences in y-axes. The Transboundary and North Alaska regions had no land classified as cropland.

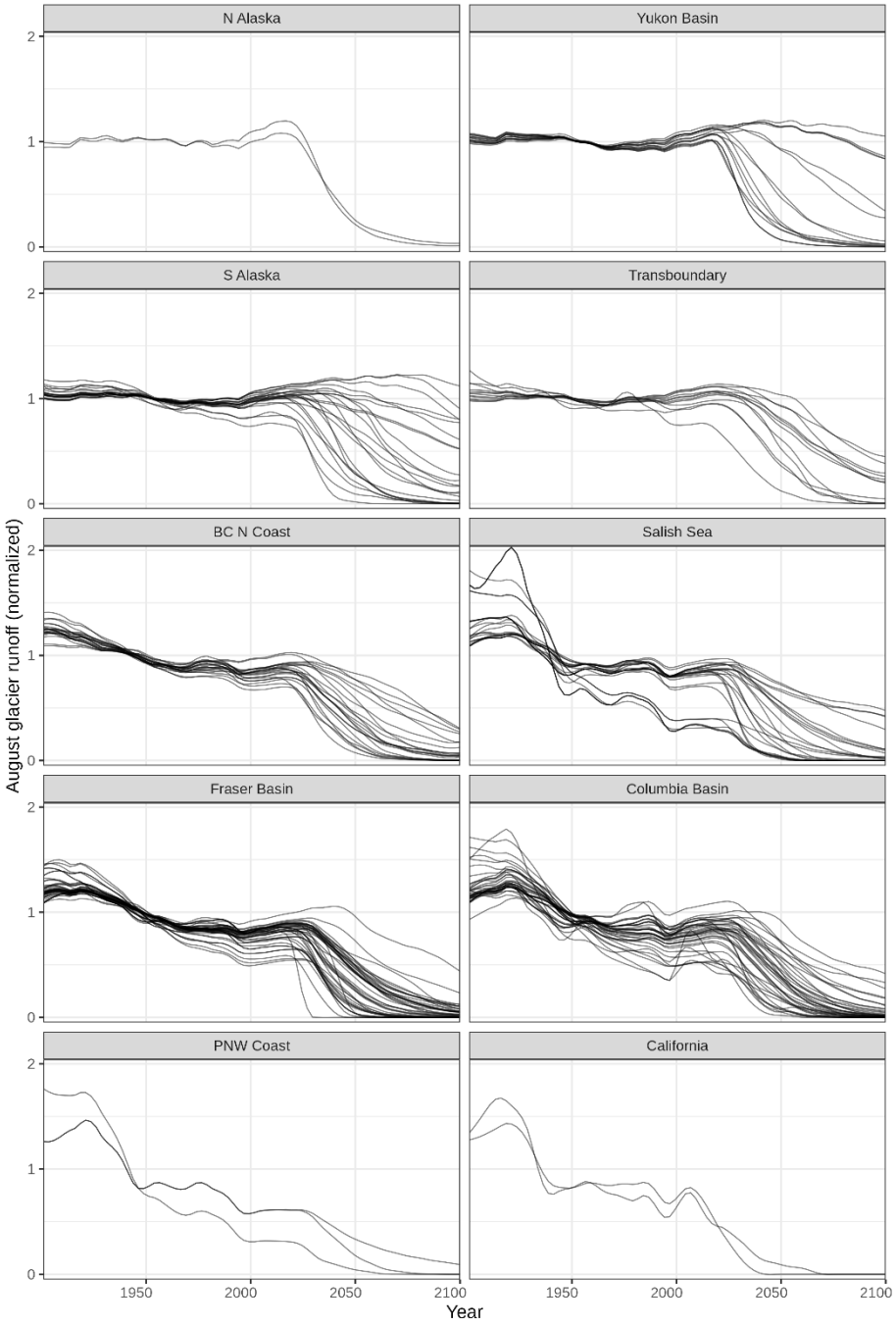

Fig. S16.

Peak water has been passed in most watersheds. The August glacier runoff, normalized by its 20th-century mean, is shown for each of the 183 watersheds with >0.01% glacier cover. The projection period corresponds to SSP 2-4.5.

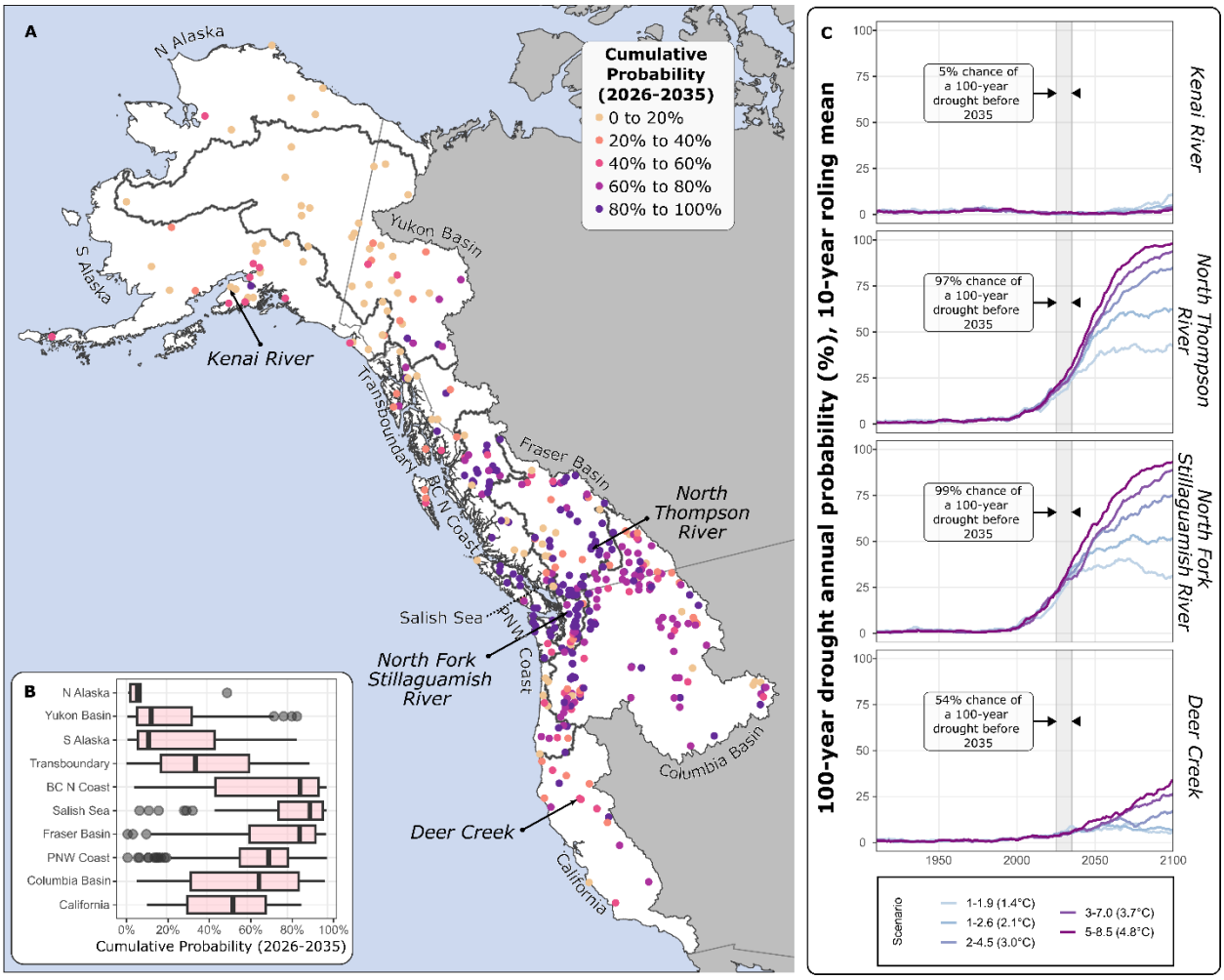

Fig. S17.

Probability of 100-year August droughts. **(A)** Cumulative probability of 100-year droughts occurring between 2026-2035. The baseline probability under a stationary climate would be ~9.6%. **(B)** Boxplots of data in A summarized across streams in each region. **(C)** Annual probability of a 100-year August drought for the sentinel rivers.

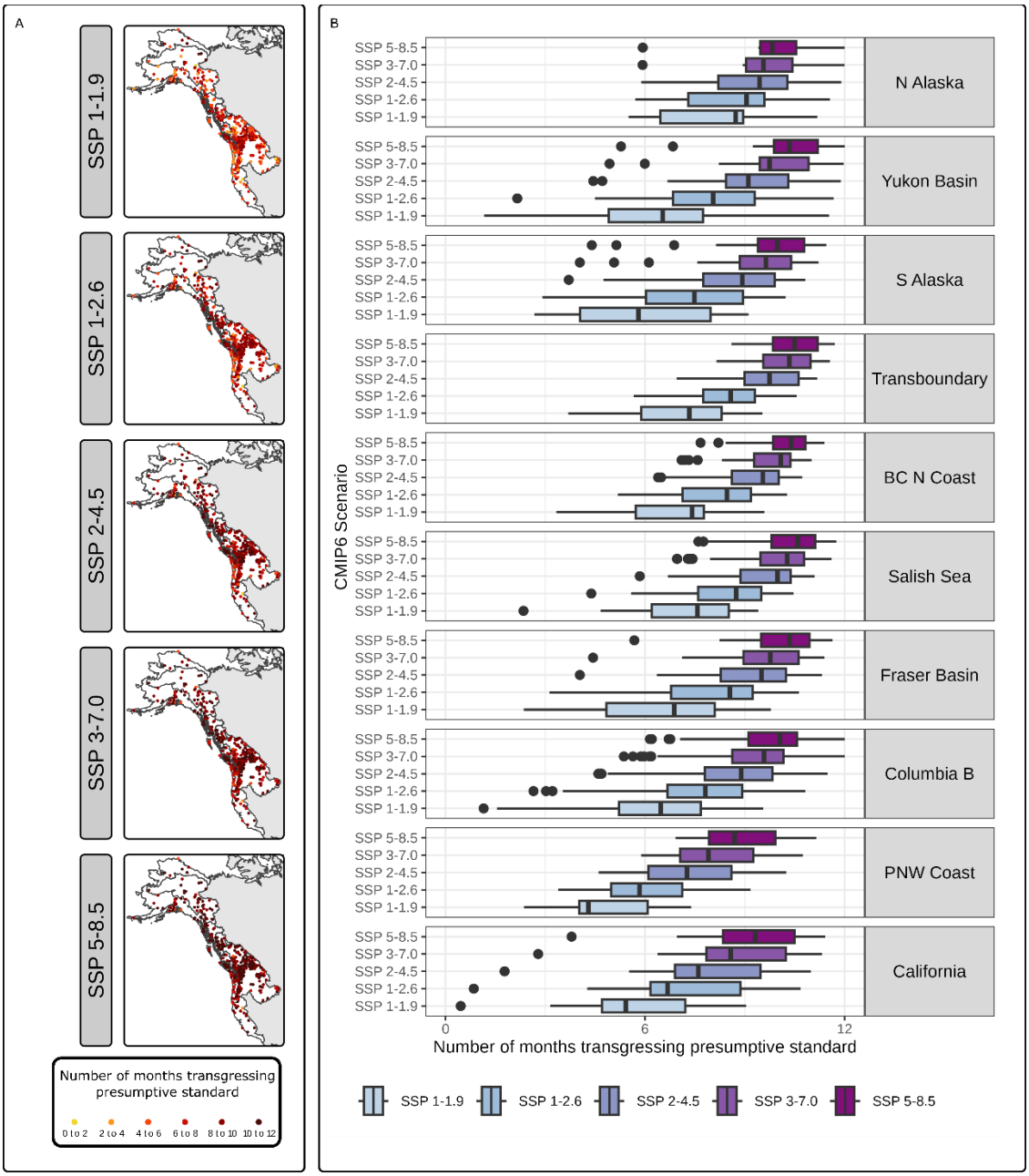

Fig. S18.

Number of months with transgressions of the presumptive standard for the end-of-century (2070-2099) under five emissions scenarios. (A) maps of the 399 catchments, number of months exceeding the presumptive standard. (B) Boxplots for each region and scenario.

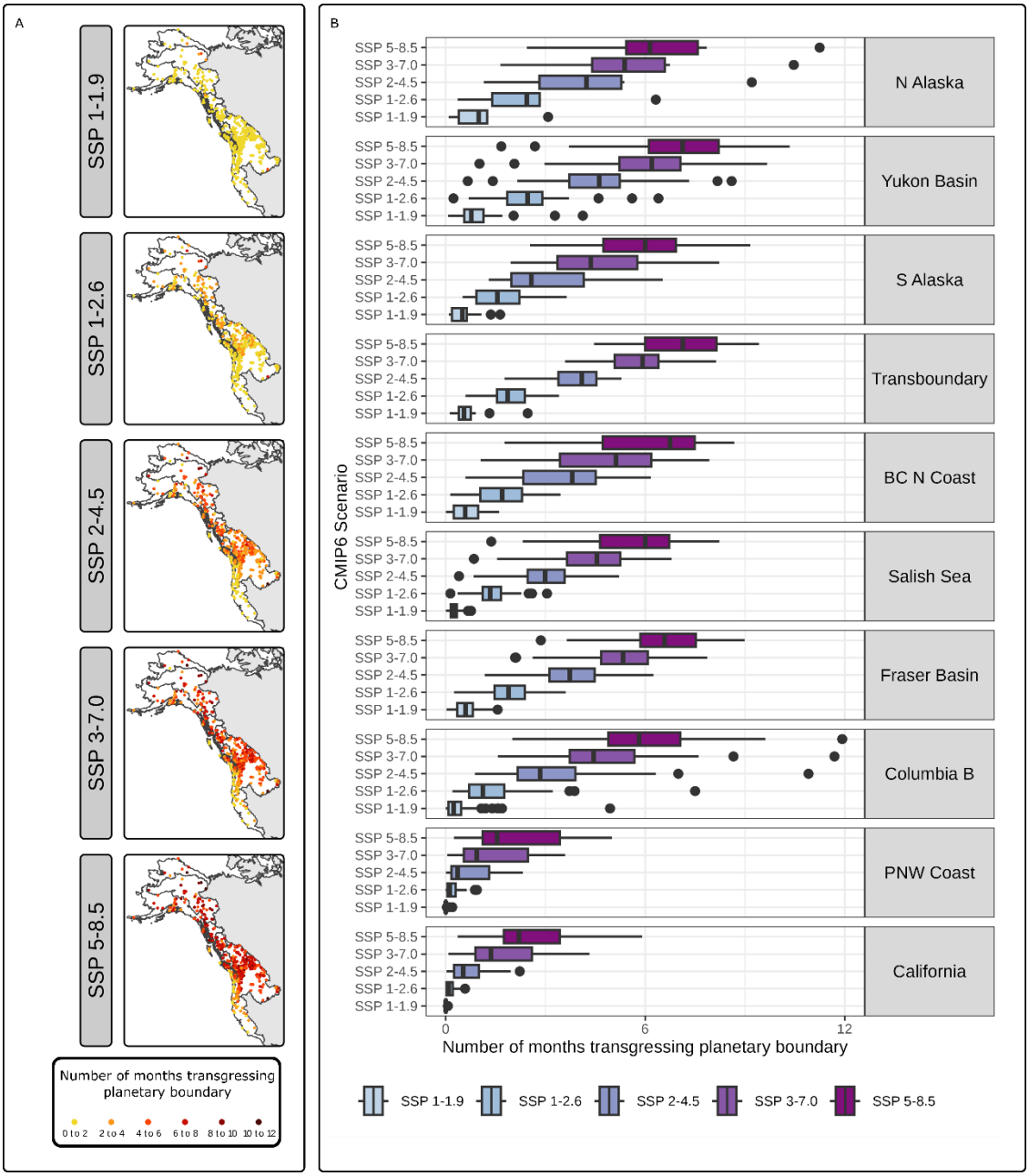

Fig. S19.

Number of months with permanent transgressions of the planetary by 2090 under five emissions scenarios. (A) maps of the 399 catchments, number of months exceeding the planetary boundary. (B) Boxplots for each region and scenario.

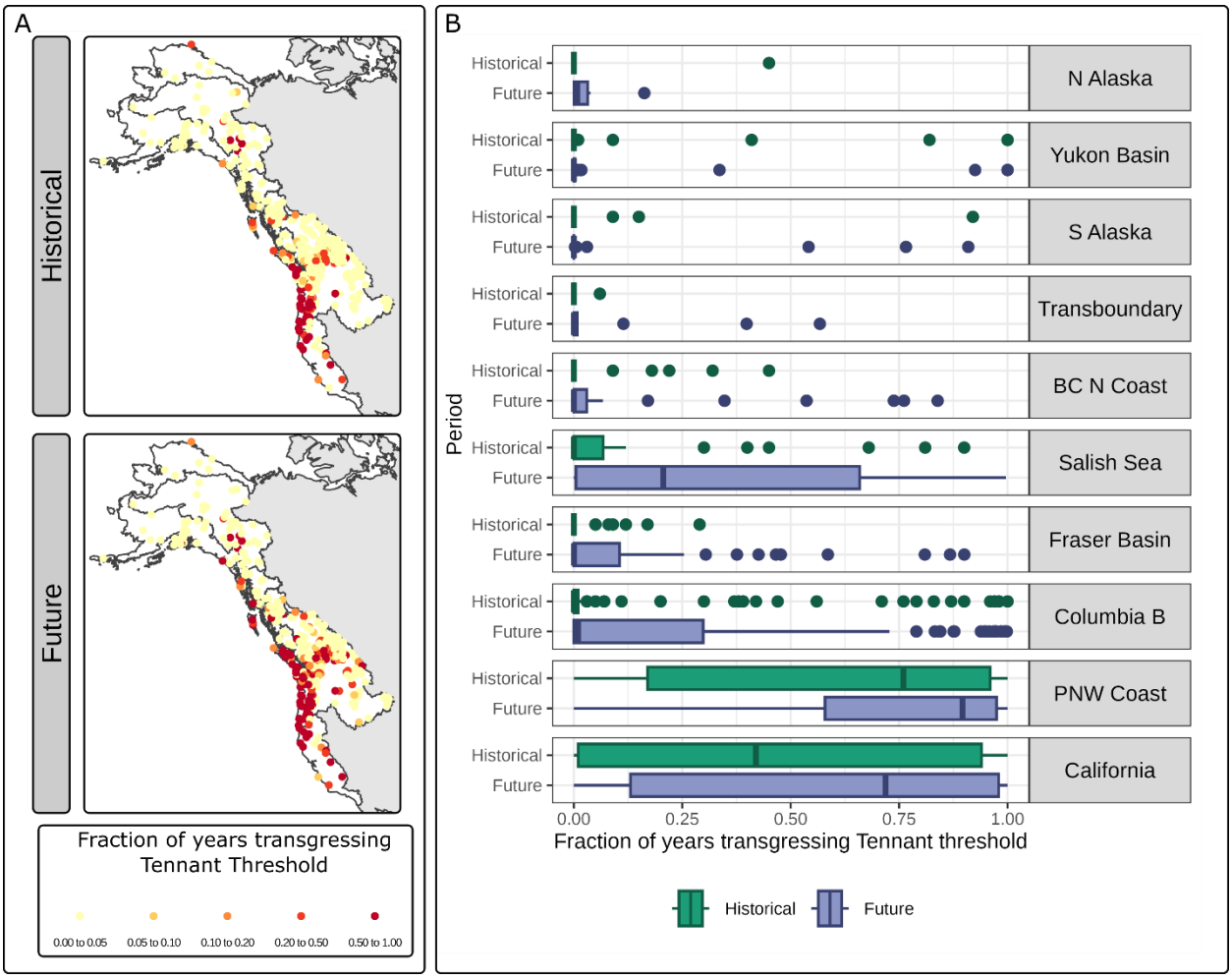

Fig. S20.

Historical and future transgression of the Tennant flow threshold (10% of the long-term mean annual discharge) for the historical (1901-2000) and future (2070-2099, SSP 2-4.5) periods. Transgressions are predicted to become more frequent in the five southern regions.

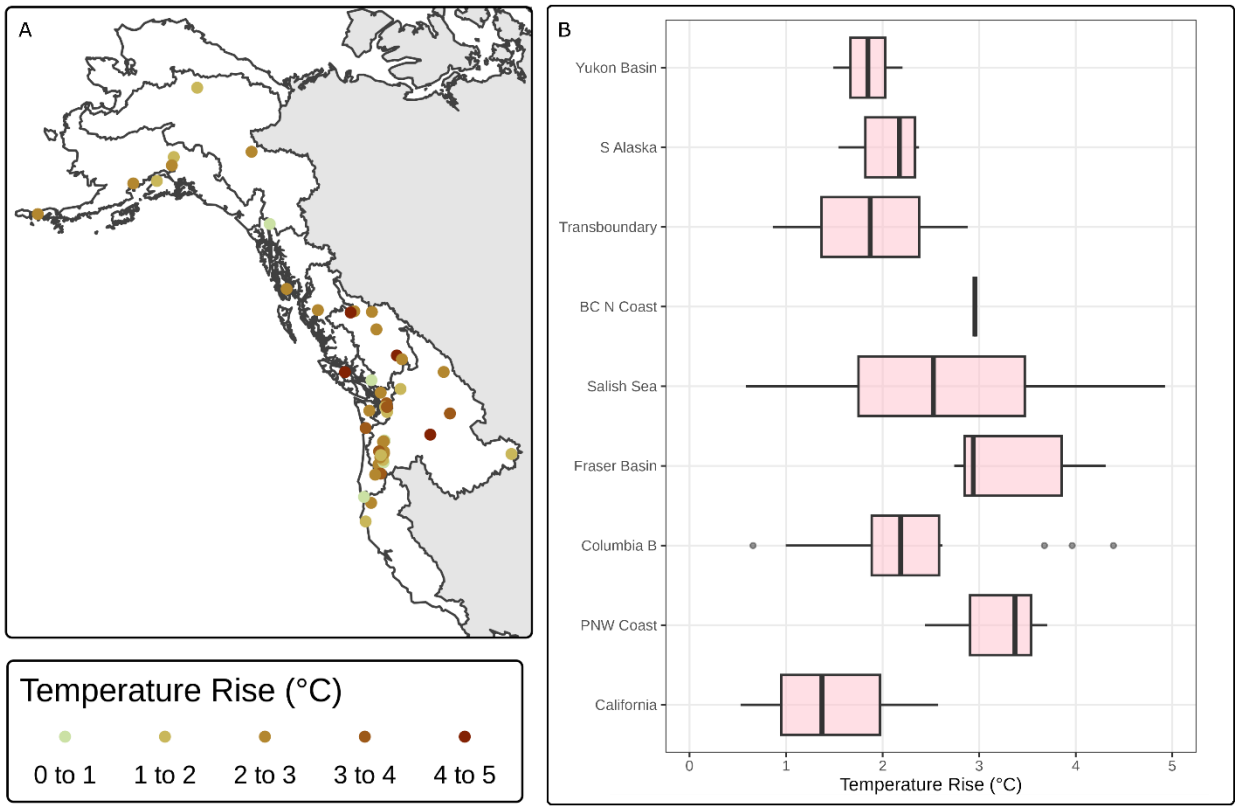

Fig. S21.

Projected increase in water temperature at 47 stream gauges that also had long water temperature records. (A) Map of temperature rise at 47 gauges. (B) Boxplots of temperature rise by region.

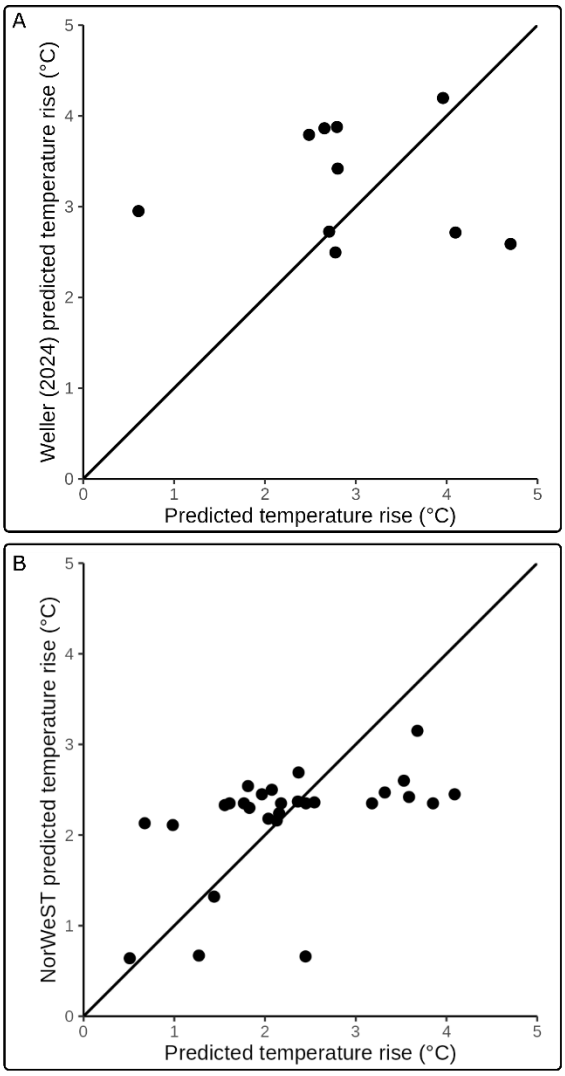

Fig. S22.

Comparison of projected water temperature rise by the end of the century to two published studies. (A) Comparison to (*85*) for ten stream gauges in British Columbia. (B) Comparison to (*127*) for 28 stream gauges in the western United States.

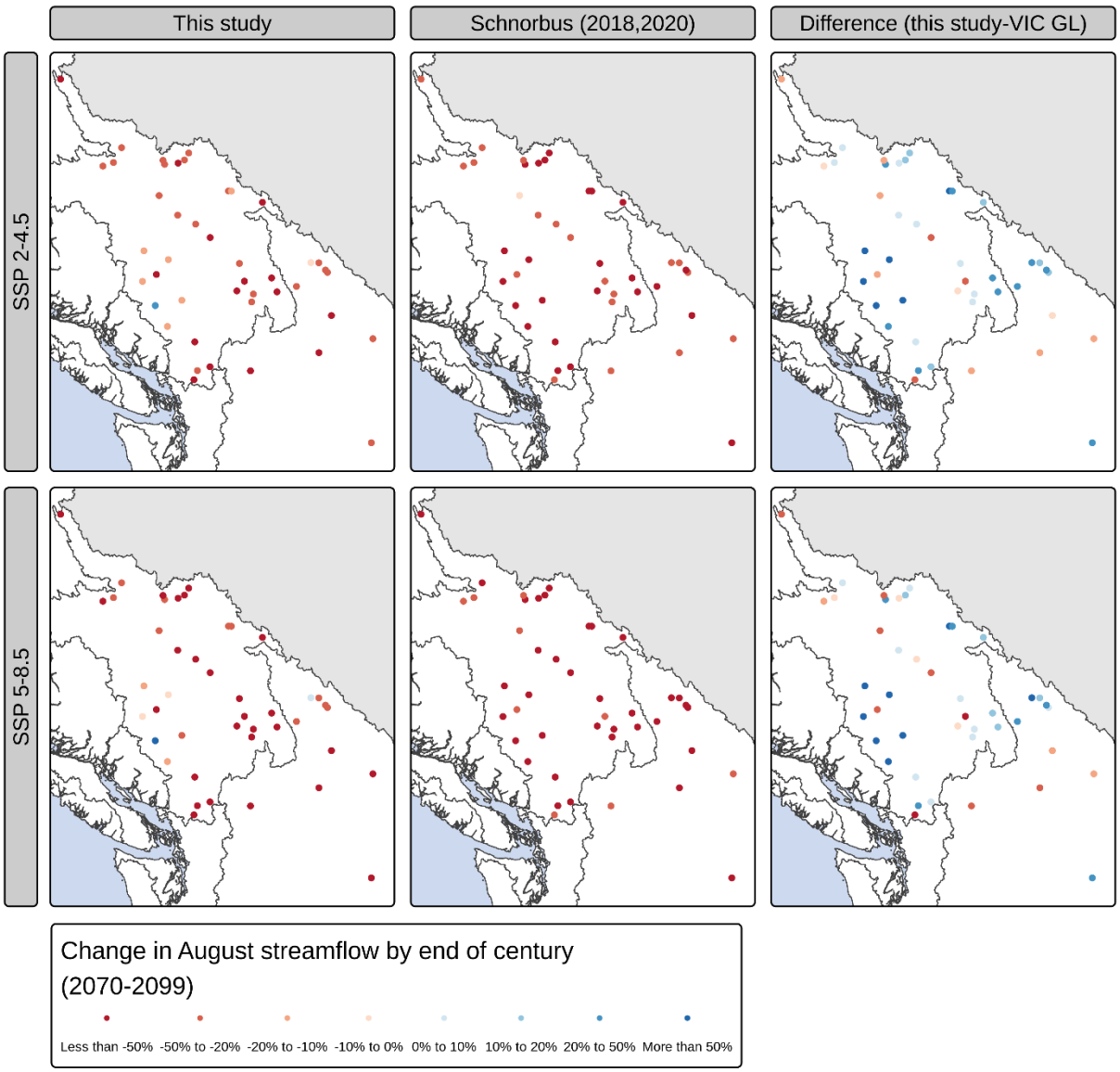

Fig. S23.

Comparison of projected streamflow changes by the end of the century to VIC-GL simulations for the Fraser Basin by Schnorbus (*29*, *156*).

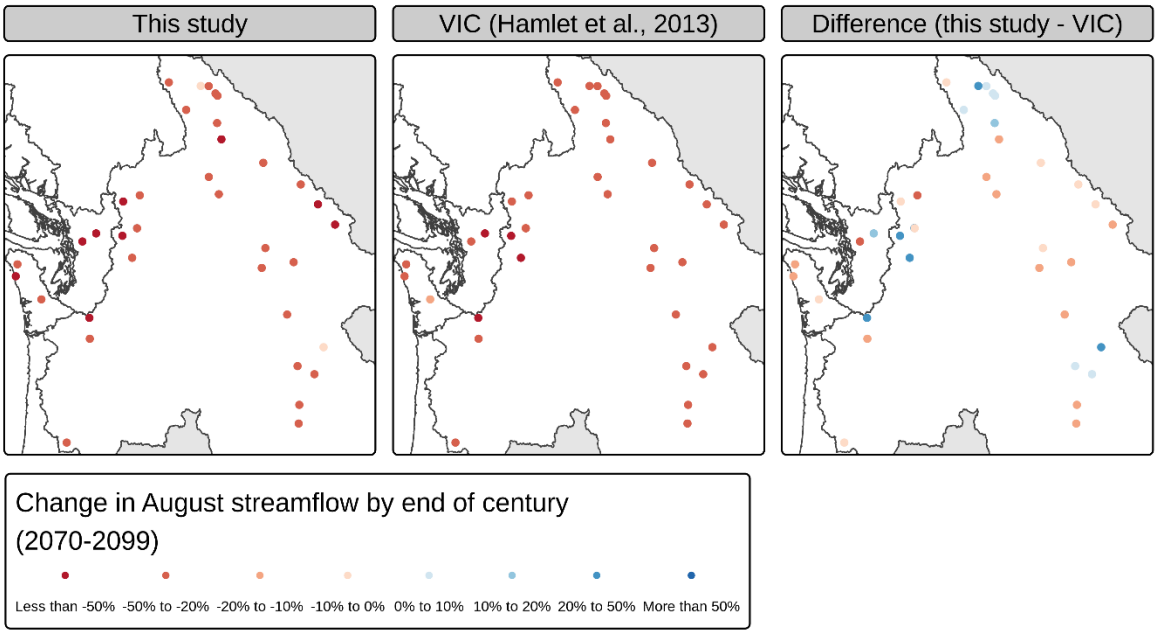

Fig. S24.

Comparison of projected streamflow changes by the end of the century to VIC simulations for the Columbia Basin and coastal Washington and Oregon by Hamlet *et al.* (*28*).

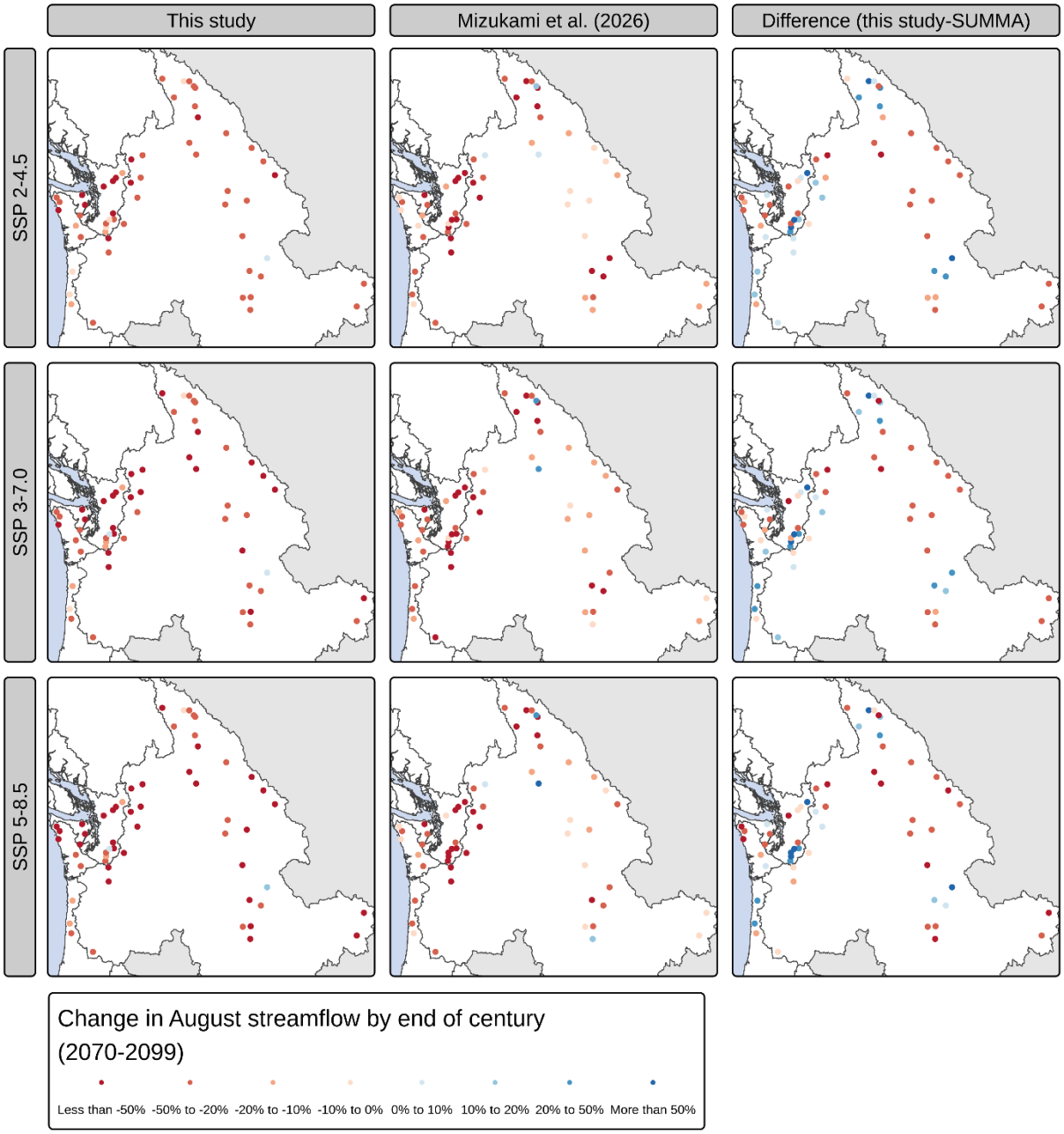

Fig. S25.

Comparison of projected streamflow changes by the end of the century to SUMMA simulations for the Columbia Basin and coastal Washington and Oregon by Mizukami (*63*).

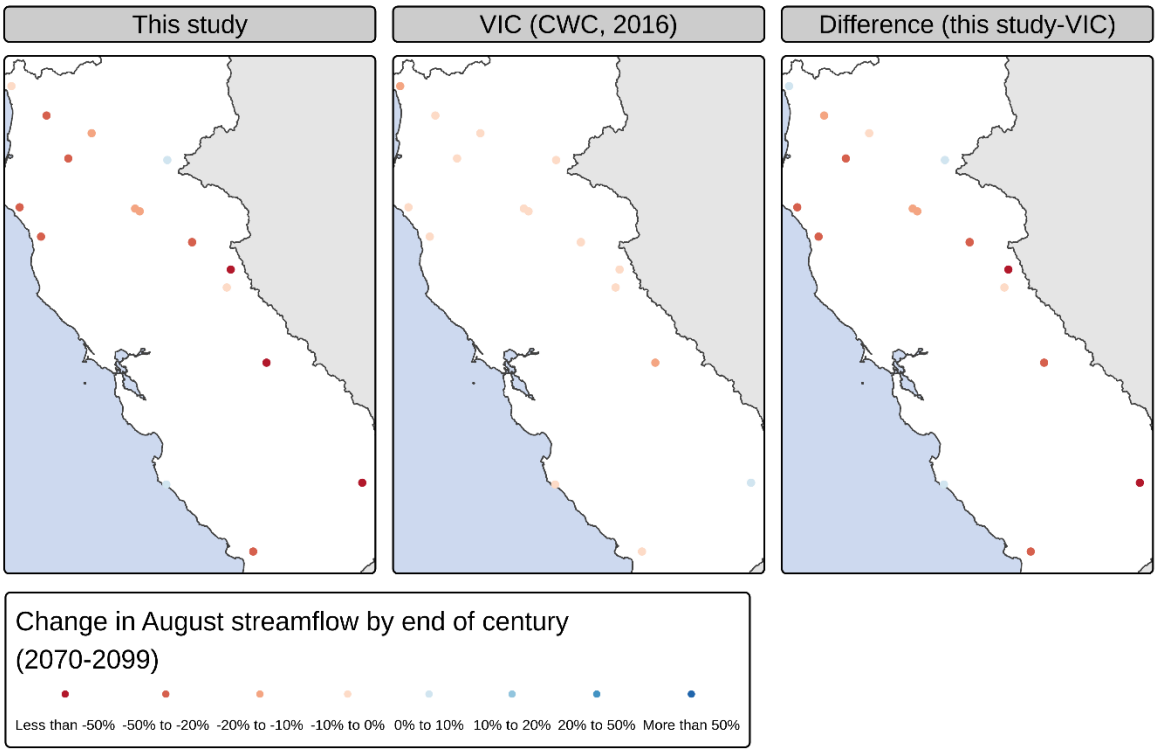

Fig. S26.

Comparison of projected streamflow changes by the end of the century to VIC-GL simulations for California by the California Water Commission (*64*).

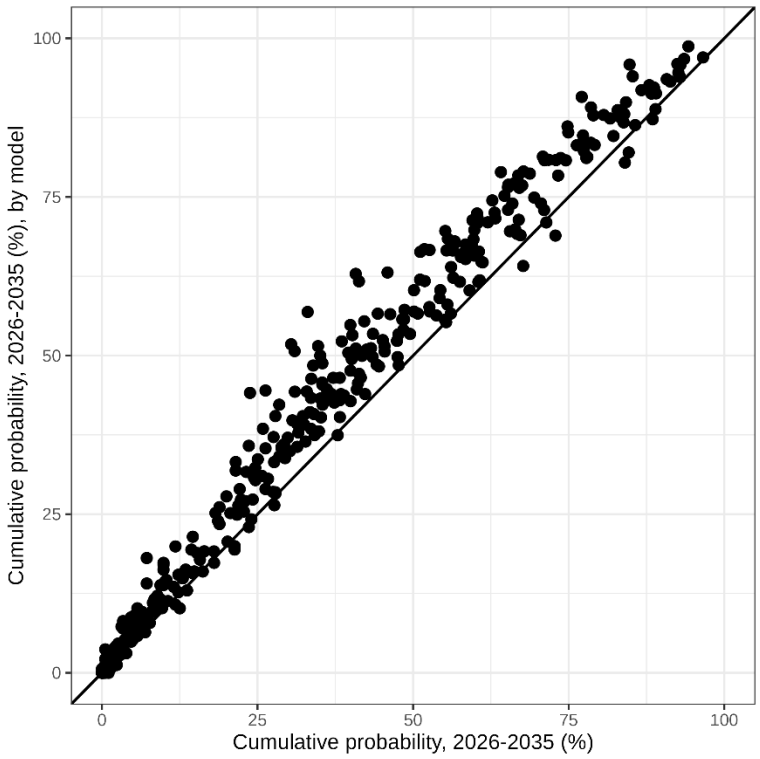

Fig. S27.

Robustness of 500-year drought predictions to calculating return levels for each model independently. The return levels were calculated separately for each model with at least ten ensemble members for the historical period (y-axis). This approach results in slightly higher probabilities than the approach presented in the main text.

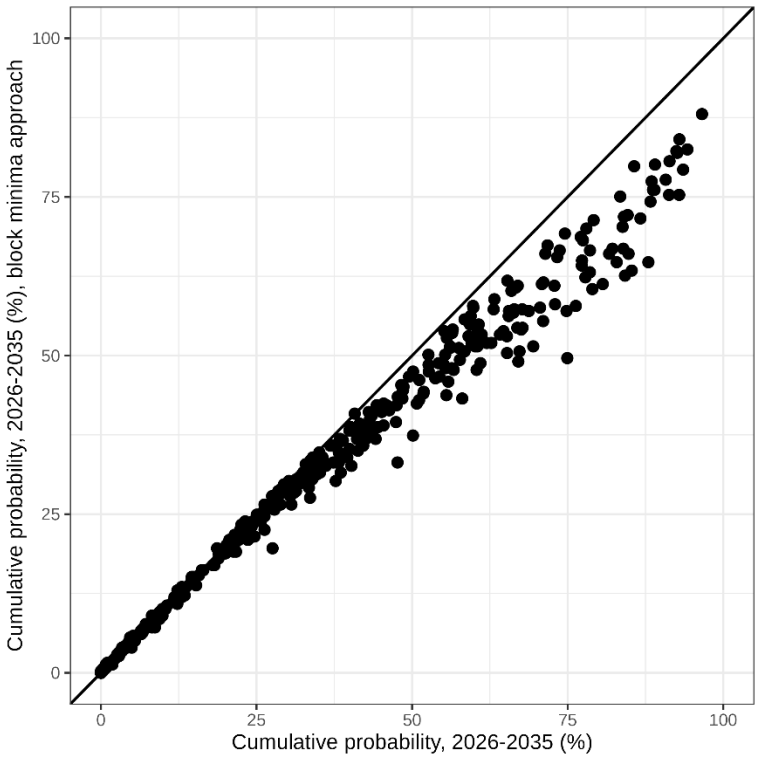

Fig. S28.

Robustness of 500-year drought predictions to using a 10-year block minima approach. The 2nd percentile of the decadal minimum mean August streamflow for 6180 decades of historical simulations is used to calculate the 500-year return level, and the probability is calculated as the number of ensembles members with at least one year below this return level for the from 2026-2035. The block minima approach results in slightly lower probabilities than the approach presented in the main text.

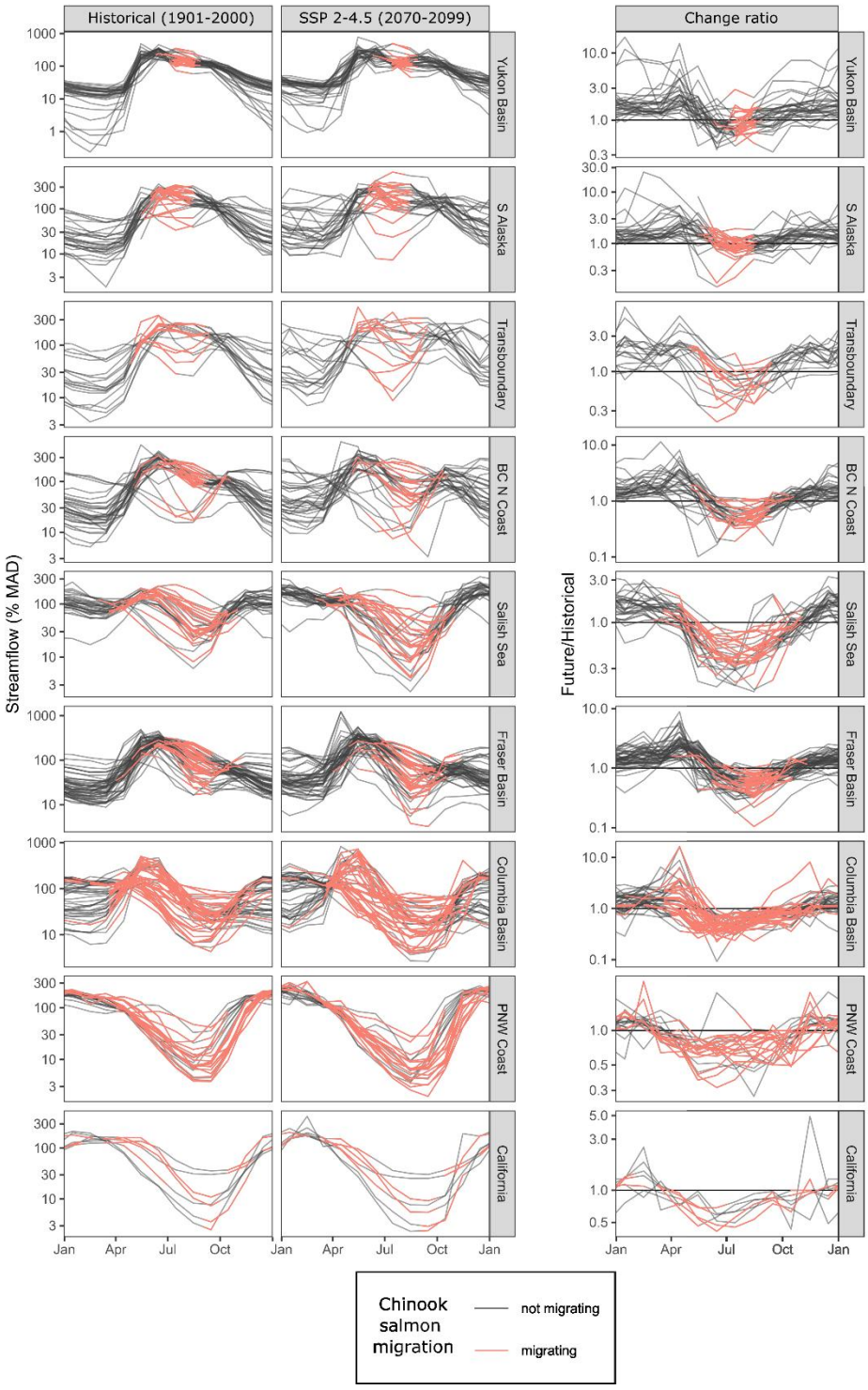

Fig. S29.

Historical and future monthly hydrographs, along with change ratio. Hydrographs are coloured pink when Chinook salmon are migrating.

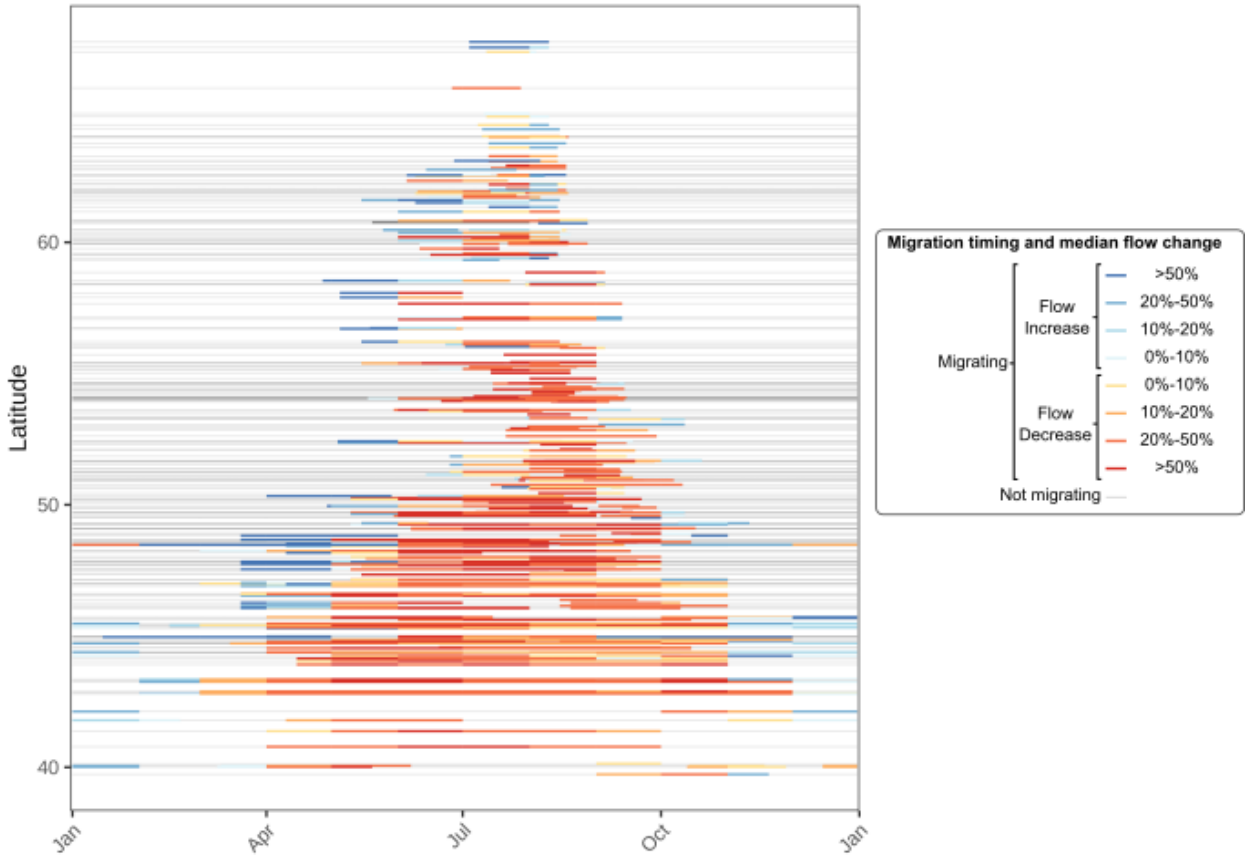

Fig. S30.

Projected change in median flows during salmon migration, by latitude. The color indicates the percentage change from historical (1901-2000) conditions for the end of the century (2070—2099) under SSP 2-4.5. Lines are coloured when Chinook salmon are migrating in the vicinity of the stream gauge.

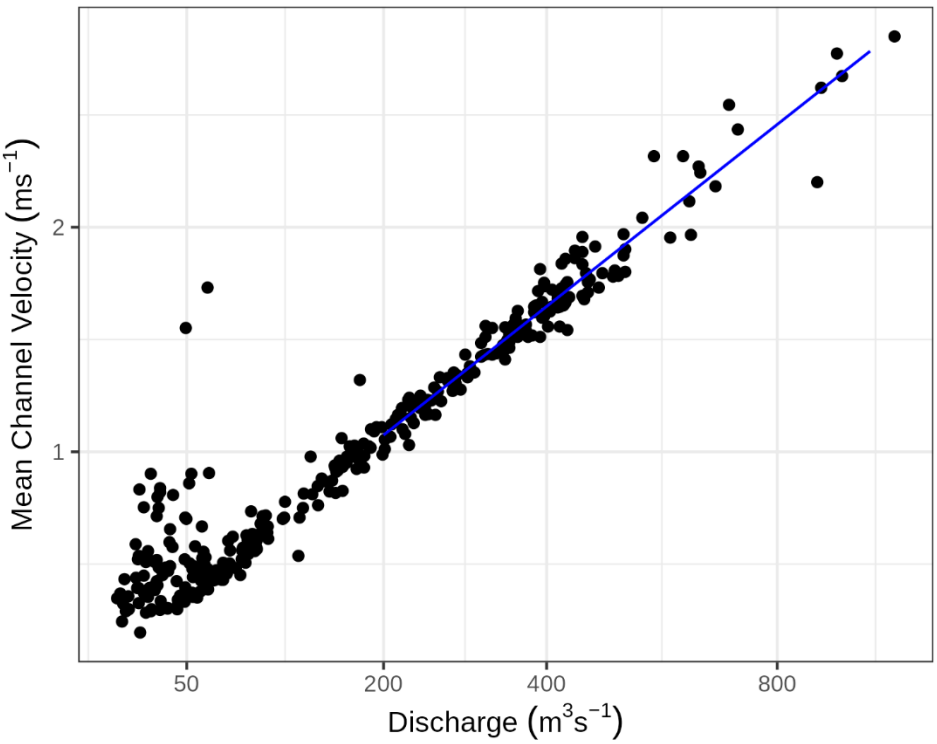

Fig. S31.

Kenai River velocity-discharge relationship. The mean channel velocity is plotted against the square root of discharge.

Table S1.

Models for Performance Comparison. Listed are 17 models against which we benchmarked our regression models. Under Model Location, CONUS is the Contiguous United States. The Number of Shared Catchments is the count of catchments modelled in the comparison model that we also modelled in this study; the performance comparison is only on these catchments. The Evaluation Data Partition indicates whether the published simulation data, which we use for the performance comparison, are from years excluded in model training (temporal holdout), gauges excluded in model training (spatial holdout), gauges and years included in model training/calibration, or a mix.

Model	Source	Model Location	# Shared Catchments	Evaluation Data Partition
LSTM (Kratzert et al, 2024)	(*62*)	CONUS	70	Temporal holdout
mHm (Mizukami et al, 2019)	(*155*, *158*)	CONUS	62	Temporal holdout
SAC-SMA (Newman et al., 2017)	(*158*, *159*)	CONUS	86	Temporal holdout
FUSE (Addor)	(*158*)	CONUS	74	Temporal holdout
HBV (Seibert et al., 2018)	(*158*, *160*)	CONUS	86	Temporal holdout
VIC (Newman et al., 2017)	(*158*, *159*)	CONUS	86	Temporal holdout
FUSE (Thébault, 2026a)	(*117*)	Canada and USA (excluding Alaska)	182	Temporal holdout
FUSE (Thébault, 2026b)	(*118*)	CONUS	60	Temporal holdout
δHBV (Song et al., 2025)	(*161*)	CONUS	125	Mixed
LSTM (Nearing et al., 2024)	(*61*)	Global	119	Spatial Holdout
GloFAS (Nearing et al., 2024)	(*61*)	Global	119	Mixed
National Water Model (Cosgrove et al., 2024)	(*60*)	CONUS	149	Temporal holdout
National Hydrologic Model (Regan et al., 2019)	(*162*)	CONUS	149	Calibration (in-sample)
Grid-LSTM (Yang et al., 2025)	(*163*)	Global	147	Spatial holdout
VIC-GL (Schnorbus, 2018)	(*29*, *156*)	Peace, Fraser, and Columbia basins	44	Calibration (in-sample)

VIC (Hamlet et al., 2013)	(*28*)	Columbia Basin and coastal Washington and Oregon	34	Calibration (in-sample) + bias correction of streamflow
SUMMA (Mizukami et al., 2026)	(*63*)	Columbia Basin and coastal Washington and Oregon	52	Mixed

Table S2.

Alaska basin screening. The 33 gauged basins in this table were not evaluation by (*130*). We screened these basins to determine whether they were reference quality (Ref), *ie*. free from regulation, mining, urban land use, and agricultural land use. Annual data reports can be accessed from the USGS at https://rconnect.usgs.gov/water-year-summary/.

Gauge ID	CLASS	Annual data report referenced	Screening Comments
15008000	Ref	2013	"Records are fair"
15024800	Ref	2013	Stikine River is free-flowing
15040000	Non-ref		Dams on Dororthy Lake and Bart Lake:
15052500	Ref	2013	Located within Tongass National Forest Special Interest Area
15052800	Ref	2012	"Records are poor"
15100000	Ref	2013	"Records are fair"
15129000	Ref	2012	"Records are poor"
15219000	Ref		Located within a "Chugach National Forest Research Natural Area"
15225997	Non-ref		Solomon Lake Dam
15238648	Non-ref	2013	"Water is diverted, 300 ft. upstream from gage, into Bradley River drainage since July 29, 1990"
15238990	Non-ref	2013	"Flow diverted from Upper Nuka River into Upper Bradley River drainage since July 29, 1990."
15239001	Non-ref		Bradley Lake Dam
15239070	Non-ref	2013	"Intermittent regulation during construction at the Bradley River dam site began in November 1986. Flow has been regulated since the reservoir began filling April 26, 1991"
15243900	Ref	2009	Upstream of water diversions into Kenai Lake; "EXTREMES OUTSIDE PERIOD OF RECORD.--Glacier-dammed lake outburst flood about August 31, 1967, 55,000 ft^3/s from rating curve extended above 27,000 ft^3/s, gage-height 42.60 ft from floodmarks, site and datum then in use."
15274600	Non-ref		Urban watershed
15281000	Ref	2013	"Maximum discharge, 355,000 ft^3/s, July 26, 1961, gage-height 24.30 ft., site then in use, caused by release of stored water (Lake George) behind Knik Glacier"
15292400	Ref	2013	Golden Zone Mine is quite far upstream and seems unlikely to substantially affect streamflow
15295700	Non-ref		Terror Lake Dam
15300500	Ref		No dams or mines
15304000	Ref	2013	"It is the longest free flowing river in the United States." - Wikipedia

15320100	Ref	2013	“Records Poor; Prior to June 19, 1997, recording gage was at a site 700 ft downstream at a different datum”
15348000	Ref	2013	“Records fair; Prior to October 16, 1912 at site 6.8 mi downstream at different datum”
15453500	Ref	2013	Minimal flow regulation on the Yukon River
15485500	Non-ref	2013	Part of river flows through Salchaket Slough and is ungauged
15493700	Non-ref	2011	3.1 mi downstream from Moose Creek Dam
15514000	Non-ref	2013	“Regulation during high-flow periods began July 9, 1981 at Moose Creek Dam 31.8 mi upstream”
15515500	Non-ref	2013	“Records are fair”; two mines in basin and Chena River is regulated
15564900	Ref		No dams or mines
15565447	Ref	2013	Minimal flow regulation on the Yukon River
15744500	Ref	2012	“Records are fair”
15798700	Ref		Small (2.9 sq miles) basin near Utqiagvik
15875000	Ref	2013	“Records fair”
15896000	Ref	2013	“Records fair”

Table S3.

CMIP6 Models used. ECS is equilibrium climate sensitivity (the average global temperature change for a doubling of atmospheric carbon dioxide). TCR the transient climate response (the average global temperature change per teratonne of carbon emitted). The weights are derived using the method proposed by (*113*) to match the assessed distribution of ECS (*112*).

Model	# variants (historical and future)	# variants (only historical)	ECS (ºC)	TCR (ºC TtC^{-1})	Weight	Model Reference	ECS & TCR Reference
ACCESS-CM2	10	0	4.66	1.96	0.006	(*164*)	(*111*)
ACCESS-ESM1-5	40	0	3.88	1.97	0.055	(*165*)	(*111*)
AWI-CM-1-1-MR	1	4	3.16	2.03	0.035	(*166*)	(*111*)
AWI-ESM-1-REcoM	1	0	3.6	NA	0.029	(*167*)	(*168*)
BCC-CSM2-MR	1	2	3.02	1.55	0.035	(*169*)	(*111*)
CAMS-CSM1-0	2	1	2.29	1.73	0.031	(*170*)	(*111*)
CAS-ESM2-0	2	0	3.4	NA	0.055	(*171*)	(*171*)
CESM2	3	8	5.15	2	0.007	(*172*)	(*111*)
CESM2-WACCM	1	2	4.68	1.91	0.005	(*172*)	(*111*)
CIESM	1	2	5.63	2.25	0.004	(*173*)	(*111*)
CMCC-CM2-SR5	1	10	3.56	2.14	0.032	(*174*)	(*111*)
CMCC-ESM2	1	0	3.58	1.92	0.034	(*175*)	(*111*)
CNRM-CM6-1	6	23	4.9	2.22	0.004	(*176*)	(*111*)
CNRM-CM6-1-HR	1	0	4.34	2.46	0.012	(*176*)	(*111*)
CNRM-ESM2-1	5	10	4.79	1.83	0.005	(*177*)	(*111*)
CanESM5	50	15	5.64	2.71	0.004	(*178*)	(*111*)
CanESM5-1	2	0	5.64	2.71	0.003	(*179*)	Assumed equal to CanESM5
CanESM5-CanOE	3	0	5.64	2.71	0.004	(*180*)	(*111*)
EC-Earth3	57	17	4.26	2.3	0.029	(*181*)	(*111*)

EC-Earth3-Veg	7	0	4.33	2.66	0.011	(*181*)	(*111*)
EC-Earth3-Veg-LR	3	0	4.33	2.66	0.014	(*181*)	Assumed equal to EC-Earth3-Veg
FGOALS-f3-L	1	2	3	1.94	0.033	(*182*)	(*111*)
FGOALS-g3	4	2	2.87	1.5	0.05	(*183*)	(*111*)
FIO-ESM-2-0	3	0	4.27	2.22	0.013	(*184*)	(*185*)
GFDL-ESM4	1	2	2.65	1.63	0.026	(*186*)	(*111*)
GISS-E2-1-G	14	31	2.64	1.8	0.027	(*187*)	(*111*)
GISS-E2-1-H	10	15	3.12	1.87	0.028	(*187*)	(*111*)
GISS-E2-2-G	5	0	2.43	1.71	0.032	(*188*)	(*111*)
HadGEM3-GC31-LL	1	54	5.55	2.49	0.004	(*189*)	(*111*)
IITM-ESM	1	0	2.37	1.66	0.034	(*190*)	(*111*)
INM-CM4-8	1	0	1.83	1.3	0.003	(*191*)	(*111*)
INM-CM5-0	1	9	1.92	1.41	0.004	(*192*)	(*111*)
IPSL-CM6A-LR	6	27	4.7	2.35	0.006	(*193*)	(*111*)
KACE-1-0-G	3	0	4.75	2.04	0.005	(*194*)	(*111*)
KIOST-ESM	1	0	3.36	NA	0.038	(*195*)	(*111*)
MCM-UA-1-0	1	1	3.76	1.9	0.035	(*196*)	(*111*)
MIROC-ES2H	1	0	2.6	NA	0.024	(*197*)	(*111*)
MIROC-ES2L	10	21	2.66	1.49	0.023	(*197*)	(*111*)
MIROC6	50	0	2.6	1.55	0.024	(*198*)	(*111*)
MPI-ESM1-2-HR	2	8	2.98	1.64	0.044	(*199*)	(*111*)
MPI-ESM1-2-LR	50	1	3.02	1.82	0.032	(*199*)	(*111*)
MRI-ESM2-0	5	1	3.13	1.67	0.032	(*200*)	(*111*)
NESM3	2	3	4.72	2.72	0.005	(*201*)	(*111*)
NorESM2-LM	1	2	2.56	1.49	0.022	(*202*)	(*111*)
NorESM2-MM	1	1	2.49	1.22	0.022	(*202*)	(*111*)
TaiESM1	1	1	4.36	2.27	0.009	(*203*)	(*111*)
UKESM1-0-LL	5	14	5.36	2.77	0.007	(*204*)	(*111*)

Table S4.

Water license curtailments by ministerial order, 2016-2025. Orders can be viewed at https://www.bclaws.gov.bc.ca/civix/content/mo/?xsl=/templates/browse.xsl

Year	Ministerial Order #	Watershed	Critical flow threshold (L/s)	Species
2025	287/2025	Besette Creek	1000	Chinook salmon
2025	286/2025	Salmon River	1270	Chinook salmon
2023	241/2023	Tsolum River	215	Steelhead trout
2023	238/2023	Salmon River	1270	Chinook salmon
2023	249/2023	Koksilah River	180	Steelhead trout
2023	239/2023	Bessette River	1000	Chinook salmon
2021	335/2021	West Kettle River	670	Rainbow trout
2021	327/2021	Bessette River	826	Chinook salmon
2021	328/2021	Salmon River	1270	Chinook salmon
2021	324/2021	Koksilah River	180	Coho salmon, steelhead and resident trout
2019	280/2019	Koksilah River	180	Steelhead and resident trout

Interactive map S1. (separate file)

https://sruzzante.shinyapps.io/streamflow_projections/

Interactive visualization of projections for all streams, as well as links to summary documents and data for each stream.